AD NUMBER:	AD0885817

LIMITATION CHANGES

TO:

Approved for public release; distribution is unlimited.

FROM:

Distribution authorized to U.S. Gov't. agencies only; Test and Evaluation; 19 Jul 1971. Other requests shall be referred to the Office of Naval Research, Code 468 (Acoustic Programs), Washington, DC 20360. Export Controlled.

AUTHORITY

29 Aug 1973, ONR ltr

SPERRY RAND

(20)

AD885817

INTERIM REPORT

ANALYSIS OF ACOUSTIC BAFFLES FOR UNDERWATER NOISE REDUCTION

CONTRACT N00014-67-C-0303

Prepared for

OFFICE OF NAVAL RESEARCH
DEPARTMENT OF THE NAVY
WASHINGTON, D.C. 20360

[redacted] Office of Naval Research, Acoustics Program (Code 468), ~~Washington, D.C. 20360~~ Arl, Va. 22217

SPERRY GYROSCOPE DIVISION
GREAT NECK, NEW YORK 11020

SGD-4230-0430
JUNE 1971

90

SPERRY RAND

INTERIM REPORT

ANALYSIS OF ACOUSTIC BAFFLES FOR UNDERWATER NOISE REDUCTION

CONTRACT N00014-67-C-0303

Prepared for

OFFICE OF NAVAL RESEARCH
DEPARTMENT OF THE NAVY
WASHINGTON, D.C. 20360

SGD-4230-0430
JUNE 1971

SPERRY GYROSCOPE DIVISION
GREAT NECK, NEW YORK 11020

UNCLASSIFIED

Security Classification

DOCUMENT CONTROL DATA - R & D

(Security classification of title, body of abstract and indexing annotation must be entered when the overall report is classified)

1. ORIGINATING ACTIVITY (Corporate author) Sperry Gyroscope Division Sperry Rand Corporation Great Neck, N.Y. 11020	2a. REPORT SECURITY CLASSIFICATION Unclassified 2b. GROUP None

3. REPORT TITLE

ANALYSIS OF ACOUSTIC BAFFLES FOR UNDERWATER NOISE REDUCTION

4. DESCRIPTIVE NOTES (Type of report and inclusive dates)

Research Report

5. AUTHOR(S) (First name, middle initial, last name)

Brian E. Owens, George Rand, Barry Schwartz

6. REPORT DATE	7a. TOTAL NO. OF PAGES	7b. NO. OF REFS
June 1971	69	5

8a. CONTRACT OR GRANT NO. N00014-67-C-0303 b. PROJECT NO. c. d.	9a. ORIGINATOR'S REPORT NUMBER(S) SGD-4230-0430 9b. OTHER REPORT NO(S) (Any other numbers that may be assigned this report)

10. DISTRIBUTION STATEMENT

This d[redacted] su[redacted] to special ex[redacted] controls and [redacted] tran[redacted]al
to f[redacted] f[redacted] ma[redacted]val
of Office Of Naval Res[redacted] Acoustics [redacted] ing[redacted] D.C.20360

11. SUPPLEMENTARY NOTES	12. SPONSORING MILITARY ACTIVITY
	Department of the Navy Office of Naval Research Acoustics Programs (Code 468) ~~Washington, D.C. 20360~~

13. ABSTRACT

This is an interim report on the study of underwater noise reduction techniques being conducted by the Sperry Division ~~for the~~ Office of Naval Research, Acoustics Programs, under Contract No. N00014-67-C-0303. Included in this report is a description of the work being done on various types of acoustic baffles. The theoretical analysis of a multilayer cylindrical baffle is given; spring-mass type baffles are analyzed using a lumped-parameter approach. For both of these baffles, good agreement is obtained between analytical and experimental data. Also presented are both theoretical and experimental results of a new baffle material, Sonite, which shows promise of operating at deep depths without the need for pressure compensation.

DD FORM 1 NOV 65 1473 (PAGE 1)

S/N 0101-807-6801

UNCLASSIFIED

Security Classification

3ND PPSO 13152

14 KEY WORDS	LINK A		LINK B		LINK C	
	ROLE	WT	ROLE	WT	ROLE	WT
Acoustic baffles						
Waterborne noise reduction						

DD FORM 1 NOV 65 1473 (BACK)
(PAGE 2)

FOREWORD

This is an interim report on the study of underwater noise reduction techniques being conducted by the Sperry Division for the Office of Naval Research, Acoustics Programs, under Contract No. N00014-67-C-0303. Included in this report is a description of the work being done on various types of acoustic baffles. The theoretical analysis of a multilayer cylindrical baffle is given; spring-mass type baffles are analyzed using a lumped-parameter approach. For both of these baffles, good agreement is obtained between analytical and experimental data. Also presented are both theoretical and experimental results of a new baffle material, Sonite, which shows promise of operating at deep depths without the need for pressure compensation.

TABLE OF CONTENTS

LIST OF ILLUSTRATIONS

LIST OF ILLUSTRATIONS (Cont'd)

SECTION 1

INTRODUCTION

The effectiveness of the acoustic baffle is often a determining factor in the maximum capability of a sonar system. Basically, the baffle is a structure, placed between an unwanted signal or noise source and a sensor, to shield the sensor from the unwanted source. To achieve an array gain consistent with the directivity index of the array, efficient baffle structures must be provided. A further purpose of the baffle is to provide a desired response characteristic for the hydrophone array. Thus, the acoustic baffle is a primary tool for underwater noise reduction and directivity pattern control in sonar arrays.

The transmission of acoustic energy in water can be impeded by a compliant baffle. To be effective, such a baffle must be sufficiently stiff to withstand hydrostatic pressures yet it should be dynamically soft to perform as a highly reflective structure.

A reflective characteristic is acceptable for the side of the baffle facing the interfering noise source, but the portion facing the hydrophone presents a major design challenge. Unless this side is nonreflective, the interaction between the incident signal and the reflected signal from the baffle can alter the hydrophone array's response, often seriously degrading it.

Under the current program, the Sperry Division has developed a set of analytical models for predicting the reflectivity, transmittivity, and other acoustic parameters of planar multilayered baffle structures. This capability extends to the prediction of directivity pattern and response for line hydrophones at any steering angle, including end fire.

The analytical models have been incorporated into a FORTRAN IV computer program which has been described, together with its implementation and built-in plotting routines, in previous interim reports (references 1 and 2). Empirical and theoretical data have been successfully correlated with the results of the computer trials.

Several aspects of baffle technology are discussed in this report. First, the analysis of a multilayer planar baffle was extended to a multilayer cylindrical baffle. As in the planar case, the cylindrical baffle consists of random layers of fluid and elastic media. Secondly, baffle designs based on the use of mechanical springs coupled to masses, which represent a compliant steel plate structure, were also investigated. Lumped parameter models were developed, which were used to calculate insertion loss. Results of studies on a new particulate, fiber-reinforced, ceramic baffle material are presented in Section 4. This material can be fabricated into intricate shapes with conventional techniques and shows promise of operating as an effective baffle at high presures without requiring pressure compensation.

SECTION 2

MULTILAYER CYLINDRICAL BAFFLES

2.1 INTRODUCTION

The analysis of cylindrical baffles is a natural extension of the work done on planar baffles during previous phases of this program. In this section an infinitely long cylinder, with wall composed of layers of various materials, is taken to represent the baffle configuration. A plane wave, parallel to the cylindrical axis, is the excitation (see figure 2-1). An analysis was performed to determine the acoustic pressure at any point outside of the cylinder. With this information, the response of a hydrophone placed outside the baffle, as well as the transmission loss through the baffle, can be computed.

Solution of the wave equation, consistent with the boundary conditions imposed by the multilayer cylinder, forms the basis of the analysis. The fundamental equations for this approach are contained in Section 2.2 of reference 3.

A description of a computer program, which calculates the response of a hydrophone outside the cylindrical baffle, is presented in this section following the theoretical analysis. The results of the program are compared to experimental measurements and are also presented. A list of symbols is included at the end of the section (paragraph 2.7).

2.2 BASIC SOLUTIONS TO THE WAVE EQUATION

The equation of motion for a homogeneous isotropic elastic medium is

$$\rho \ddot{\underline{u}} = (\lambda + 2\mu) \text{ grad div } \underline{u} - \mu \text{ curl curl } \underline{u} \quad (1)$$

where $\underline{u}$ is the particle displacement vector, λ and μ are constants characteristic of the medium, and ρ is the density. It can be shown that the most general solution of (1) has the form

$$\underline{u} = \text{grad } P + \text{curl } \underline{Q} \quad (2)$$

where the scalar P and the vector $\underline{Q}$ satisfy

$$\rho \ddot{P} = (\lambda + 2\mu) \nabla^2 P \qquad (3.1)$$

$$\rho \ddot{\underline{Q}} = \mu \nabla^2 \underline{Q} \qquad (3.2)$$

In the case of a fluid, μ is set equal to 0 and λ is replaced by the bulk modulus k.

For the present application, equations (3) may be specialized in two ways. First, motion at a single frequency will be assumed; the components of $\underline{u}$ will then be complex numbers representing the phase and amplitude of the displacement components along the coordinate axes. The actual physical displacement vector is the real part of $\underline{u} \exp(-i\omega t)$. Second, it will be assumed that all components of $\underline{u}$ are independent of z, and that the z-component vanishes identically. These are natural assumptions when considering normal incidence on an infinite cylinder. One may then write

$$\underline{Q} = S\hat{\underline{z}} \qquad (4)$$

$$\text{curl } \underline{Q} = \text{grad } S \times \hat{\underline{z}}$$

where $\underline{z}$ is the unit vector in the z direction. Equations (3) now take the form

$$\nabla^2 P + n^2 P = 0 \qquad (5.1)$$

$$\nabla^2 S + m^2 S = 0 \qquad (5.2)$$

where the compressional and rotational wave numbers n and m are given by

$$n^2 (\lambda + 2\mu) = \omega^2 \rho = m^2 \mu \qquad (6)$$

The multilayer cylindrical baffle, with the z coordinate suppressed, becomes in effect a set of concentric rings. Solutions to equations (5), valid for specific values of m and n, can only apply to the zone between two circular boundaries. To facilitate matching the solutions on opposite sides of a boundary, so that continuity of stress and displacement can be maintained, the use of polar coordinates is indicated. Solutions of the form P = BR, where B is a function of bearing b only, and R depends only on range r, will be especially useful. Transforming the operator ∇^2 into polar coordinates, equation (5.1) gives

$$B''/r^2 B + R'/rR + R''/R = -n^2 \qquad (7)$$

as the condition for B and R.

Since B''/B in (7) can be expressed as a function of r only, while in fact it is a function of b only, it must be a constant. Hence B must be a linear combination of sin pb and cos pb for some number p. Furthermore, when the bearing b increases by 2π, the values of B must repeat. Thus, p must be an integer. The condition for R is then

$$R'' + R'/r + \left[n^2 - (p/r)^2\right] R = 0 \tag{8}$$

which requires R to be a linear combination of $J_p(nr)$ and $H_p(nr)$; by J_p is denoted the Bessel function of the first kind, and by H_p the Hankel function $H_p^{(1)}$.

Replacing n by m provides solutions S to equation (5.2). The next step is to form more complex solutions, for both P and S, by combining the basic solutions. For instance, letting $B_p(b)$ denote a linear combination of sin pb and cos pb, and using $R_p(x)$ to indicate a linear combination of $J_p(x)$ and $H_p(x)$, the series

$$\sum_{p=o}^{\infty} B_p(b)\, R_p(kr) \tag{9}$$

will provide a general solution for P when k = n and for S when k = m.

A solution of the form (9) is required for each zone of constant n and m. The constants used in forming the linear combinations B_p and R_p must be adjusted to make the solutions match at the boundaries between zones. Section 2.3 discusses how the matching is done.

2.3 BOUNDARY CONDITIONS

At the boundaries separating regions of different wave velocities, two types of conditions must be met. First, the stress vector must be continuous across the boundary. Second, the displacement normal to the boundary must be continuous as the boundary is crossed; and in the case of a solid-solid boundary, the tangential displacement must also be continuous (assuming secure bonding of the surfaces).

The stress vector $\underline{t}$ acting on a surface may be expressed in terms of the displacements by the formula

$$\underline{t} = \underline{a}\,\lambda\,\mathrm{div}\,\underline{u} + \mu\,\underline{a}\cdot(\nabla\underline{u} + \underline{u}\nabla) \tag{10}$$

where $\underline{a}$ is the unit normal to the surface. Using polar coordinates and setting $\underline{a}$ equal to $\underline{r}$ (the unit vector in the range direction), the stress components normal and tangential to the boundary are

$$\left.\begin{aligned} t_r &= \lambda\,\mathrm{div}\,\underline{u} + 2\mu\,\partial u_r/\partial r \\ t_b &= \mu\left[(1/r)\,\partial u_r/\partial b - u_b/r + \partial u_b/\partial r\right] \end{aligned}\right\} \tag{11}$$

where u_r and u_b are the displacements normal and tangential to the boundary, respectively.

At the outer boundary, the displacements and stresses must be compatible with the assumed input conditions. In this analysis, an incident plane wave parallel to the cylinder axis is assumed. The displacements in the fluid surrounding the cylinder are thus the sum of an incident plane wave and waves scattered from the cylinder. Assuming that axis b=o points toward the source of the incident wave, it may be described as

$$P_{01} = \exp(-inr \cos b)$$

$$= \sum_{o}^{\infty} \epsilon_p (-i)^p J_p (nr) \cos pb \qquad (12)$$

where ϵ_p equals 2 for positive p and 1 for p=o. The scattered waves may be written

$$P_{02} = \sum_{o}^{\infty} c_p H_p (nr) \cos pb \qquad (13)$$

where the coefficients c_p are to be determined. Note that the scattered waves do not make use of a fully general expansion in the form (9). The function R_p is restricted to a pure Hankel function so that, for large r, each term of (13) will correspond to an outgoing circular wave. The function B_p is restricted to the cosine for symmetry reasons: with the incident wave coming in along the b=o axis, displacement and stresses normal to the circular boundaries will be even functions of b, and displacements and stresses tangent to the boundaries will be odd functions of b. The relations

$$\left.\begin{aligned} u_r &= \partial P/\partial r + (1/r)\, \partial S/\partial b \\ u_b &= (1/r)\, \partial P/\partial b - \partial S/\partial r \end{aligned}\right\} \qquad (14)$$

and also equation (11), indicate that the functions P must have even symmetry in b, while the functions S must have odd symmetry. In short, the expansions of form (9) for P and S have predetermined choices of B_p; only R_p is open to selection. Except for the restriction on the scattered waves, one may generally choose R_p freely; however, in the innermost zone one must select pure Bessel functions to avoid a pole at the origin.

The entire process of matching displacements and stresses at the boundaries must be carried out separately for each p, until the terms in (12) become negligible. For a given p, let F and G denote the choices for R_p in the expansions of P and S, respectively; then

$$\left.\begin{aligned} F(r) &= C_{11} J_p (nr) + C_{12} H_p (nr) \\ G(r) &= C_{21} J_p (mr) + C_{22} H_p (mr) \end{aligned}\right\} \qquad (15)$$

Substituting $P = F \cos pb$ and $S = G \sin pb$ into (14) and (11), and noting that $\text{div}\ \underline{u} = -n^2 P$, gives the p^{th} terms in the sine or cosine series for the displacement and stress components. Using capital letters to denote the series coefficients, so that, for instance

$$u_r = \sum_{0}^{\infty} U_{rp} \cos pb$$

one finds directly that

$$\left.\begin{aligned} U_{rp} &= F' + (p/r)\ G \\ U_{bp} &= -\left[G' + (p/r)\ F\right] \end{aligned}\right\} \quad (16)$$

Some additional calculation shows that the coefficients in the expansions for the stress components are

$$T_{rp} = -\lambda n^2 F + 2\mu F'' + 2\mu (p/r^2)\ (rG' - G) \qquad (17.1)$$

$$T_{bp} = -\mu m^2 G - 2\mu G'' - 2\mu (p/r^2)\ (rF' - F) \qquad (17.2)$$

where (8) has been used to modify equation (17.2).

It is the quantities given in (16) and (17) which must show continuity at the boundaries, with the exception of U_{bp} in the fluid/solid case. The next step is to represent these displacement and stress coefficients explicity as linear functions of the constants C_{ij} appearing in equations (15). This will be done in Section 2.4, where the procedure for solving the equations is discussed.

2.4 NUMERICAL METHODS

Upon substituting (15) into (16) and (17) the following explict formulas are obtained giving the Fourier coefficients of the displacement and stress components. The symbols x and y are used for nr and mr, respectively.

$$rU_{rp} = x\ J_p'(x)\ C_{11} + x\ H_p'(x)\ C_{12} + p\ J_p(y)\ C_{21} + p\ H_p(y)\ C_{22} \qquad (18.1)$$

$$-rU_{bp} = p\ J_p(x)\ C_{11} + p\ H_p(x)\ C_{12} + y\ J_p'(y)\ C_{21} + y\ H_p'(y)\ C_{22} \qquad (18.2)$$

$$\begin{aligned} r^2\,T_{rp} = {} & x^2 \left[2\mu J_p''(x) - \lambda\ J_p(x)\right] C_{11} \\ & + x^2 \left[2\mu H_p''(x) - \lambda\ H_p(x)\right] C_{12} \\ & + 2\mu p \left[y\ J_p'(y) - J_p(y)\right] C_{21} \\ & + 2\mu p \left[y\ H_p'(y) - H_p(y)\right] C_{22} \end{aligned} \qquad (18.3)$$

$$
\begin{aligned}
-r^2\,T_{bp} = {} & 2\mu p\left[x\,J_p'(x) - J_p(x)\right]C_{11} \\
& + 2\mu p\left[x\,H_p'(x) - H_p(x)\right]C_{12} \\
& + \mu y^2\left[2\,J_p''(y) + J_p(y)\right]C_{21} \\
& + \mu y^2\left[2\,H_p''(y) + H_p(y)\right]C_{22}
\end{aligned}
\tag{18.4}
$$

As previously stated, all the quantities (18) except (18.2) must show continuity at every boundary, and at a solid/solid boundary (18.2) also must show continuity. The meaning of this is that if a quantity such as (18.3) is evaluated on the outer side of a boundary $r = r_o$ using the physical constants λ^I, μ^I, n^I, m^I, $x^I = n^I r_o$ and $y^I = m^I r_o$ pertaining to the outer medium, and the values $C_{ij}{}^I$ describing the wave in the outer medium, then the resultant value of (18.3) will be the same as that found on the inner side of the boundary using the physical constants λ^{II}, μ^{II}, n^{II}, m^{II}, $x^{II} = n^{II} r_o$ and $y^{II} = m^{II} r_o$ pertaining to the inner medium and the values $C_{ij}{}^{II}$ describing the wave in the inner medium.

Thus, at each boundary a set of equations may be set up, expressing the requirements of continuity. The equations may be written

$$
\left.
\begin{aligned}
(r\,U_{rp})^I - (r\,U_{rp})^{II} &= 0 \\
(-r\,U_{bp})^I - (-r\,U_{bp})^{II} &= 0 \\
(r^2\,T_{rp})^I - (r^2\,T_{rp})^{II} &= 0 \\
(-r^2\,T_{bp})^I - (-r^2\,T_{bp})^{II} &= 0
\end{aligned}
\right\}
\tag{19}
$$

where superscripts I and II indicate evaluation in the outer and the inner medium, respectively. It must be noted, however, that not all the equations are required at every boundary. At a fluid/fluid boundary, only the first and third equations are needed, since the fourth is satisfied automatically when $\mu = o$ in both media. At a fluid/solid boundary all but the second are needed, and all are needed at a solid/solid boundary. The number of equations (19) needed to express the continuity requirements can thus be two, three, or four, depending on the type of boundary.

When the continuity equations have been written for all the boundaries, one has a number of simultaneous linear equations. The unknowns are the various C_{ij} which describe the waves within the various zones of constant velocity. There will always be just enough equations to allow a solution to be found, based on the given values of C_{11} in the outermost zone. When the equations have been solved for the value of C_{12} in the outermost zone, all this being for a particular value of p, the p^{th} coefficient in the expansion (13) has been calculated. When sufficient coefficients have been determined, the overall displacement potential in the outermost medium may be calculated from

$$P = P_{01} + P_{02}$$

where the notations P_{01} and P_{02} refer to (12) and (13), respectively.

The actual rms pressure in the outermost medium equals $\omega^2 \rho$ times 0.707 $|P|$.

2.5 COMPUTER PROGRAM

This subsection contains an annotated listing of CYLBAF, a program to calculate the response of a multilayer cylindrical baffle to normally incident waves. The program language employed is time sharing FORTRAN.

The principal function of the program is to find the coefficients in the scattered-wave expansion, equation (13). These coefficients form a one-dimensional array C02 in the program: one value for each azimuth harmonic used in the incident-wave expansion, equation (12). (The order of the harmonic is indicated by N in the program, instead of the symbol p used in the equations.)

To find the scattered-wave coefficient for any N, it is necessary to set up the matrix A showing the combined boundary conditions (18) for all the boundaries present. The structure of the matrix for a baffle of three layers is illustrated in figure 2-2. Each boundary is assigned a number (NCON in the program) of rows, involving the parameters of two adjacent zones. Blocks marked "I" involve the parameters of the zone on the inner side of the boundary, while blocks marked "II" involve the zone on the outer side. Each zone is assigned NCOE columns. Unmarked blocks are zero-filled.

For each marked block, sufficient Bessel functions are computed to allow the coefficients of equation (18) to be calculated. Then, depending on the type of boundary, the proper coefficient values are put into the matrix. When the entire matrix has been filled in this way, it is solved for the scattered-wave coefficient.

Finally, the coefficients are stored on a disc-file. Also, the pressure at various points of interest is calculated and stored on a separate file. Thus, immediate results are available, but also, the stored coefficients may be used to obtain further results at a later time.

ANNOTATED LISTING OF COMPUTER PROGRAM

```
*CYLBAF: PRØGRAM TØ CALCULATE RESPØNSE ØF MULTILAYER CYLINDRICAL
BAFFLE TØ NØRMALLY-INCIDENT PLANE WAVE. CAN HANDLE UP TØ 5 LAYERS.
     DIMENSIØN IDENT(4),TH(7),D(7),C(7),B(7),LA(7),MU(7),TMU(7),
& NCØE(7),NCØN(6),XSQ(6,2),X(6,2),YSQ(6,2),Y(6,2),BF(5,12,4),
& BV(2,3,4),BVC(3,4),A(23,24),CO2(50)
     REAL LA,MU
     CØMPLEX BVC,A,CO2,CO1
     EQUIVALENCE (BV,BVC)
*USE ØF BV FACILITATES HANDLING REAL AND IMAGINARY PARTS ØF BVC.
     CALL ØPENF(1,"CYLDAT")
*"CYLDAT" CØNTAINS PHYSICAL PARAMETERS DESCRIBING BAFFLE AND INCIDENT
WAVE. FIRST READ RUN IDENTIFICATIØN AND NUMBER ØF CØNSTANT-VELØCITY
ZØNES, INCLUDING CØRE AND EXTERNAL ZØNES.
     READ(1,500) IDENT,NZØN
 500FØRMAT(4A3,2XI1)
     NBDD= NZØN-1
*NBDD IS THE NUMBER ØF INTERZØNE BØUNDARIES. NEXT READ PARAMETERS
FØR EACH ZØNE: TH= LAYER THICKNESS (DUMMY VALUE REQUIRED FØR CØRE
AND EXTERNAL ZØNES), D= DENSITY, C= CØMPRESSIØNAL-WAVE SPEED,
B= RØTATIØNAL-WAVE SPEED.
     DØ 5 K=1,NZØN
     READ(1,) T1,T2,T3,T4
*FREE-FIELD FØRMAT
     TH(K)= T1
     D(K)= T2
     C(K)= T3
   5B(K)= T4
*READ ØUTER RADIUS ØF CYLINDER. READ INCIDENT-WAVE FREQUENCY AND
CØNVERT TØ RADIANS/SEC.
     READ(1,) R,T1
     ØMEGA= FP1(2*T1)
*FØR EACH ZØNE CØMPUTE LAME PARAMETERS LA AND MU, AND NCØE= NUMBER
ØF CØEFFICIENTS NEEDED. FØR EACH BØUNDARY CØMPUTE SPECIAL SYMBØLS
X AND Y, AND NCØN= NUMBER ØF ØONTINUITY CØNDITIØNS (EQS 18).
     T2= R
     NCØN(NBDD)= 1
     DØ 10 L=1,NZØN
     K= NZØN-L+1
     LA(K)= D(K)*C(K)**2 - TMU(K)= 2*MU(K)= D(K)*B(K)**2
     IF(L.EQ.1)GØTØ 10
     T1= ØMEGA*T2
     XSQ(K,2)= (X(K,2)= T1/C(K+1))**2
     YSQ(K,2)= (Y(K,2)= T1/B(K+1))**2
*SECØND SUBSCRIPT = 2 FØR ØUTER MEDIUM, = 1 FØR INNER
     XSQ(K,1)= (X(K,1)= T1/C(K))**2
           1)= (Y(K,1)= T1/B(K))**2
```

```
      NCØE(K)= 4
      IF(B(K).EQ.0.) NCØE(K)= 2
      NCØN(K)= NCØN(K) + NCØE(K)/2
*THIS IS INNER-MEDIUM CØNTRIBUTIØN TØ NCØN. NØW MAKE ØUTER-MEDIUM
CØNTRIBUTIØN FØR NEXT BØUNDARY, AND UPDATE RADIUS.
      IF(K.EQ.1)GØTØ 10
      NCØN(K-1)= NCØE(K)/2
      T2= T2-TH(K)
   10CØNTINUE
*ADJUST NCØE(1) FØR LACK ØF HANKEL FUNCTIØNS IN CØRE ZØNE.
      NCØE(1)= NCØE(1)/2
*FØR EACH ØRDER N, WILL NØW WRITE MATRIX A FØR CØNTINUITY CØNDITIØNS.
FIRST MAKE SURE UNSPECIFIED A-VALUES ARE ZERØ.
      DØ 12 I=1,23
      DØ 12 J=1,24
   12A(I,J)= 0
      CO1= 1
*CO1 IS CØEFFICIENT IN INCIDENT-WAVE EXPANSIØN (EQ 12).
      N= -1
   15N= N+1
      IBM= -1
      IO= JO= 1
*IO AND JO INDEX UPPER-LEFT ELEMENT ØF MATRIX BLØCK. II WILL INDEX
BØUNDARIES, JJ ZØNES.
      DØ 70 II=1,NBDD
      DØ 65 LL=1,2
*LL= 1 FØR INNER MEDIUM, = 2 FØR ØUTER MEDIUM.
      JJ= II+LL-1
      KK= 2*II+LL-2
*KK IS INDEX FØR BESSEL-FUNCTIØN VALUES.
      IF(N.GT.0)GØTØ 30
*FØR N=0 CØMPUTE BESSEL FUNCTIØNS ØF ØRDER -2 THRØUGH 2.
      DØ 20 K=3,5
      CALL BESS(BF(K,KK,1),BF(K,KK,2),K-3,X(II,LL))
   20CALL BESS(BF(K,KK,3),BF(K,KK,4),K-3,Y(II,LL))
      DØ 25 K=1,4
      BF(1,KK,K)= BF(5,KK,K)
   25BF(2,KK,K)= -BF(4,KK,K)
      GØTØ 40
*IF N>0, SHIFT ØVER ØLD BESSEL FUNCTIØN VALUES AND CØMPUTE NEW
FUNCTIØNS, ØF ØRDER N+2.
   30DØ 35 K=1,4
      DØ 35 L=1,4
   35BF(K,KK,L)= BF(K+1,KK,L)
      CALL BESS(BF(5,KK,1),BF(5,KK,2),N+2,X(II,LL))
      CALL BESS(BF(5,KK,3),BF(5,KK,4),N+2,Y(II,LL))
```

```
  40SIGN= 3-2*LL
*THIS IS THE CENTRAL (MINUS) SIGN IN EQS 19. NØW FØRM SIGNED J- AND
H-FUNCTIØNS, TØGETHER WITH FIRST AND SECØND DERIVITIVES, FRØM
THE J- AND Y- FUNCTIØN VALUES BF.
    DØ 50 K=2,4,2
    DØ 45 L=1,2
*HANKEL FUNCTIØNS FIRST.
    I= K+L-2
    BV(L,1,K)= SIGN*BF(3,KK,I)
    BV(L,2,K)= .5*SIGN*(BF(2,KK,I)-BF(4,KK,I))
  45BV(L,3,K)= .25*SIGN*(BF(1,KK,I)-2*BF(3,KK,I)+BF(5,KK,I))
*THEN J-FUNCTIØNS.
    DØ 50 J=1,3
  50BVC(J,K-1)= BV(1,J,K)
*NØW FILL IN A MATRIX BLØCK. IBM= 1 FØR II= LL= 1, WHEN H-FUNCTIØNS
FØRBIDDEN. AFTER THAT IBM STAYS = 2.
    IBM= (IBM+3)/2
    DØ 55 IB=1,IBM
*IB= 1 FØR J-FUNCTIØN CØEFFICIENT, = 2 FØR H-FUNCTIØN CØEFFICIENT.
    J= J0+IB-1
*CØMPRESSIØNAL-WAVE CØEFFICIENTS, EQS 18.1 AND 18.3:
    A(I0,J)= X(II,LL)*BVC(2,IB)
    A(I0+1,J)= XSQ(II,LL)*(TMU(JJ)*BVC(3,IB)-LA(JJ)*BVC(1,IB))
    IF(NCØN(II).EQ.2)GØTØ55
*CØMPRESSIØNAL-WAVE CØEFFICIENTS, EQ 18.4:
    A(I0+2,J)= TMU(JJ)*N*(X(II,LL)*BVC(2,IB)-BVC(1,IB))
    IF(NCØN(II).EQ.3)GØTØ 55
*CØMPRESSIØNAL-WAVE CØEFFICIENTS, EQ 18.2:
    A(I0+3,J)= N*BVC(1,IB)
  55CØNTINUE
    IF(B(JJ).EQ.0)GØTØ 65
*NØW RØTATIØNAL-WAVE CØEFFICIENTS, IF ANY.
    DØ 60 IB=1,IBM
    J= J0+IB-1+IBM
*EQS 18.1 AND 18.3:
    A(I0,J)= N*BVC(1,IB+2)
    A(I0+1,J)= TMU(JJ)*N*(Y(II,LL)*BVC(2,IB+2)-BVC(1,IB+2))
    IF(NCØN(II).EQ.2)GØTØ 60
*EQ 18.4:
    A(I0+2,J)= YSQ(II,LL)*(TMU(JJ)*BVC(3,IB+2)+MU(JJ)*BVC(1,IB+2))
    IF(NCØN(II).EQ.3)GØTØ 60
*EQ 18.2:
    A(I0+3,J)= Y(II,LL)*BVC(2,IB+2)
  60CØNTINUE
*UPDATE J0 IN PASSING FRØM INNER TØ ØUTER MEDIUM.
  65J0= J0 + (2-LL)*NCØE(II)
  70I0= I0 + NCØN(II)
```

```
*ALL MATRIX ENTRIES HAVE BEEN CØMPUTED. INTERCHANGE LAST TWØ
CØLUMNS ØF A, AND MULTIPLY (NEW) LAST CØLUMN BY -CO1.
     KK= IO-NCØN(NBDD)
     LL= IO-1
     DØ 75 I=KK,LL
     Ø1= A(I,JO-1)
     A(I,JO-1)= -CO1*A(I,JO-2)
   75A(I,JO-2)= Ø1
*NØW SØLVE MATRIX FØR SCATTERED-WAVE CØEFFICIENT CO2 (EQ 13).
     CALL SØLV(A,IO-1,CO2(N+1))
*UPDATE CO1 AND TEST FØR EXHAUSTIØN ØF INCIDENT-WAVE EXPANSIØN.
     IF(N.GT.0)GØTØ 80
     CO1= 2
   80CO1= CO1*CMPLX(0.,-1.)
     IF(ABS(BF(3,2*NBDD,1))+ABS(BF(4,2*NBDD,1))+ABS(BF(5,2*NBDD,1))
&.GT.1E-5)GØTØ 15
*CALCULATIØN ØF SCATTERED-WAVE CØEFFICIENTS CØMPLETE. STØRE THEM
FØR FUTURE USE.
     CALL ØPENF(2,"CYLCØE")
     I= N+1
     WRITE(2,505) IDENT,I
  505FØRMAT(4A3,":",I4,"  CØEFFICIENTS")
     DØ 85 J=1,I
     Ø1= CO2(J)
   85WRITE(2,510) Ø1
  510FØRMAT(2E17.10)
*IF IMMEDIATE PRESSURE READINGS ARE DESIRED, TAKE LØCATIØNS FØR
READINGS FRØM "CYLLØC" AND PUT VALUES INTØ "CYLVAL".
     CALL ØPENF(3,"CYLLØC")
     CALL ØPENF(4,"CYLVAL")
     FACTØR= SQRT(.5)*D(NZØN)*ØMEGA**2
     WRITE(4,515) IDENT
  515FØRMAT("VALUES FØR ",4A3)
   90READ(3,,END=999) GAP,ANGLE
     T1= (R+GAP)*ØMEGA/C(NZØN)
     T2= FPI(ANGLE/180)
     T3= -T1*CØS(T2)
*INCIDENT-WAVE PØTENTIAL:
     Ø1= CMPLX(CØS(T3),SIN(T3))
*ADD TERMS ØF SCATTERED-WAVE PØTENTIAL TØ GET TØTAL PØTENTIAL.
     DØ 95 J=0,N
     CALL BESS(T3,T4,J,T1)
   95Ø1= Ø1 + CO2(J+1)*CMPLX(T3,T4)*CØS(J*T2)
*CØMPUTE AND STØRE PRESSURE VALUE.
     T1= FACTØR*CABS(Ø1)
     WRITE(4,520) GAP,ANGLE,T1
  520FØRMAT(F7.2,F6.0,E14.6)
*GØ BACK AND READ NEXT LØCATIØN.
     GØTØ 90

*DESCRIPTIØN ØF SUBRØUTINES:
SUBRØUTINE BESS(B1,B2,K,X) CØMPUTES BESSEL FUNCTIØN B1 ØF FIRST KIND
AND B2 ØF SECØND KIND FØR ARGUMENT X AND ØRDER K.
SUBRØUTINE SØLV(A,K,X) TAKES THE FIRST K RØWS AND K+1 CØLUMNS ØF A
AND APPLIES RØW ØPERATIØNS TØ MAKE A(I,J)=0 FØR I>J AND A(I,I)=1.
THEN X= A(K,K+1).
  999END
```

2.6 CORRELATION WITH EXPERIMENTAL DATA

Figure 2-3 shows a comparison between the computer program prediction and experimental results on a two-layer cylindrical baffle consisting of 5/8-inch thick steel and 1/2-inch thick RAL. Good agreement exists between 2 and 8 kHz; below 2 kHz, the theory deviates from the experimental results but this is believed due to limitations in certain subroutines of the program which will be improved in the future.

Figures 2-4 and 2-5 show the predicted and experimental azimuthal responses of a hydrophone in front of the same baffle as in figure 2-3 for frequencies of 2500 Hz and 4500 Hz, respectively. The correlation is excellent. Additional comparisons of this type are necessary, however, before a proper evaluation of the program can be made.

2.7 SYMBOLS

$\underline{a}$	Unit vector normal to a surface
b	Bearing coordinate in polar system r, b, z
B, B_p	Function of b only
c_p	Coefficient in scattered-wave expansion
C_{11}, C_{12}, C_{21}, C_{22}	Coefficients in expansion of F and G (equation 15)
F	Choice of R_p for compressional waves
G	Choice of Rp for rotational waves
$H_p = H_p^{(1)}$	Hankel function of order p
J_p	Bessel function of first kind and order p
k	Bulk modulus
λ, μ	Lame elastic constants
m	Rotational wave number
n	Compressional wave number
ω	Angular frequency of sound wave
P	Compressional-wave potential
P_{01}, P_{02}	Incident and scattered wave potentials
$\underline{Q}$	Vector potential for rotational waves
r	Range coordinate in polar system r, b, z
$\hat{\underline{r}}$	Unit vector in range direction
R, R_p	Function of r only
ρ	Density

S	Scalar potential for rotational waves
t	Time
$\underline{t}$	Stress vector
t_r, t_b	Stress components in radial and tangential directions
T_{rp}, T_{bp}	Fourier coefficients of t_r and t_b
$\underline{u}$	Displacement vector
u_r, u_b	Displacement components in radial and tangential directions
U_{rp}, U_{bp}	Fourier coefficients of u_r and u_b
$x = nr$	
$y = mr$	
Z	Axial coordinate in polar system r, b, z
$\underline{\hat{Z}}$	Unit vector in axial direction

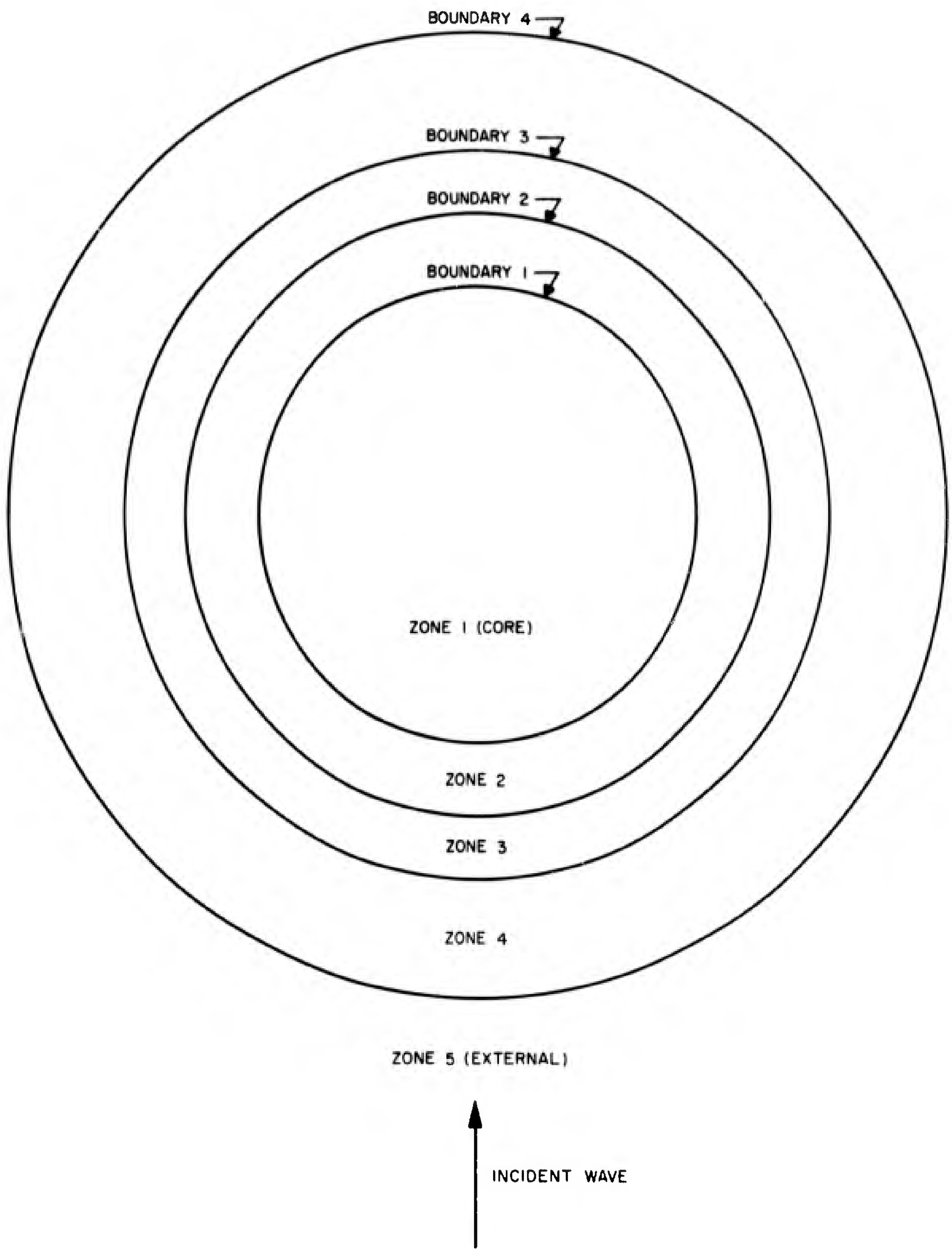

Figure 2-1. Structure of Three-Layer Cylindrical Baffle

	ZONE 1	ZONE 2	ZONE 3	ZONE 4	ZONE 5
BOUNDARY 1	I	II			
BOUNDARY 2		I	II		
BOUNDARY 3			I	II	
BOUNDARY 4				I	II

Figure 2-2. Structure of Boundary Condition Matrix for a Three-Layer Baffle

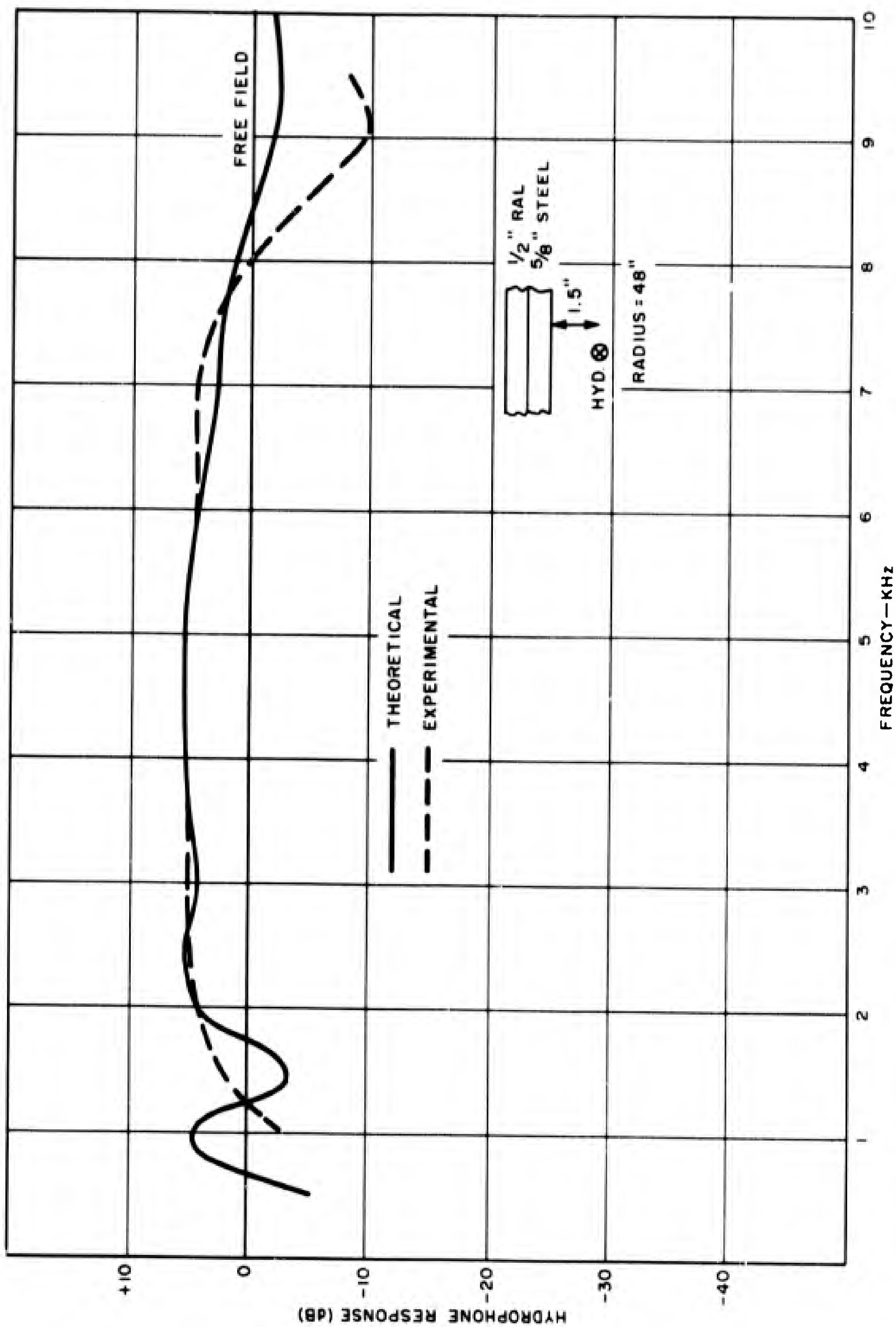

Figure 2-3. Comparison of Predicted and Experimental Results of Two-Layer Cylindrical Baffle

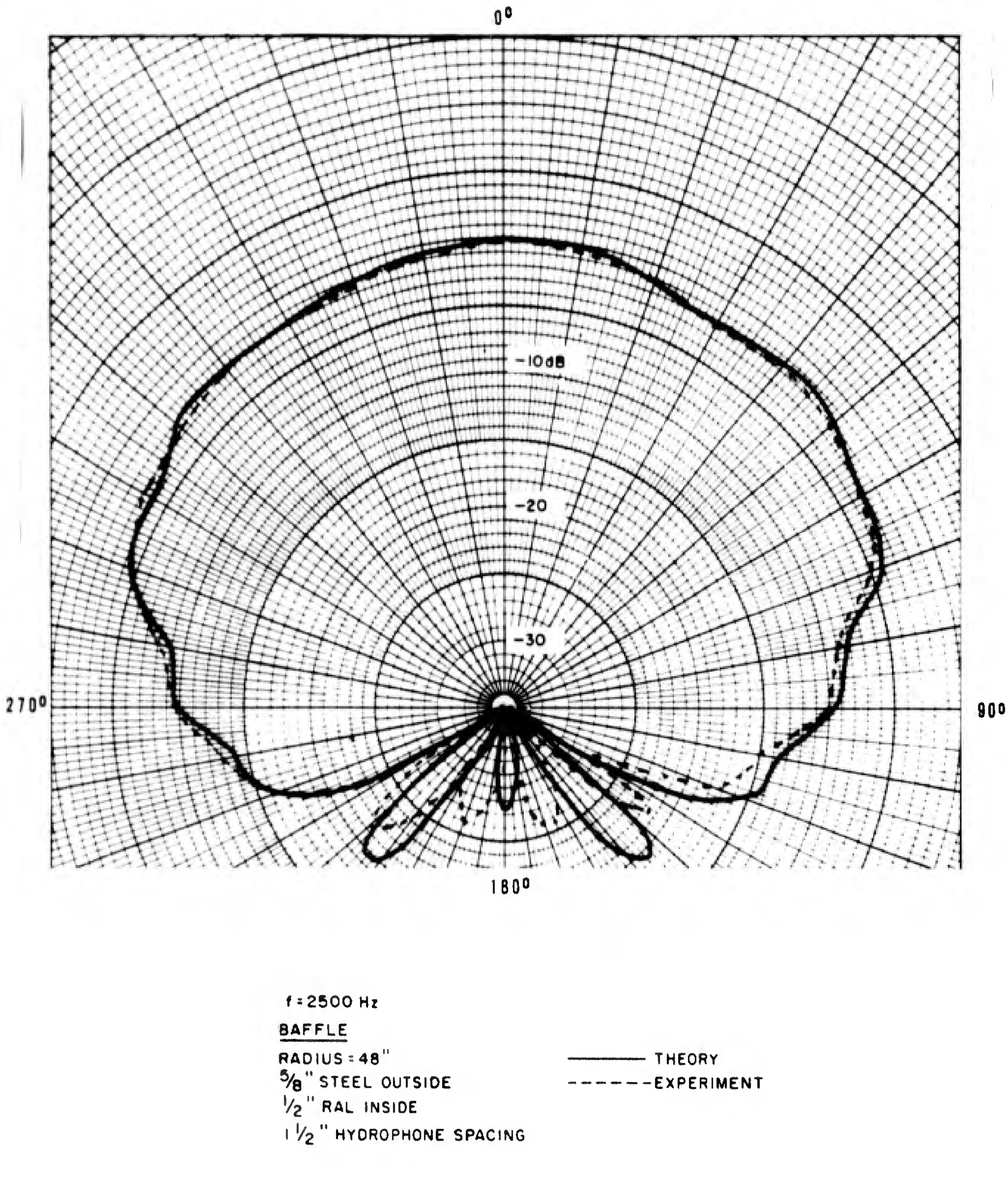

Figure 2-4. Predicted and Experimental Hydrophone/Baffle Azimuthal Response at 2500 Hz

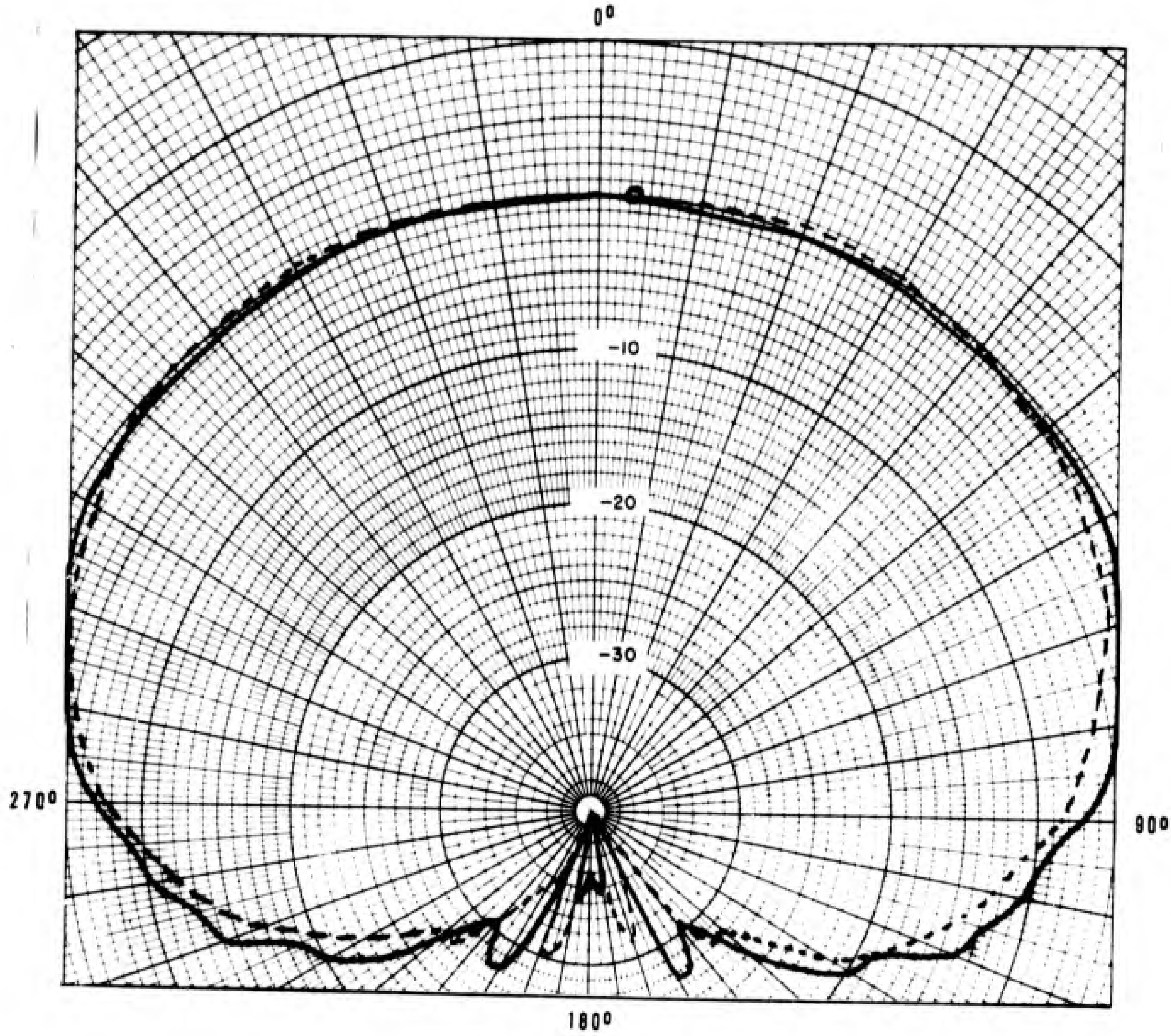

f = 4500 Hz

BAFFLE

RADIUS = 48"

5/8" STEEL OUTSIDE

1/2" RAL INSIDE

1 1/2" HYDROPHONE SPACING

——— THEORY

- - - - - EXPERIMENT

Figure 2-5. Predicted and Experimental Hydrophone/Baffle Azimuthal Response at 4500 Hz

SECTION 3

SPRING-MASS BAFFLES

3.1 INTRODUCTION

An efficient approach to preventing transfer of acoustic energy from one point in water to another point is to use a layer of material which is more compliant than water. Air is an excellent material for this purpose, as shown in figure 3-1, where the insertion loss as a function of frequency for various air thicknesses is plotted. The curve shows maximum insertion loss at $\lambda/4$, while complete transmission corresponds to multiples of a half wavelength of thickness.

The response of a hydrophone in front of this compliant layer must also be considered. Figure 3-2 shows the response of a hydrophone 1.5-inches in front of an air layer. A severe loss in response, compared to free field, occurs in the important frequency band of 1 to 3 kHz due to the 180 degree phase shift when sound is reflected from the compliant layer. One solution to this problem is to place a stiff material, such as steel, between the baffle and the hydrophone. When steel is used alone, as shown in figure 3-3, the hydrophone response improves considerably. However, the insertion loss of steel alone is low, as shown in figure 3-4. The combination of compliant baffle and the steel has only a small affect on the response as shown in figure 3-5, while still providing a high insertion loss.

In practice, an air layer by itself cannot be used as an acoustic baffle for sonar applications because of the pressure requirements. On a submarine the air layer would compress at a moderate depth and would then be useless. It is possible to build a pressure-compensated air baffle in which an arragement is made to keep the air inside at the same pressure as the water outside; however, such designs are usually complex and unreliable. The goal is to build a baffle which is statically stiff so that it can withstand the hydrostatic pressure and yet dynamically soft so that it provides the required insertion loss.

A promising approach is through the use of spring-mass baffles which consist of a sealed assembly of plates simulating springs with the outside plates behaving as masses. This section reviews spring-mass baffle design parameters and presents the results of experimental investigations utilizing full scale baffle samples.

3.2 TRANSMISSION LOSS COMPUTATION

The configuration of an uncompensated spring-mass baffle developed by Sperry is shown in figure 3-6. The assembly utilizes two hardened steel inner plates in a diaphragm mode as springs to provide high compliance. A matrix of steel pins, located on each side of the two inner plates in a staggered orientation, transforms water pressure loads from the outer plates into concentrated loads on the inner plates. This arrangement produces diaphragm-type inner plate deflections in the form of contiguous circles in each inner plate. Each circle is the result of the load from a pin on one side of one of these plates being resisted by the pins on the opposite side of the same plate. The pins, held in place by square rubber pads, fit tightly into undersized holes in the pads, which are cemented to the steel plates. The top outer plate is supported from the bottom outer plate by a perimeter rubber gasket cemented to these plates.

Under increasing static pressure, the inner and outer plates deflect; the outer plate deflections are at least an order of magnitude smaller than the inner plate deflections, both because the outer plates receive a distributed pressure load as compared to the concentrated loads from the pins on the inner plates, and because the outer plates are 1/4-inch thick as compared to the 1/8-inch thick inner plates.

The lumped-parameter model of the spring-mass baffle is shown in figure 3-7(a). In this figure, the transmitted pressure is denoted by P_T and the total pressure at the incident face is denoted by P_O. The total pressure is composed of the incident pressure P_I and the reflected puressure P_R; as follows:

$$P_O = P_I + P_R$$

All pressures and velocities are assumed to have a complex exponential time dependence. Thus, for example, the actual physical incident-wave pressure is the real part of $P_I e^{-i\omega t}$, where ω is the angular frequency of the incident wave.

Let v_1, v_2, and v_3 denote the velocities of the left-hand, center and right-hand masses in figure 3-7(a). The equations of motion are

$$-i\omega M v_1 = P_O + iK(v_2 - v_1)/\omega$$

$$-i\omega m v_2 = iK(v_1 - 2v_2 + v_3)/\omega$$

$$-i\omega M v_3 = iK(v_2 - v_3)/\omega - P_T$$

where M and m are the masses per unit area of the outer and inner plates, respectively, and K is the slope of the baffle pressure/displacement curve. By interpreting pressure as voltage and velocity as current, the equations of motion may be viewed as describing an electrical circuit equivalent in behavior to the mechanical system.

The equivalent circuit for the baffle model is shown in figure 3-7(b). The impedances are given by

$$Z_M = -j\omega M$$

$$Z_m = -j\omega m$$

$$Z_K = jK/\omega$$

The effect of damping in the springs and rubber pads of the baffle may be recognized by using complex values of K, or more explicitly, by

$$Z_K = L + jK/\omega$$

where L is the effective viscosity of the spring/pad combination.

By converting the interior π-section of figure 3-7(b) into an equivalent T-section, the equivalent circuit for the baffle is converted into the form shown in figure 3-8(a), where

$$Z_A = Z_M + Z_m Z_K/(Z_m + 2 Z_K)$$

$$Z_B = (Z_K)^2/(Z_m + 2 Z_K)$$

When the baffle is immersed in water and subjected to an incident wave of pressure P_I, the pressure/velocity relations for plane progressive waves incident upon and/or radiated from the baffle surfaces must be included. At the right-hand surface pure radiation exists, for which

$$P = P_T e^{i\omega x/c}$$

where c is the speed of sound in water and x is measured from the right-hand surface.

At the left-hand surface, both incident and reflected waves exist, so that

$$P = P_I e^{i\omega x/c} + P_R e^{-i\omega x/c}$$

where x is measured from the left-hand surface.

A water particle is subject to the general law of motion

$$\partial P/\partial x = -\rho\, \partial v/\partial t$$

which implies that $P = \rho cv$ for waves moving to the right and $P = -\rho cv$ for waves moving to the left. The quantity ρc is the characteristic impedance of water. Hence, P_T may be eliminated from the equations of motion by the substitution

$$P_T = \rho c v_3 \tag{20}$$

On the left-hand surface, the following exists

$$\rho cv = P_I e^{i\omega x/c} - P_R e^{-i\omega x/c}$$

so that by setting x = o in the equations for the left-hand surface, the following is obtained:

$$P_o = P_I + P_R$$

$$\rho cv_1 = P_I - P_R$$

from which is obtained

$$P_o = 2P_I - \rho cv_1 \tag{21}$$

Adjoining (20) and (21) to the equations of motion shows that the operation is equivalent to the circuit shown in figure 3-8(b), where Z_C is the characteristic impedance of water.

Simple circuit-analysis techniques show that the transmission loss is given by

$$TL = 20 \log |P_I/P_T|$$

where

$$P_I/P_T = (Z_A + Z_C)(Z_A + 2 Z_B + Z_C)/(2 Z_B Z_C)$$

Once appropriate values of M, m, K and L have been chosen, computer program BAF, which is listed on the following pages, plots TL against frequency.

For the Sperry baffle, M and m are 0.00022 and 0.000072 mass units/in^2, respectively. K varies from 100 lb/in^3 at shallow depths to about 3000 lb/in^3 at 700 feet, while L lies in the range 0.2 to 0.4 lb-sec/in^3. Figure 3-9 (Sheets 1 through 3) show TL versus frequency for a number of spring constants and damping values (AØM = M, AIM = m, AK = K, AL = L).

Experimental data on a spring-mass type of baffle has shown good agreement with the theoretical calculations over the low frequency band (approximately 0.5 to 3 kHz). At higher frequencies, the theory predicts larger transmission loss than measured. Also, the measurements show a peak and a null in the transmission loss curve which is an indication that the baffle thickness becomes equivalent to one-quarter and one-half wavelength at certain frequencies. When this occurs, a distributed parameter model is required. The spring-mass type of baffle becomes an appreciable part of a wavelength at even relatively low frequencies because the speed of sound through such a baffle is much lower than that through water. Experimental measurements indicate the velocity through the baffle is only one-sixth that of water.

LISTING OF COMPUTER PROGRAM TO COMPUTE TRANSMISSION LOSS OF SPRING-MASS BAFFLES

```
      PRØGRAM BAF(INPUT,ØUTPUT,TAPE1,TAPE6)
      DIMENSIØN DB(70),FMTS(8,2),FØRM(5),LINE(72),F(3,2)
      DATA PI,RC/3.14159,5.84/
      CØMPLEX Z1,Z2,Z3
      PRINT, *WHAT MODE, MATE*,
      READ, MØDE
      DATA F/1000.,200.,10000.,5.,5.,200./
      REWIND 1  $  REWIND 6
      WRITE(6,500)
  500FØRMAT(4H----)
   10READ(1,510) AØM,AIM,NUMKL  $  IF(EØF,1) 110,15
  510FØRMAT(4X2F10/4XI5)
   15DØ 100 KL=1,NUMKL
      READ(1,520) AK,AL
  520FØRMAT(4X2F10)
      I= 1  $  FREQ= F(1,MØDE)
   20T1= 2.*PI*FREQ
      Z1= CMPLX(0.,-T1*AIM)
      Z2= CMPLX(AL,AK/T1)
      Z3= Z2/(Z1+Z2+Z2)
      Z1= CMPLX(0.,-T1*AØM)+Z1*Z3
      Z2= Z2*Z3
      GØTØ(30,40) MØDE
   30Z1= Z1+RC
      DB(I)= -1000.+AINT(1000.5+20.*ALØG10(CABS(Z1*(Z1+Z2+Z2)
+     /(2.*RC*Z2))))
      GØTØ 50
   40DB(I)= -1000.+AINT(1000.5+20.*ALØG10(CABS(Z2/(Z1+Z2))))
   50I= I+1  $  FREQ= FREQ+F(2,MØDE)
      IF(FREQ.LT.F(3,MØDE)+.5*F(2,MØDE)) GØTØ 20
*WRITE PLØT HEADING
      DATA FMTS/
+     50H(////5X30HTRANSMISSION LØSS VS FREQUENCY          ),
+     30H(/4H(DB),I3,9I5,7H  (KHZ)     ),
+     50H(////5X26HVELØCITY GAIN VS FREQUENCY              ),
+     30H(/4H(DB),I3,8I5,6H  (HZ)      )/
      ENCØDE(50,600,FØRM) (FMTS(I,MØDE),I=1,5)
  600FØRMAT(5A10)
      WRITE(6,FØRM)
      WRITE(6,610) AØM,AIM,AK,AL
  610FØRMAT(/7X,4HAØM=,F8.6,7H   AIM=,F8.6,/7X4HAK =,
+     F7.0,8H    AL =,F7.2)
      ENCØDE(30,600,FØRM) (FMTS(I,MØDE),I=6,8)
      I= 2-MØDE  $  J= 190*MØDE-180  $  K= 24*MØDE-23
      WRITE(6,FØRM) (L,L=I,J,K)
```

```
*FIND DB RANGE
      DBMAX= DB(1)  $  DBMIN= DB(1)
      I= 1.5 + (F(3,MØDE)-F(1,MØDE))/F(2,MØDE)
      DØ 60 J=2,I
      DBMAX= AMAX1(DBMAX,DB(J))
   60DBMIN= AMIN1(DBMIN,DB(J))
*PLØT
      T1= DBMAX
   70LINE(1)= 6H
      IF(AMØD(T1,5.).NE.0.) GØTØ 80
      ENCØDE(5,620,LINE) T1
  620FØRMAT(F5.0)
   80DØ 90 J=1,I
      LINE(J+1)= 1H
      IF(AMØD(T1,5.)*MØD(J+MØDE-2,5).EQ.0.) LINE(J+1)= 1H.
   90IF(T1.EQ.DB(J)) LINE(J+1)= 1H*
      WRITE(6,640) LINE(1),(LINE(L+1),L=1,I)
  640FØRMAT(A6,71A1)
      T1= T1-1.
      IF(T1.GE.DBMIN) GØTØ 70
  100CØNTINUE
      GØTØ 10
  110WRITE(6,650)
  650FØRMAT(////4H----)
      ENDFILE 6  $  REWIND 6
      END
```

3.3 EXPERIMENTAL DATA

Data obtained from tests of a spring-mass baffle and associated hydrophone array are presented in this section. The array tested consisted of a 6 by 6 ft, 1-1/2-inch thick, steel plate in which the hydrophones were mounted, a 1-1/2-inch thick rubber sheet bonded to the front of the plate, and the spring-mass baffles placed behind the hydrophones. The test array contained 23 hydrophones located on the steel plate as shown in figure 3-10.

The following tests were performed:

- Single element receiving response
- Single element directivity patterns
- Sum-difference patterns
- Steered beams.

Test were conducted at depths of 100, 400, and 700 feet. Of the large number of test runs made, some representative samples showing the baffle performance have been selected. Figures 3-11 through 3-16 show the single element directivity patterns of hydrophones 1 through 6 (see figure 3-10), which are located across the array, at 2.5 kHz. It is interesting to observe how the patterns for hydrophones near the center of the array (3 and 4) are symmetrical while those at the edges (1 and 6) show a definite filling in of the pattern. This can be explained by noting that the hydrophones mounted near the array edge do not get the full effect of the baffle. These patterns were taken at a depth of 400 feet and show a front-to-back ratio of 15 to 20 dB.

Figures 3-17 through 3-19 show broadside beam patterns formed by summing the outputs of hydrophones 1 through 6 at 1, 2.5, and 3.5 kHz. The theoretical beam patterns are superimposed on the measured data. Agreement between theory and experiment is excellent in the forward-looking direction. The presence of the baffle reduces the rear response by a factor of better than 20 dB. Depth for these tests was 100 feet.

Figures 3-20 through 3-24 show steered beam patterns at 30 degrees and 45 degrees with and without shading. Hydrophones 1 through 6 were steered using delay lines; shading was added by switching in resisitive attenuators; depth was 700 feet. Theoretical patterns, calculated assuming free field hydrophones, are also shown. Agreement is good for the forward looking direction. For the broadside beams, the baffle attenuates the second main beam by more than 20 dB.

The results of these tests indicate that the spring-mass baffle is capable of effective performance over a wide range of frequencies and hydrostatic pressures. These baffles require no external pressure compensation and can be designed to be relatively light and thin. The baffles are highly compliant, thus providing large transmission loss values.

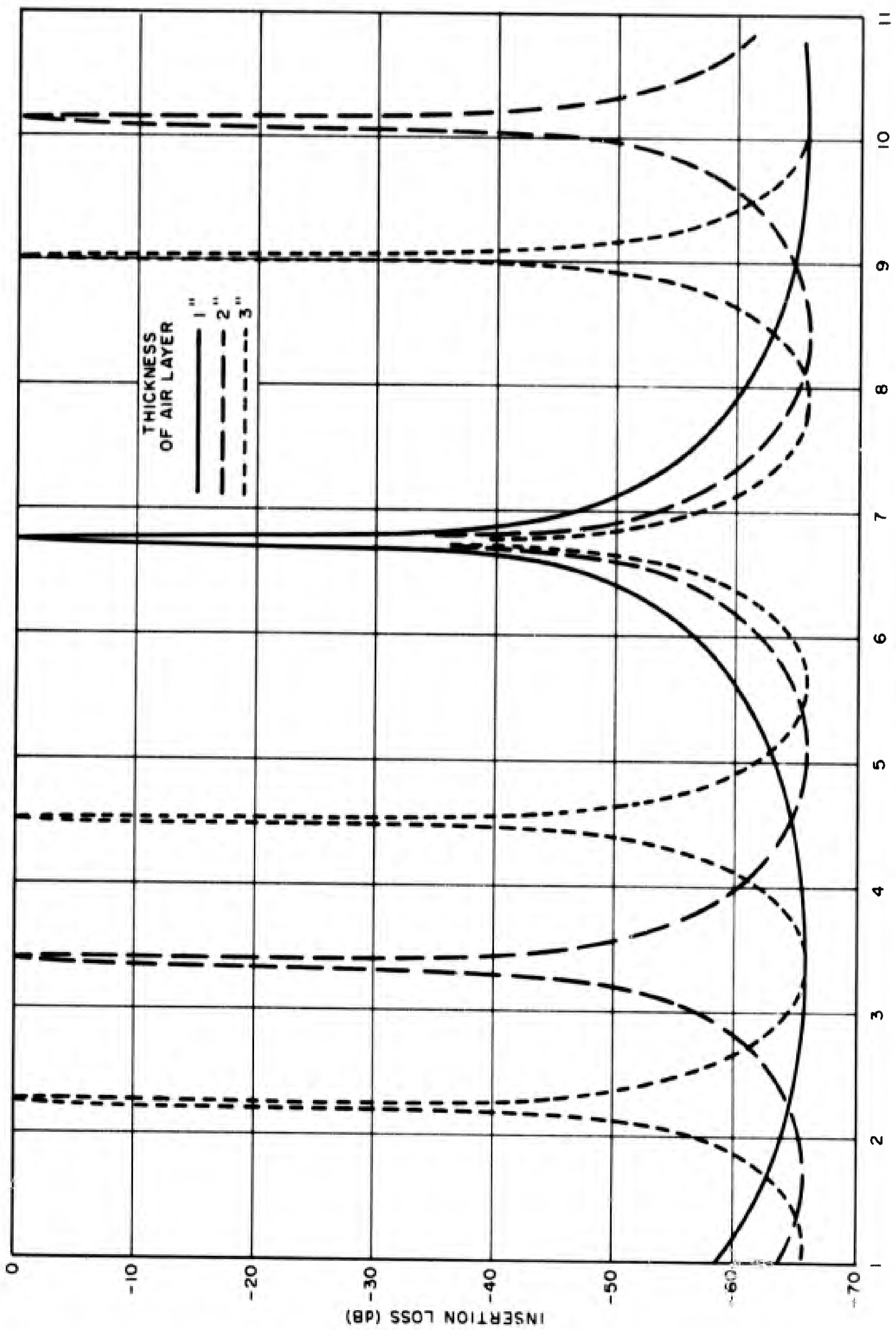

Figure 3-1. Insertion Loss Versus Frequency for Various Air Layer Thicknesses

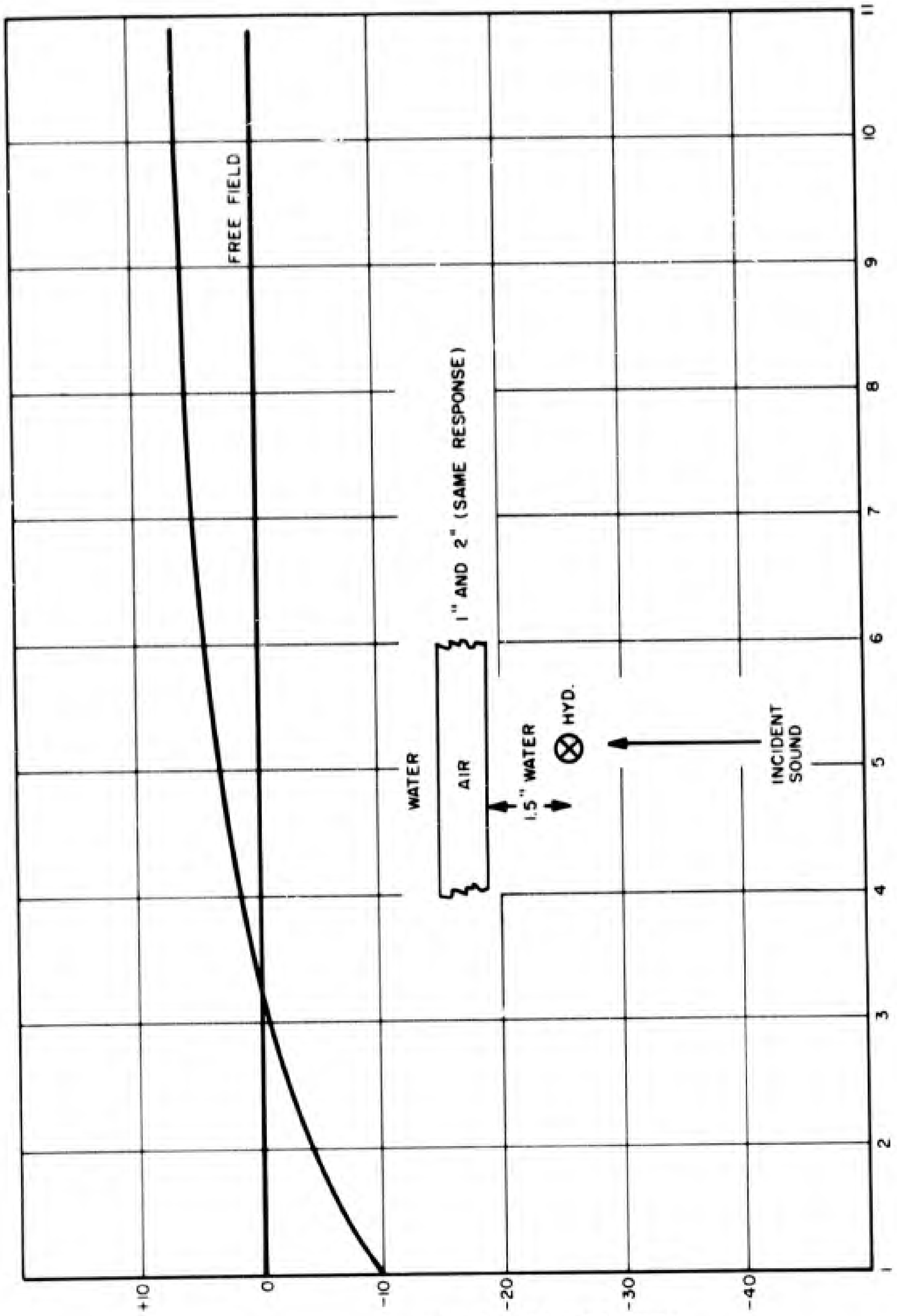

Figure 3-2. Response of a Hydrophone 1.5 Inches in Front of an Air Layer

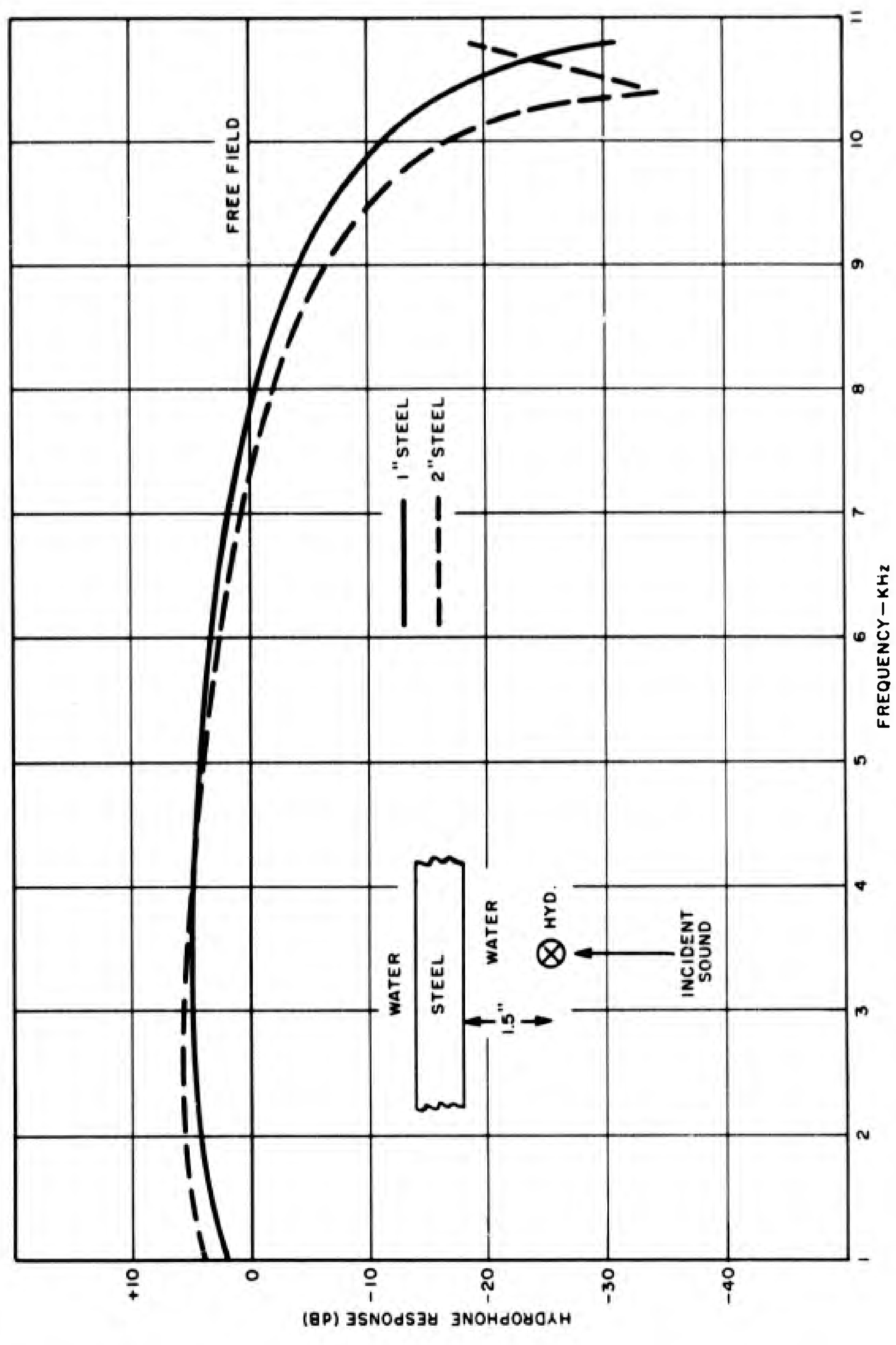

Figure 3-3. Response of a Hydrophone 1.5 Inches in Front of a Steel Layer

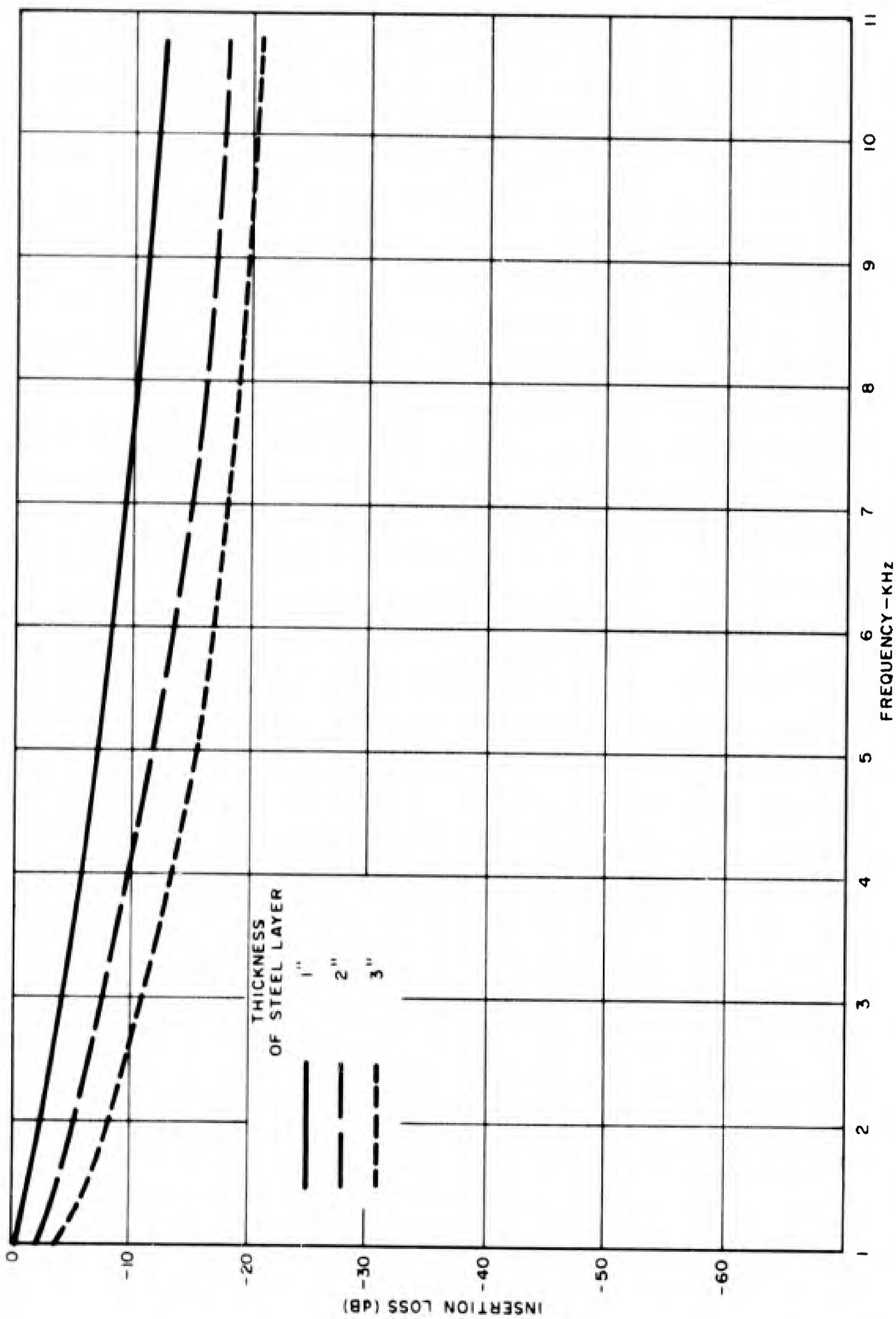

Figure 3-4. Insertion Loss Versus Frequency of Various Steel Layer Thicknesses

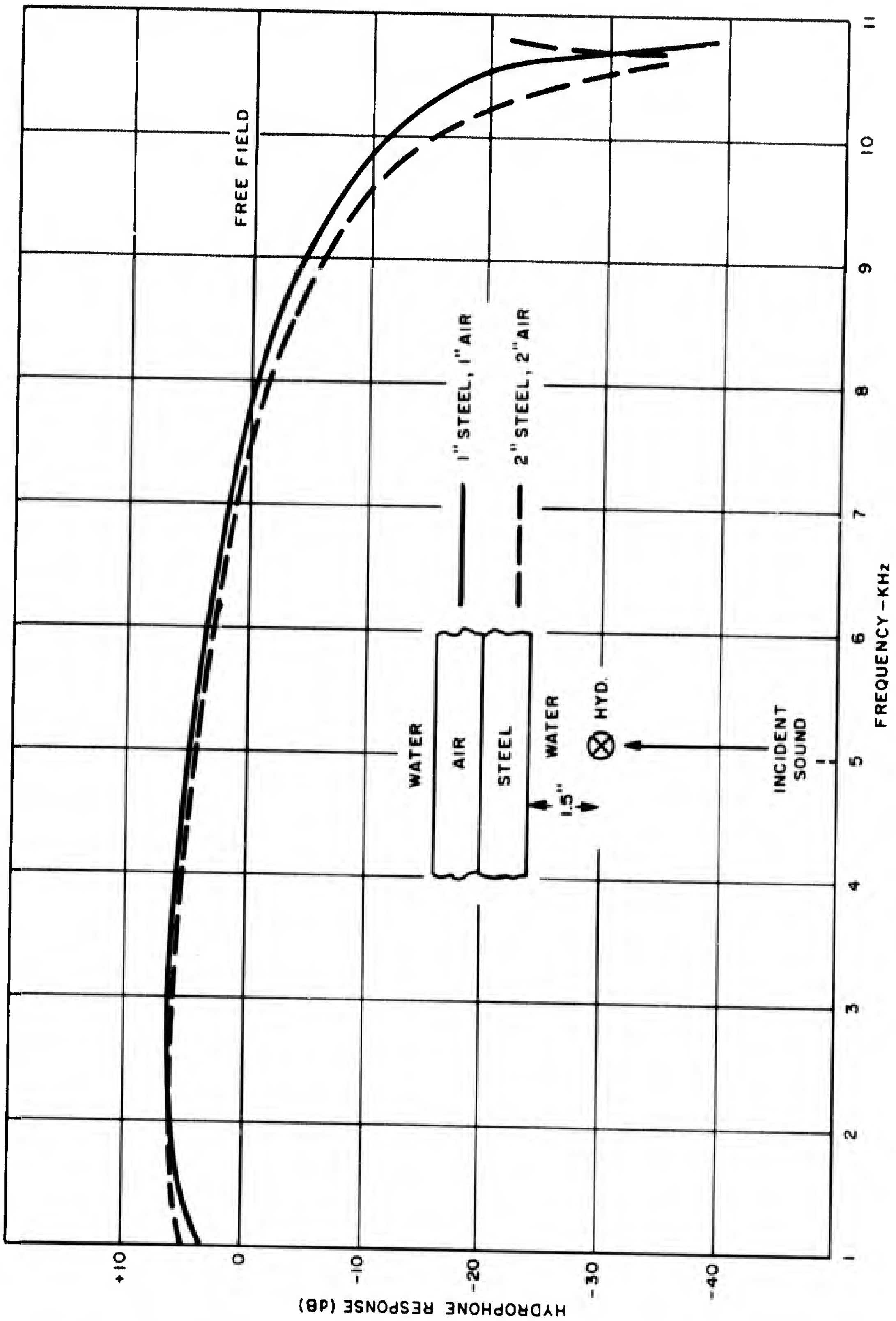

Figure 3-5. Response of a Hydrophone 1.5 Inches in Front of a Combined Air/Steel Baffle

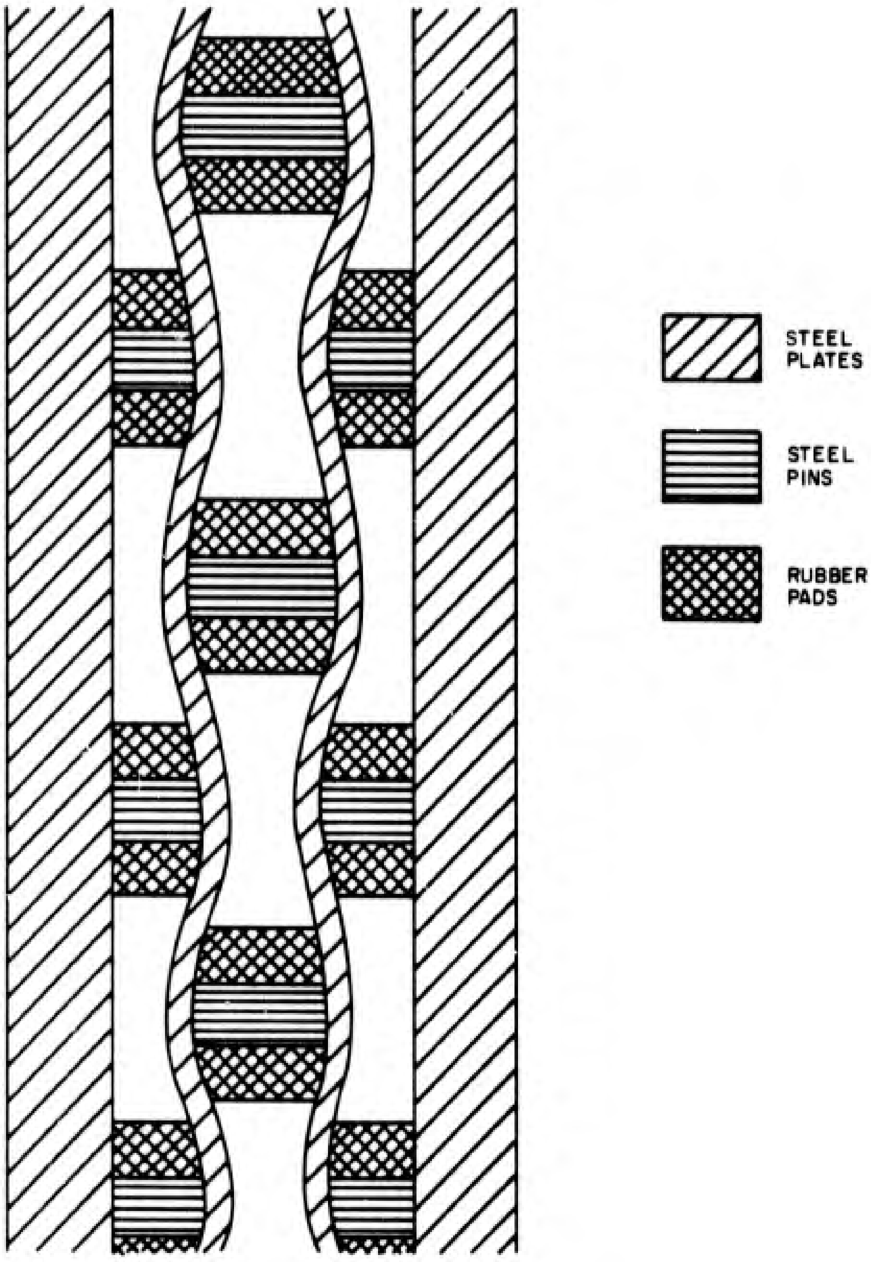

Figure 3-6. Spring-Mass Baffle Configuration Under Hydrostatic Pressure

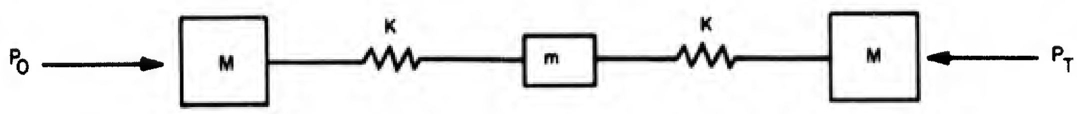

(a) Lumped-Parameter Model of Baffle

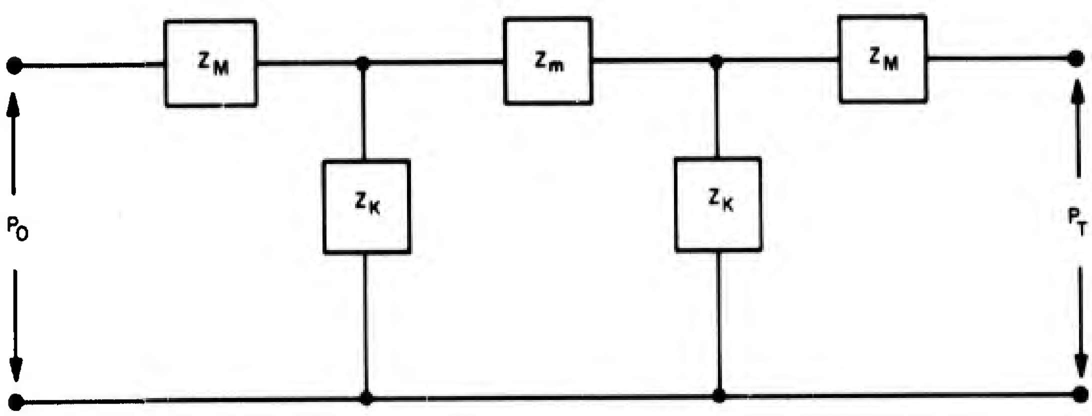

(b) Equivalent Circuit of Baffle

Figure 3-7. Lumped Parameter Model and Equivalent Circuit of Spring-Mass Baffle

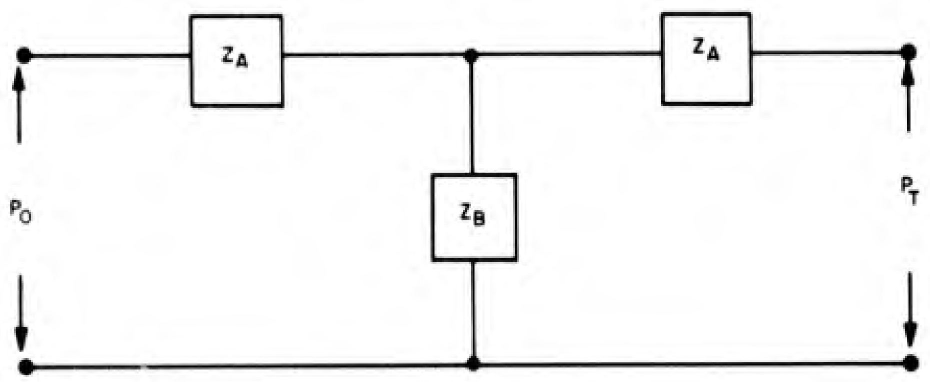

(a) Equivalent T Circuit for Baffle

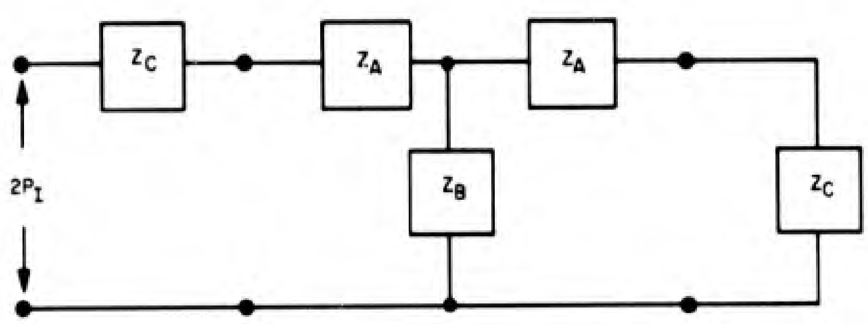

(b) Baffle Circuit in Operation

Figure 3-8. Converted Equivalent Circuit for Spring-Mass Baffle

TRANSMISSIØN LØSS VS FREQUENCY

AØM= .000220 AIM= .000072
AK = 200 AL = .20

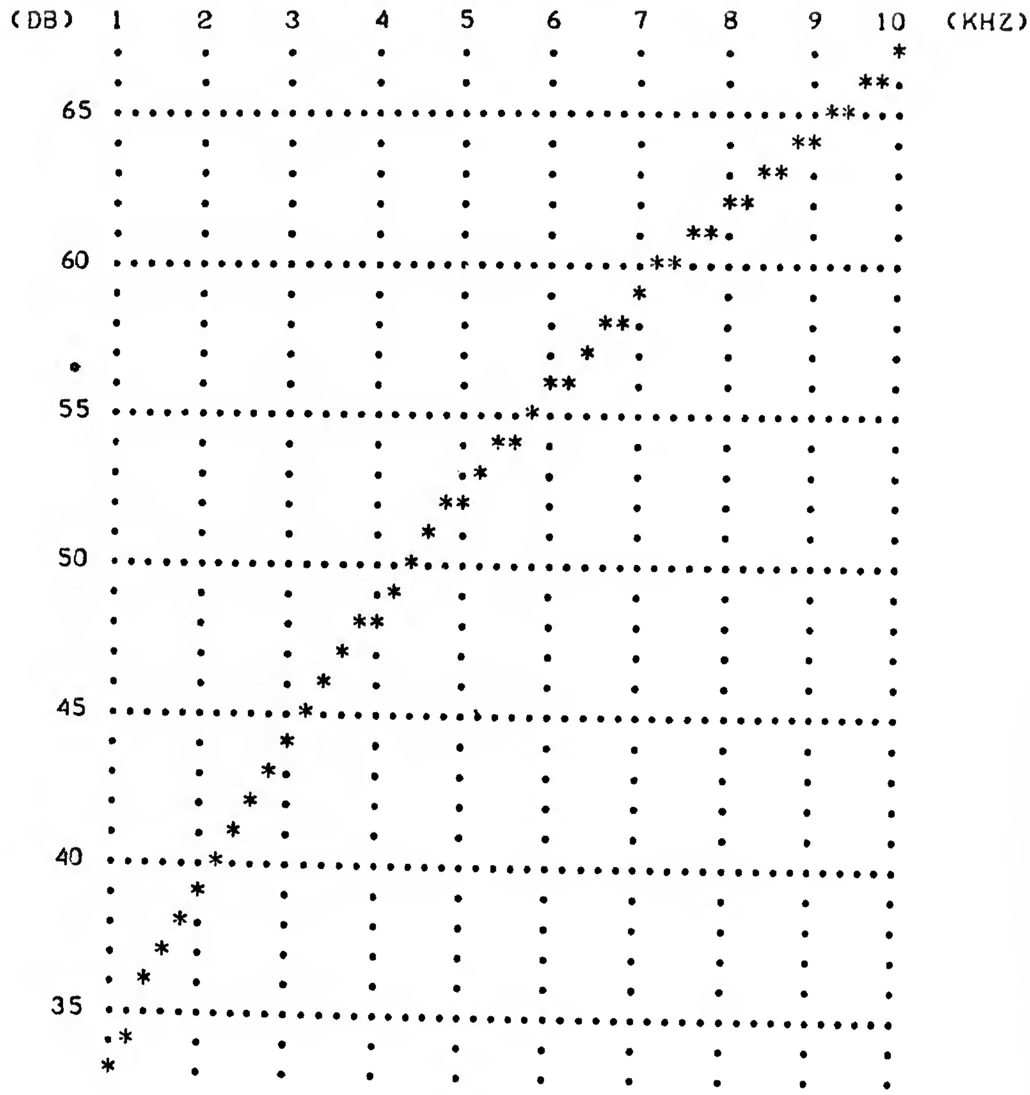

3-16a

TRANSMISSION LØSS VS FREQUENCY

AØM= .000220 AIM= .000072
AK = 600 AL = .20

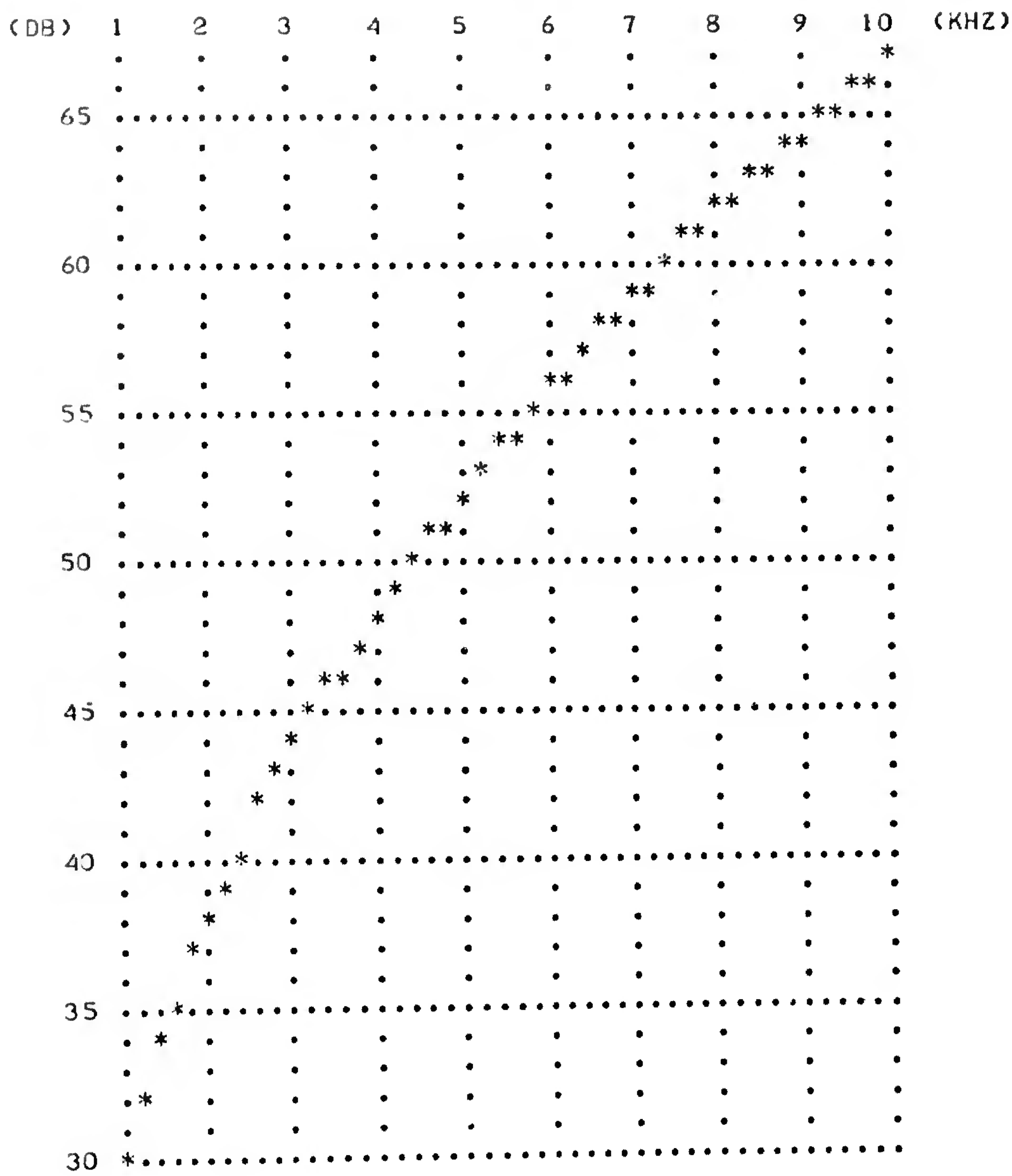

3-16-h

TRANSMISSIØN LØSS VS FREQUENCY

AØM= .000220   AIM= .000072
AK =   1000   AL =   .20

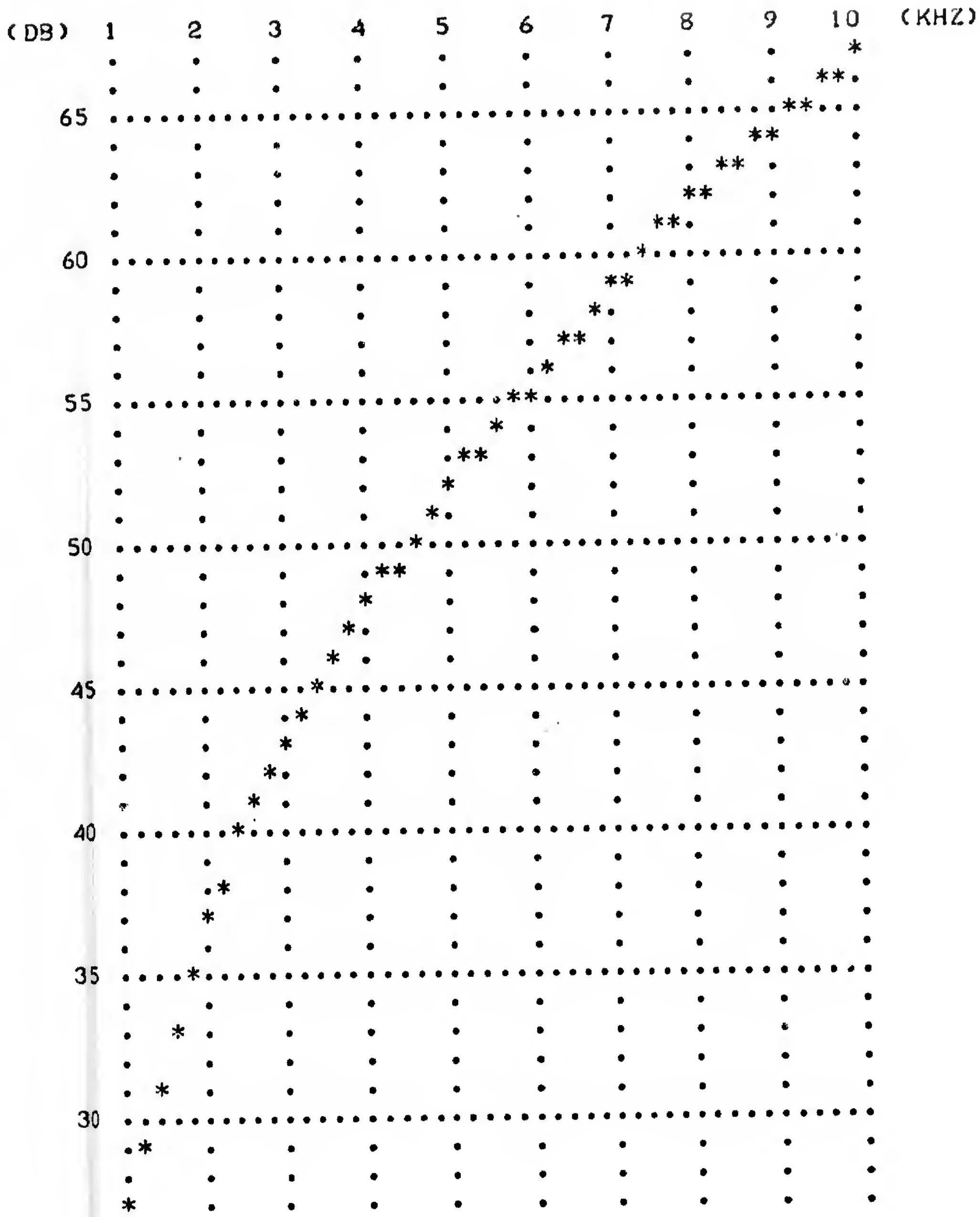

3-16-C

TRANSMISSIØN LØSS VS FREQUENCY

AØM= .000220 AIM= .000072
AK = 1000 AL = .20

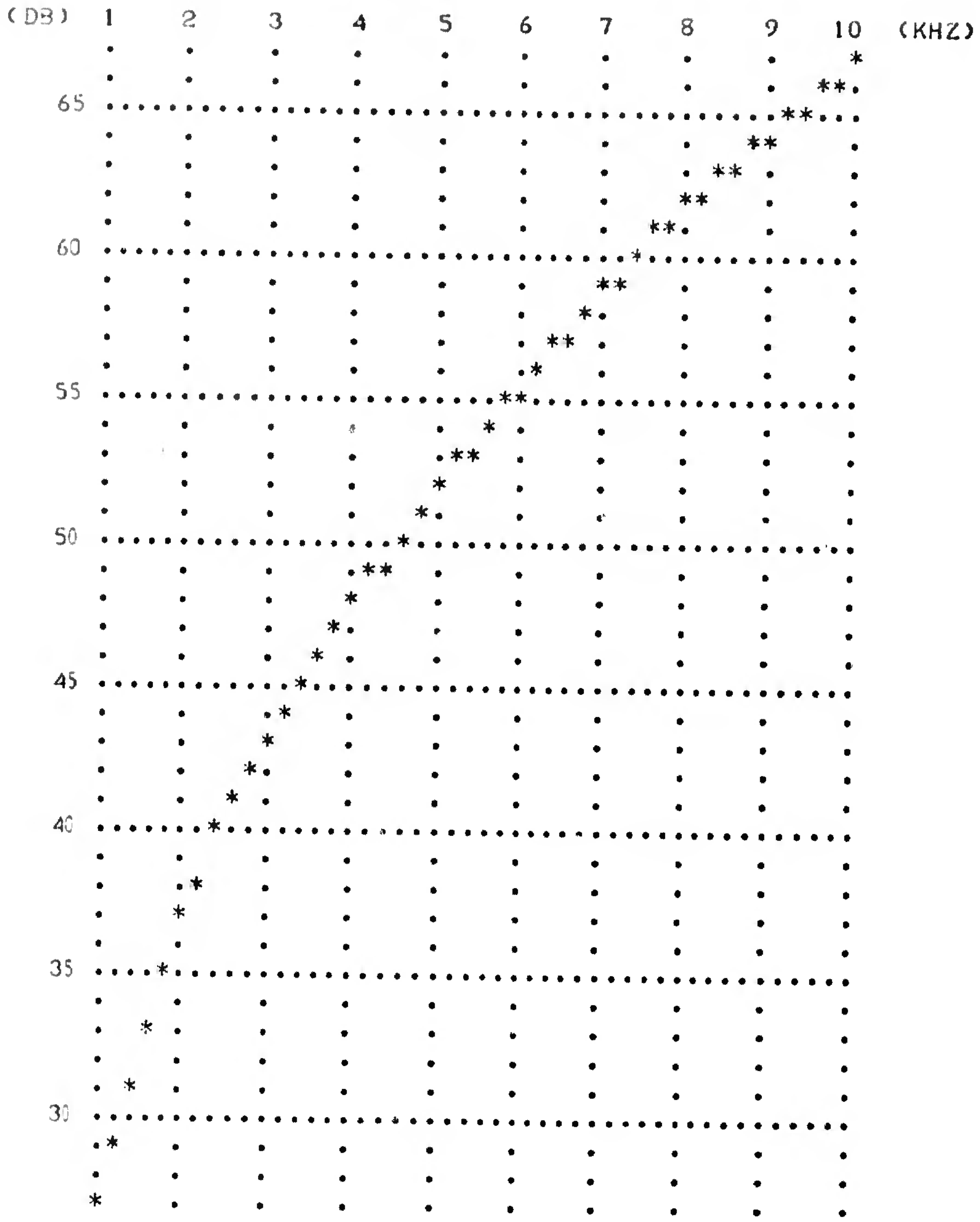

3-16-C

TRANSMISSIØN LØSS VS FREQUENCY

AØM= .000220   AIM= .000072
AK =   2000   AL =   .20

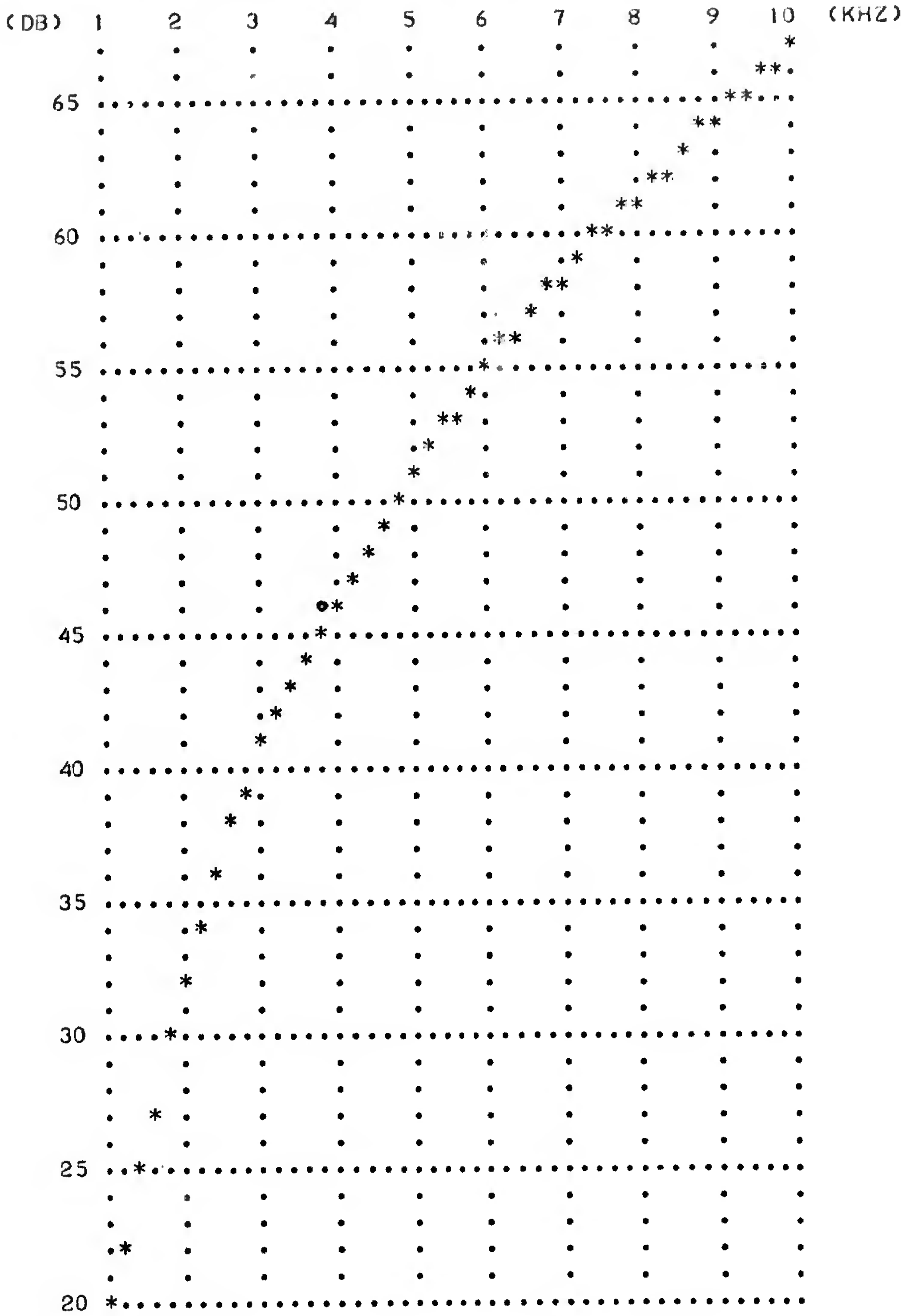

3-16-d

TRANSMISSION LØSS VS FREQUENCY

AOM= .000220 AIM= .000072
AK = 3000 AL = .20

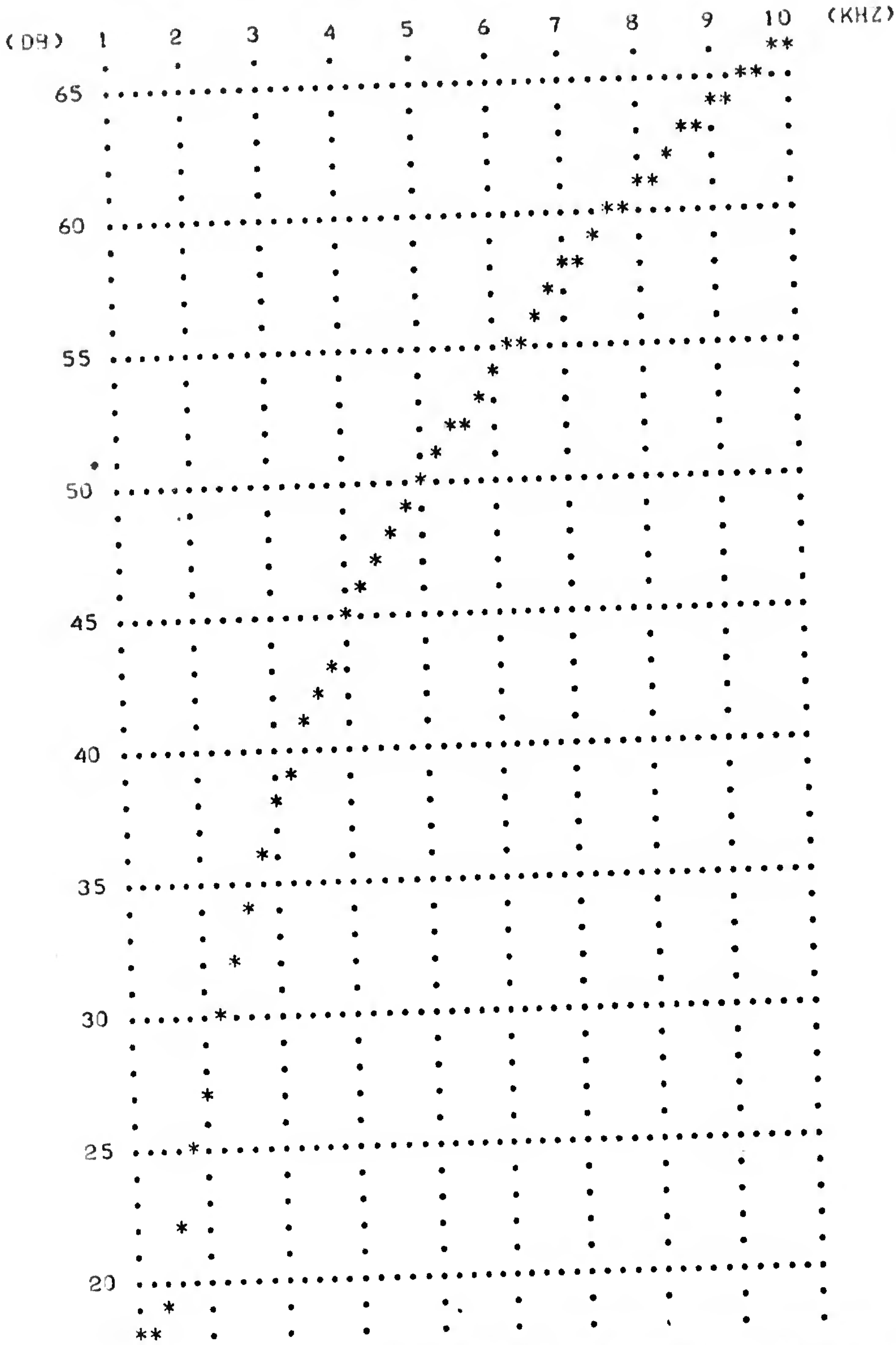

Figure 3-9. Plots of Transmission Loss Versus Frequency for Various Spring Constants and Damping Values (Sheet 1 of 3)

TRANSMISSIØN LØSS VS FREQUENCY

AØM= .000220   AIM= .000072
AK = 200   AL = .30

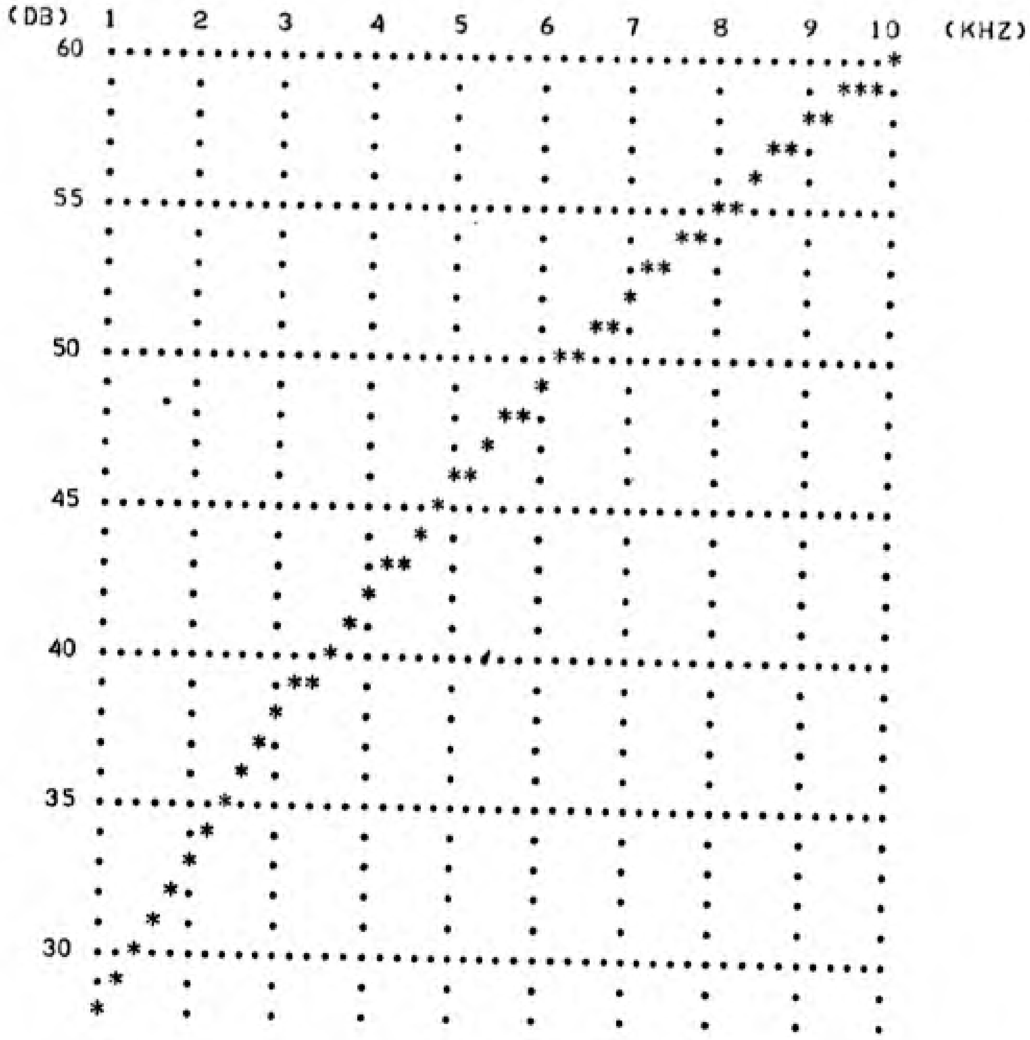

3-17-a

TRANSMISSIØN LØSS VS FREQUENCY

AØM= .000220 AIM= .000072
AK = 600 AL = .30

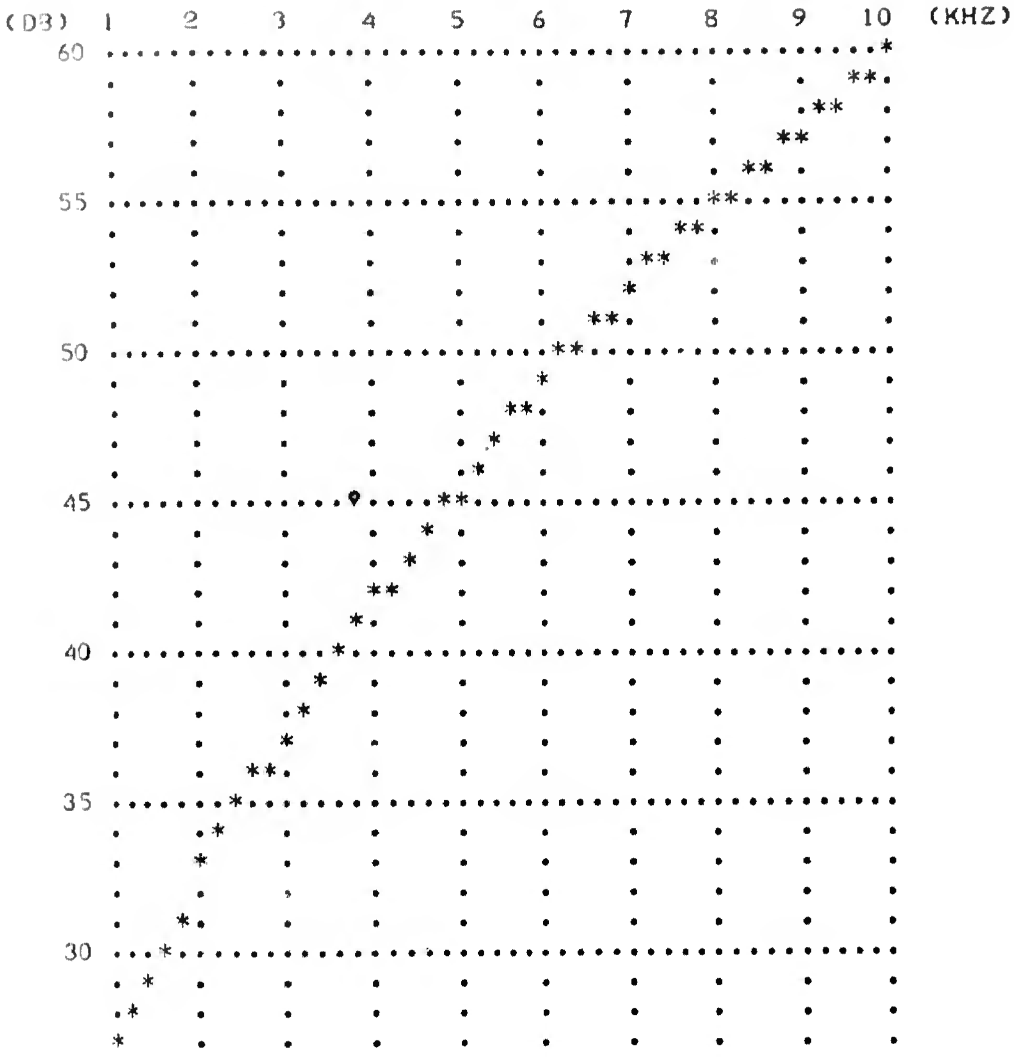

3-17 h

TRANSMISSIØN LØSS VS FREQUENCY

AØM= .000220 AIM= .000072
AK = 1000 AL = .30

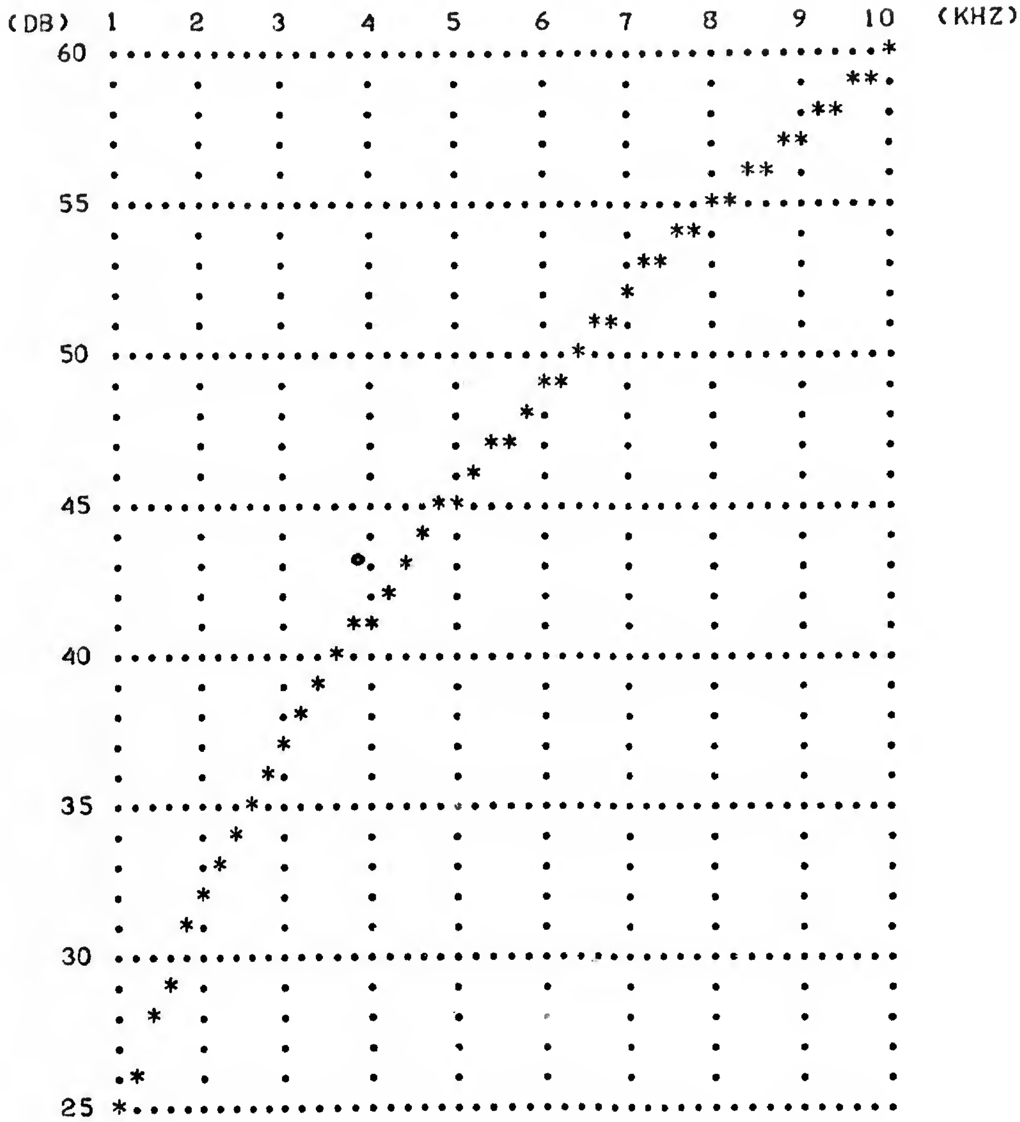

TRANSMISSIØN LØSS VS FREQUENCY

AØM= .000220 AIM= .000072
AK = 2000 AL = .30

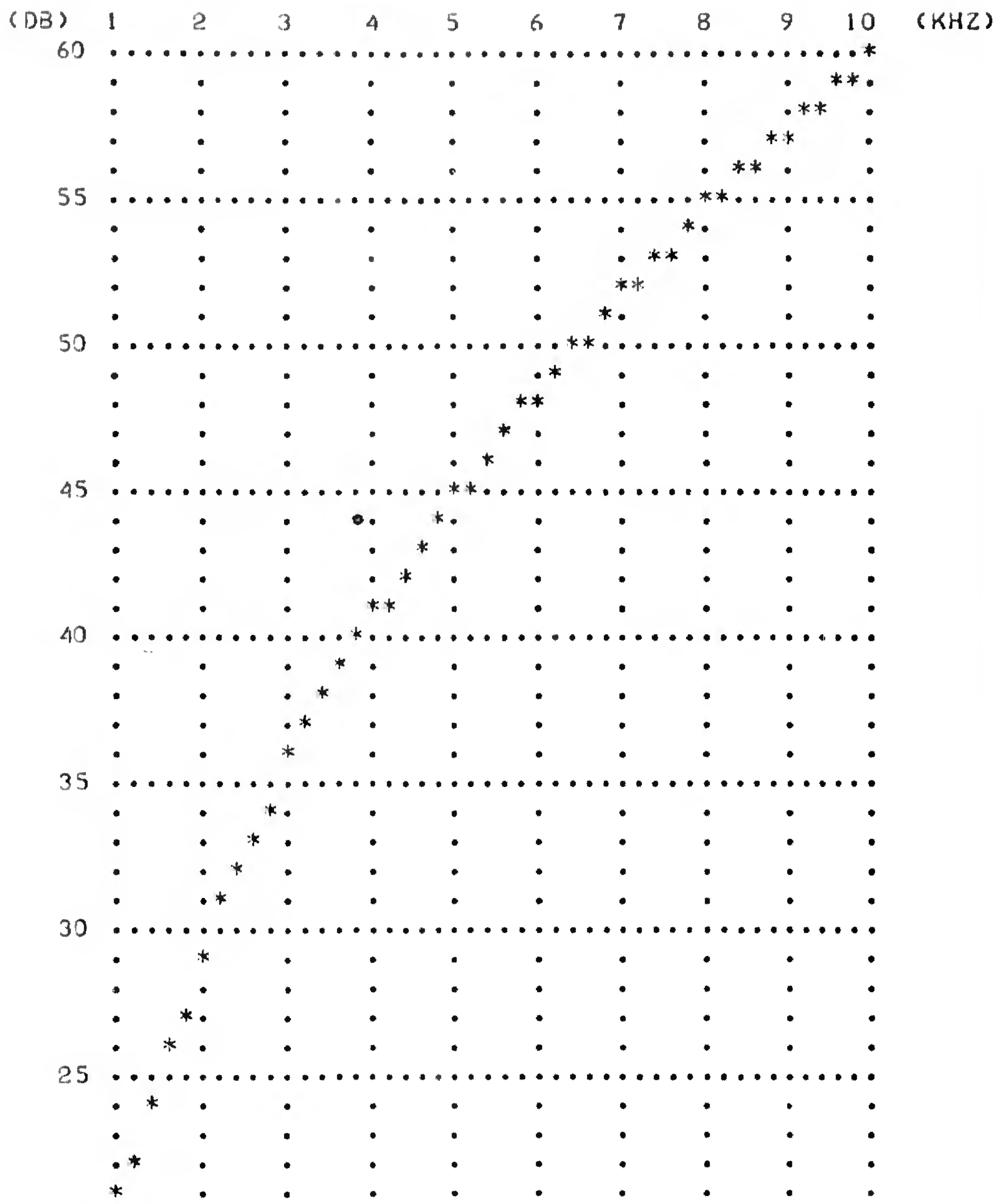

3-17-d

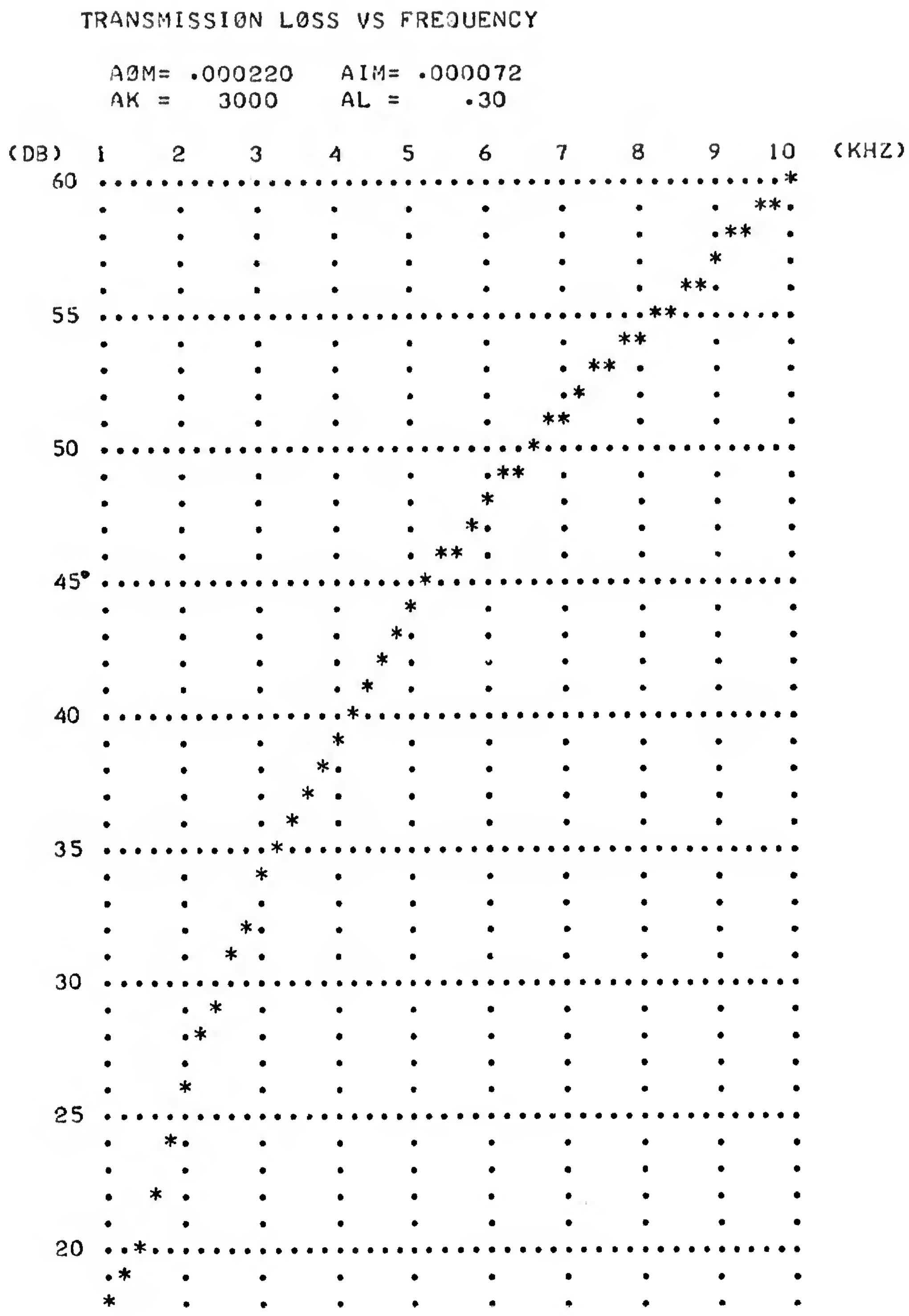

Figure 3-9. Plots of Transmission Loss Versus Frequency for Various Spring Constants and Damping Values (Sheet 2 of 3)

TRANSMISSIØN LØSS VS FREQUENCY

AØM= .000220 AIM= .000072
AK = 200 AL = .40

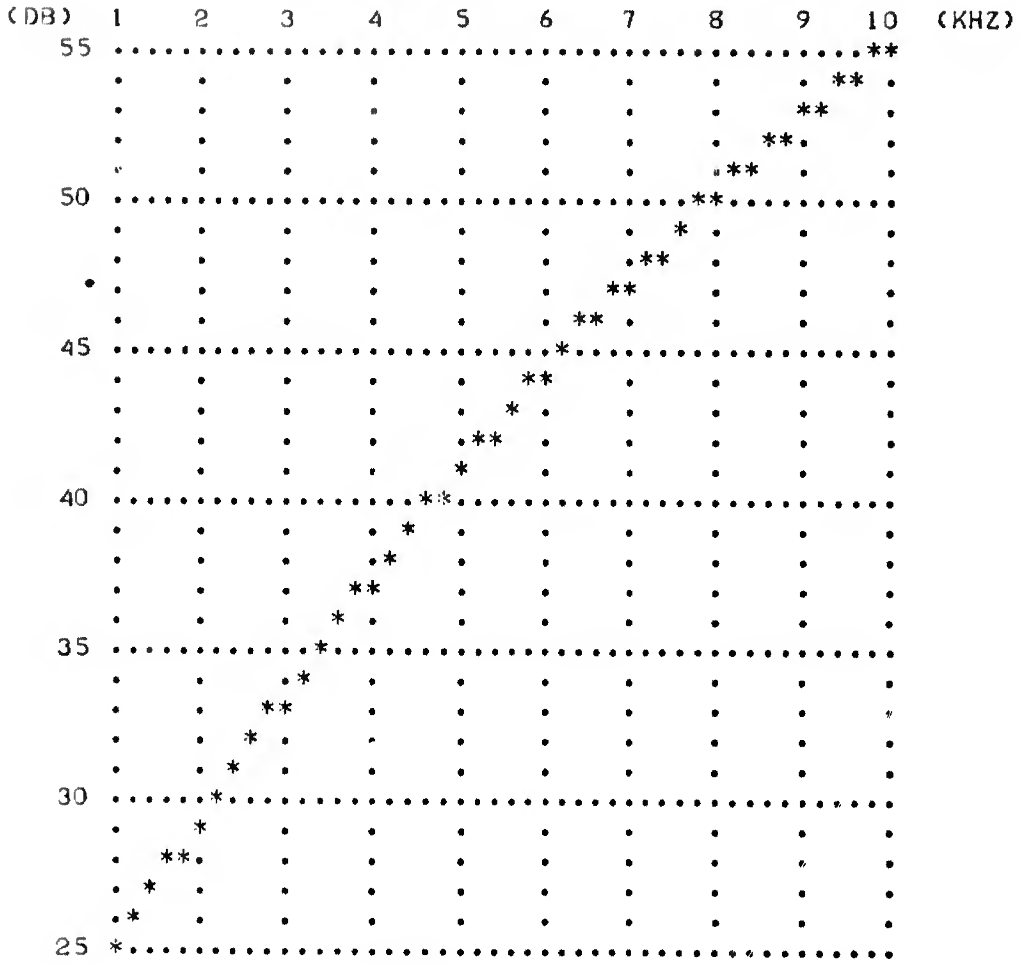

3-18-A

TRANSMISSIØN LØSS VS FREQUENCY

AØM= .000220 AIM= .000072
AK = 600 AL = .40

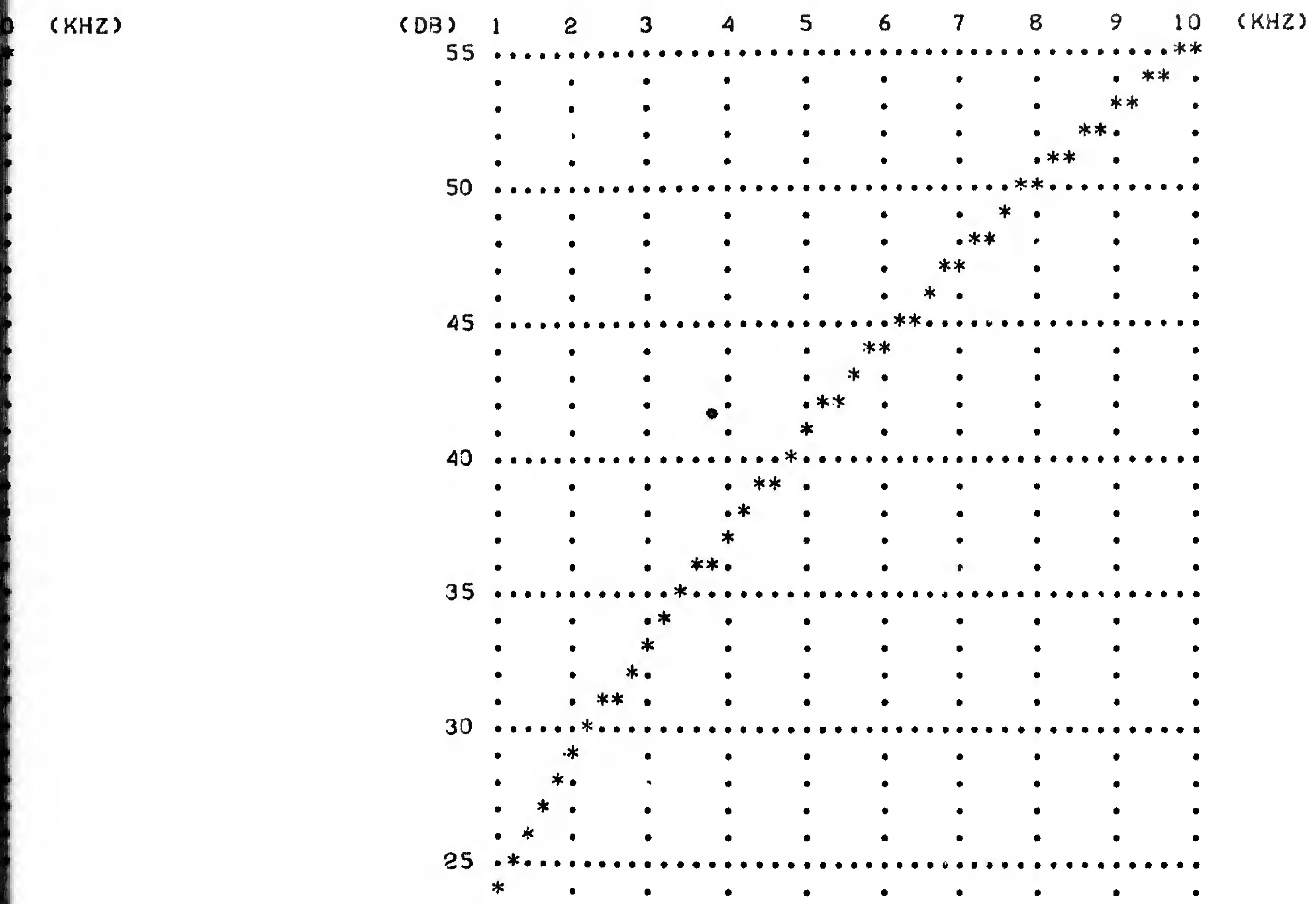

34 8-h

TRANSMISSIØN LØSS VS FREQUENCY

AØM= .000220   AIM= .000072
AK = 1000   AL = .40

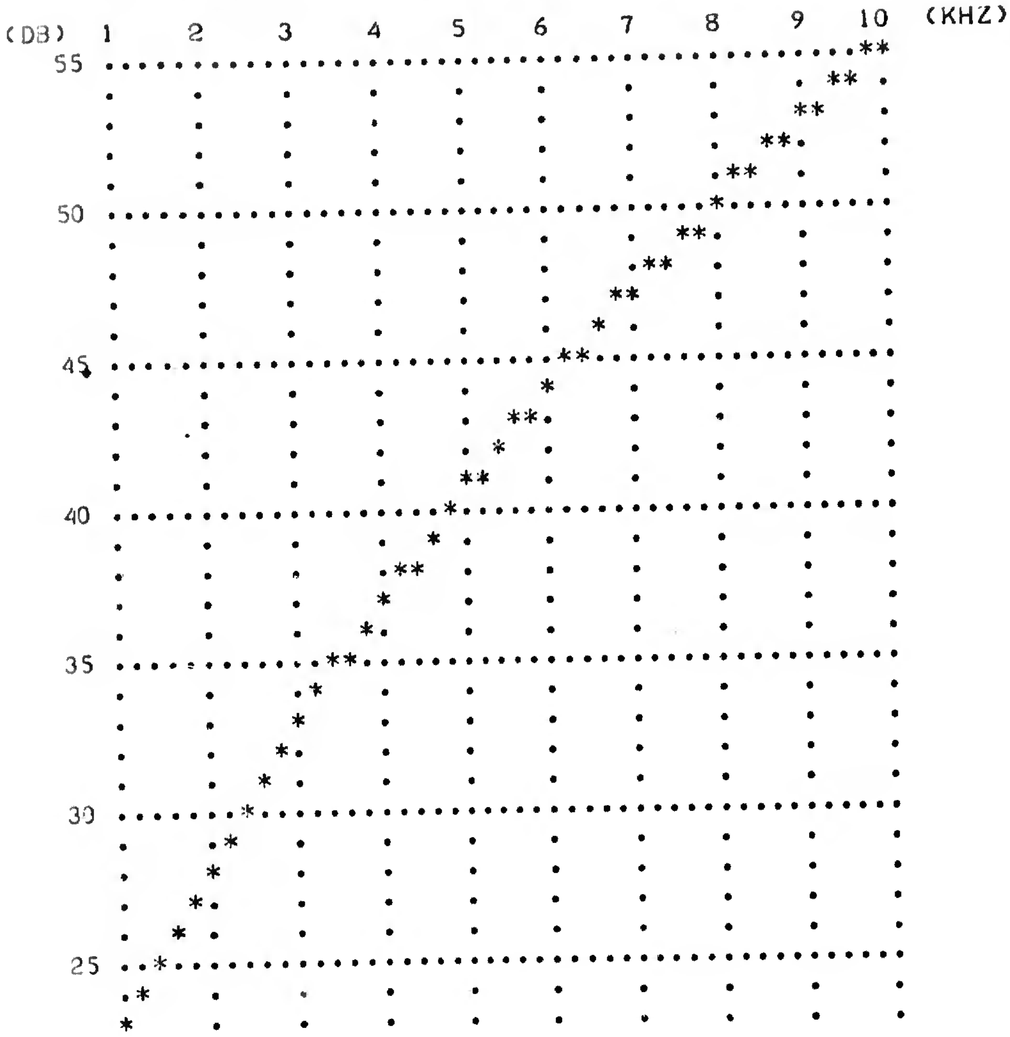

3-18-C

TRANSMISSIØN LØSS VS FREQUENCY

AØM= .000220   AIM= .000072
AK =   2000   AL =   .40

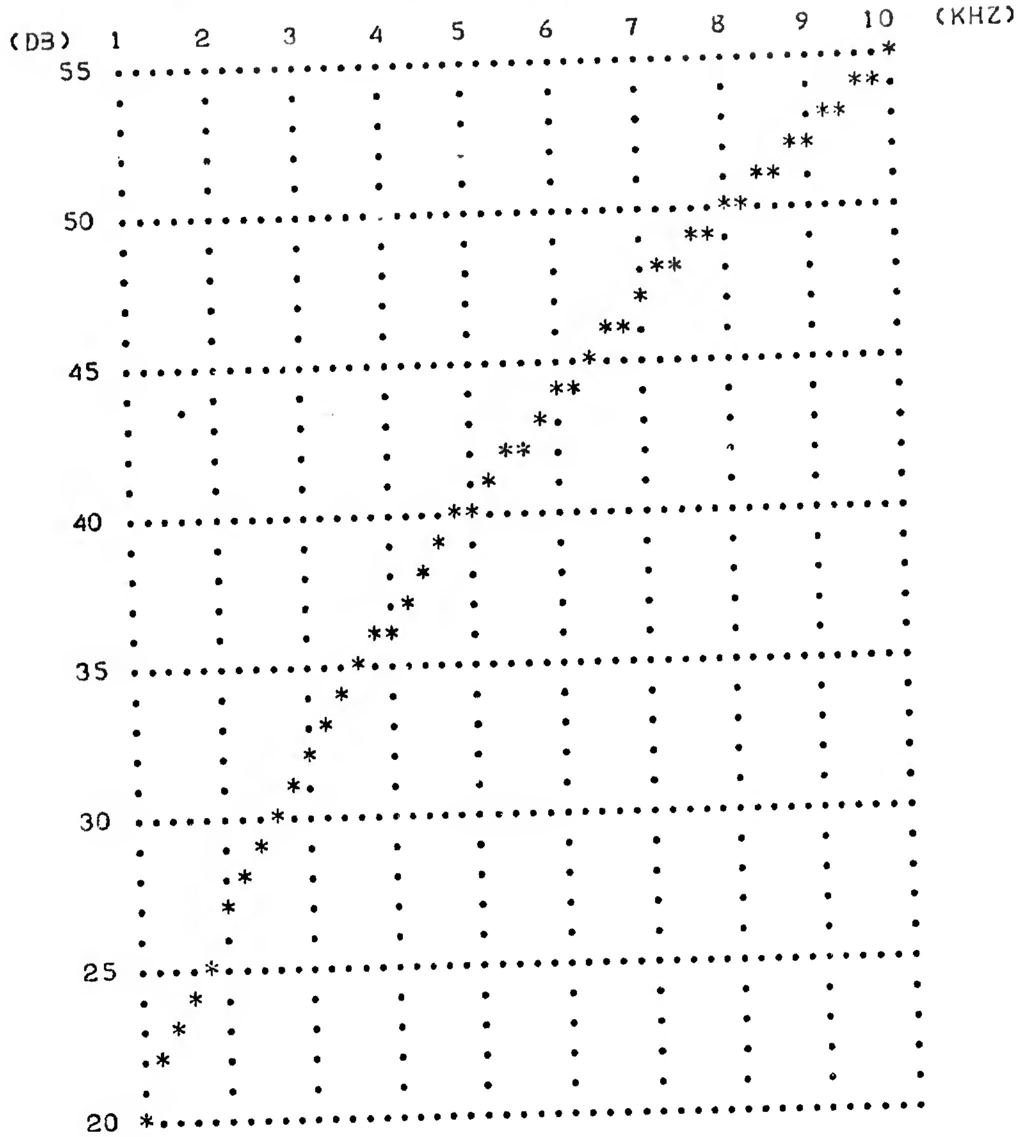

3-18-d

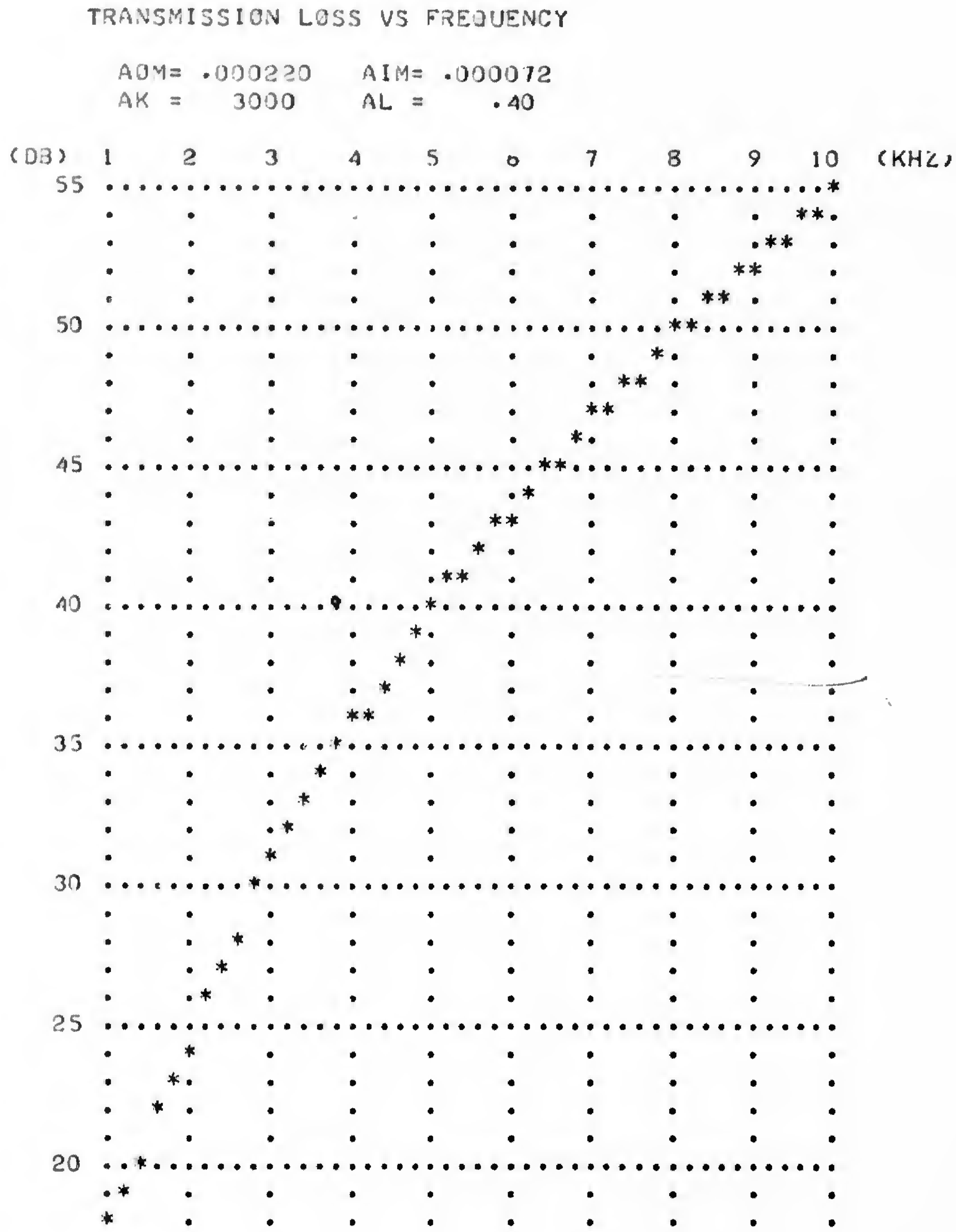

Figure 3-9. Plots of Transmission Loss Versus Frequency for Various Spring Constants and Damping Values (Sheet 3 of 3)

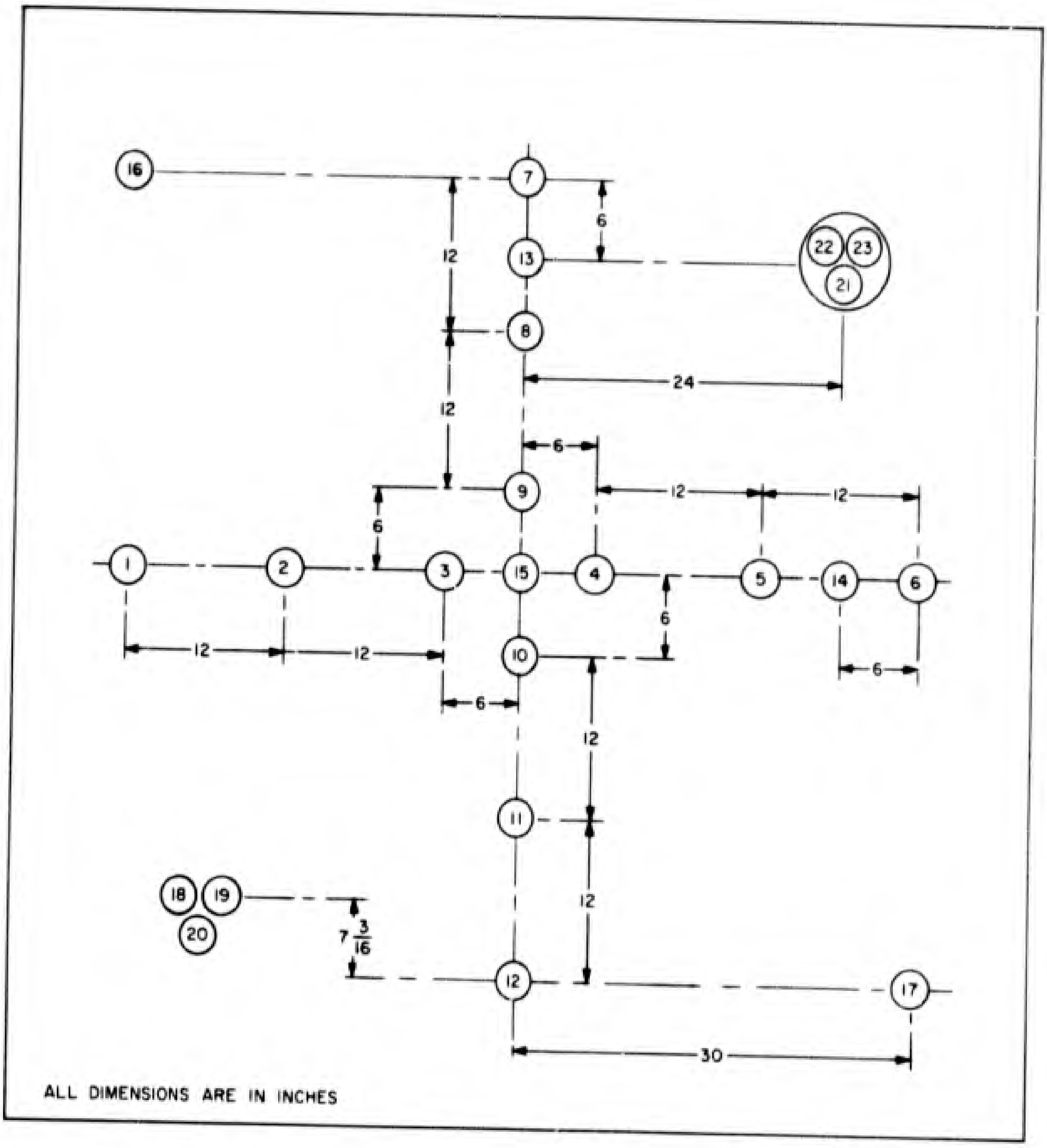

Figure 3-10. Arrangement of Test Hydrophones

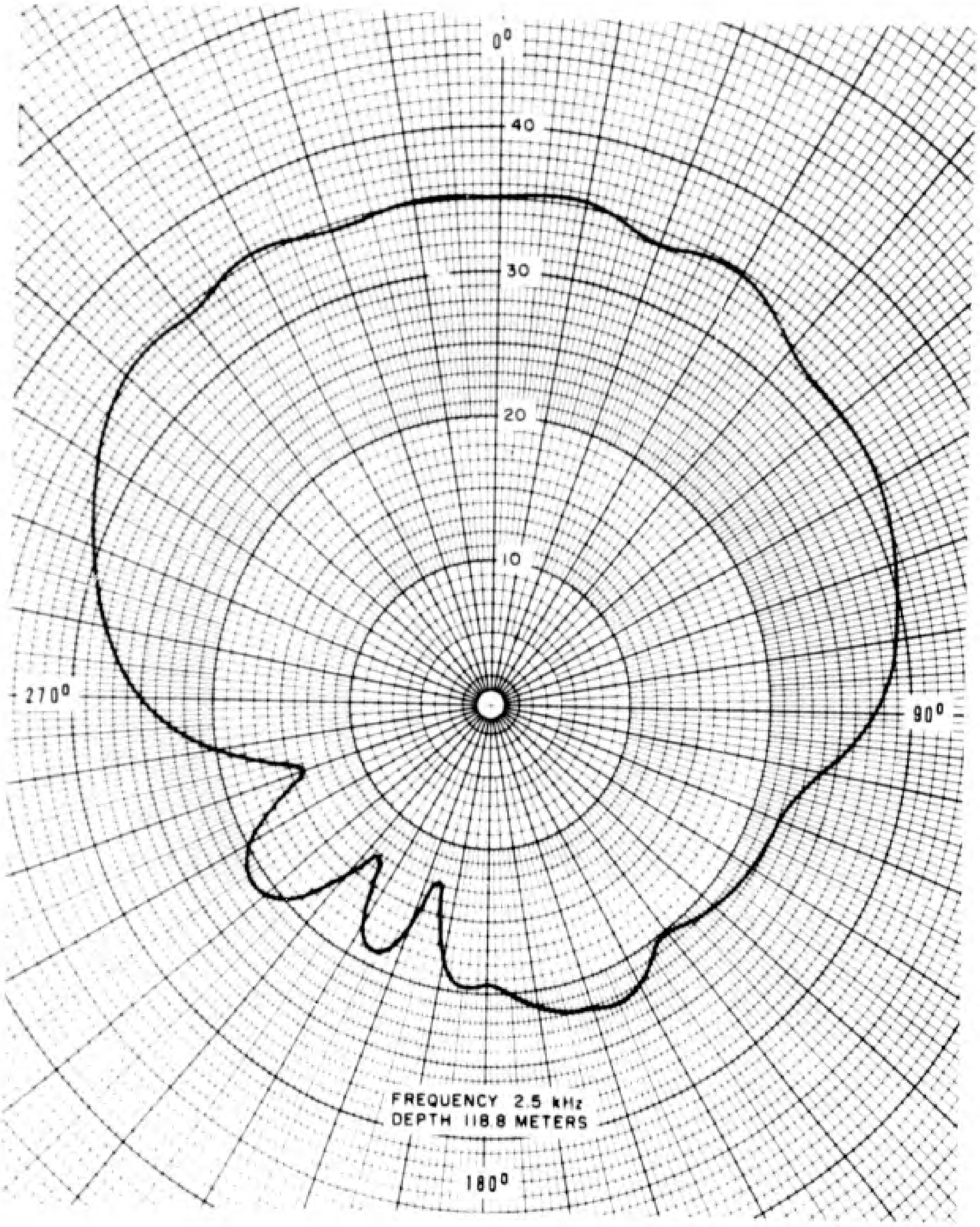

Figure 3-11. Directivity Pattern of Hydrophone 1 at 2.5 kHz

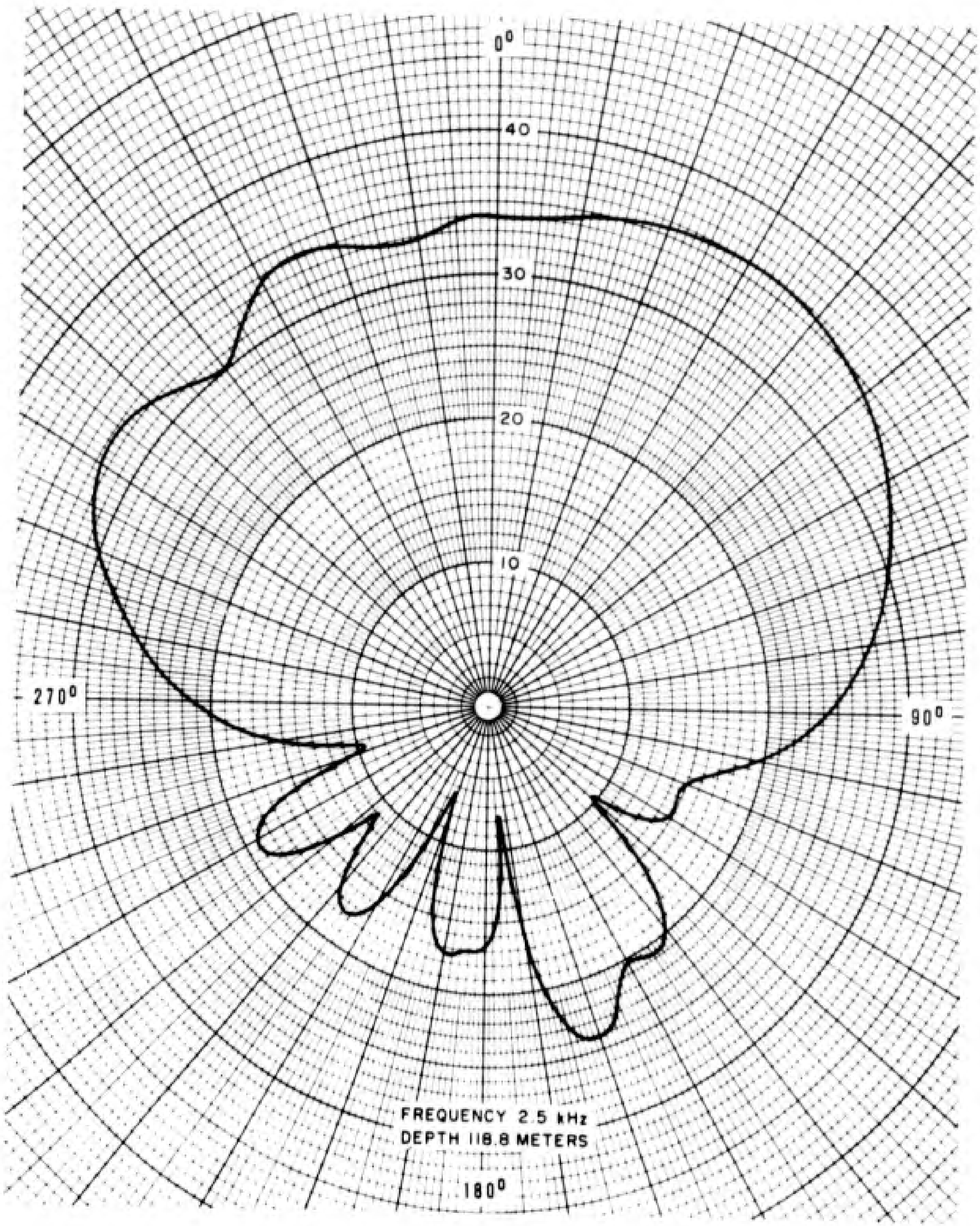

Figure 3-12. Directivity Pattern of Hydrophone 2 at 2.5 kHz

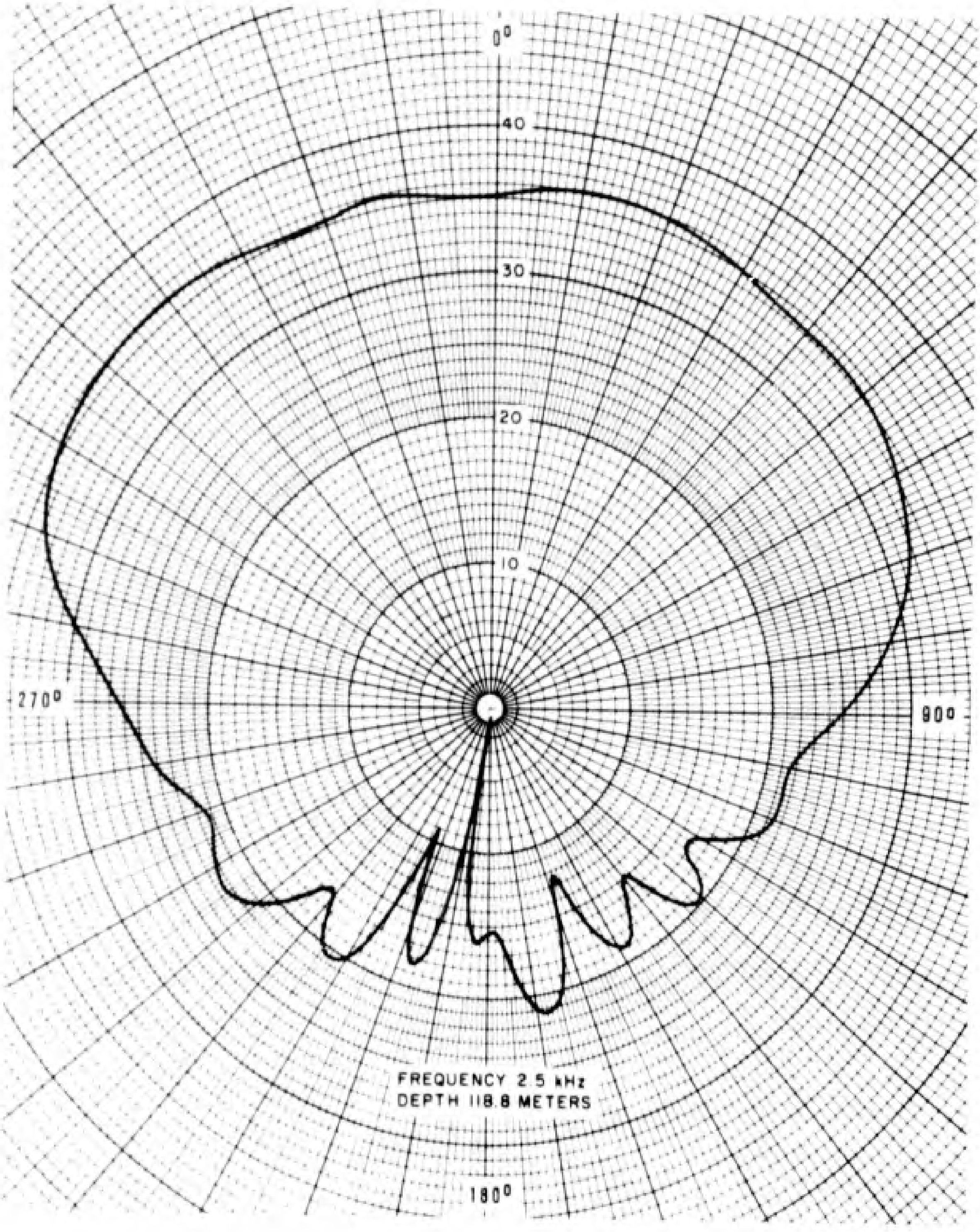

Figure 3-13. Directivity Pattern of Hydrophone 3 at 2.5 kHz

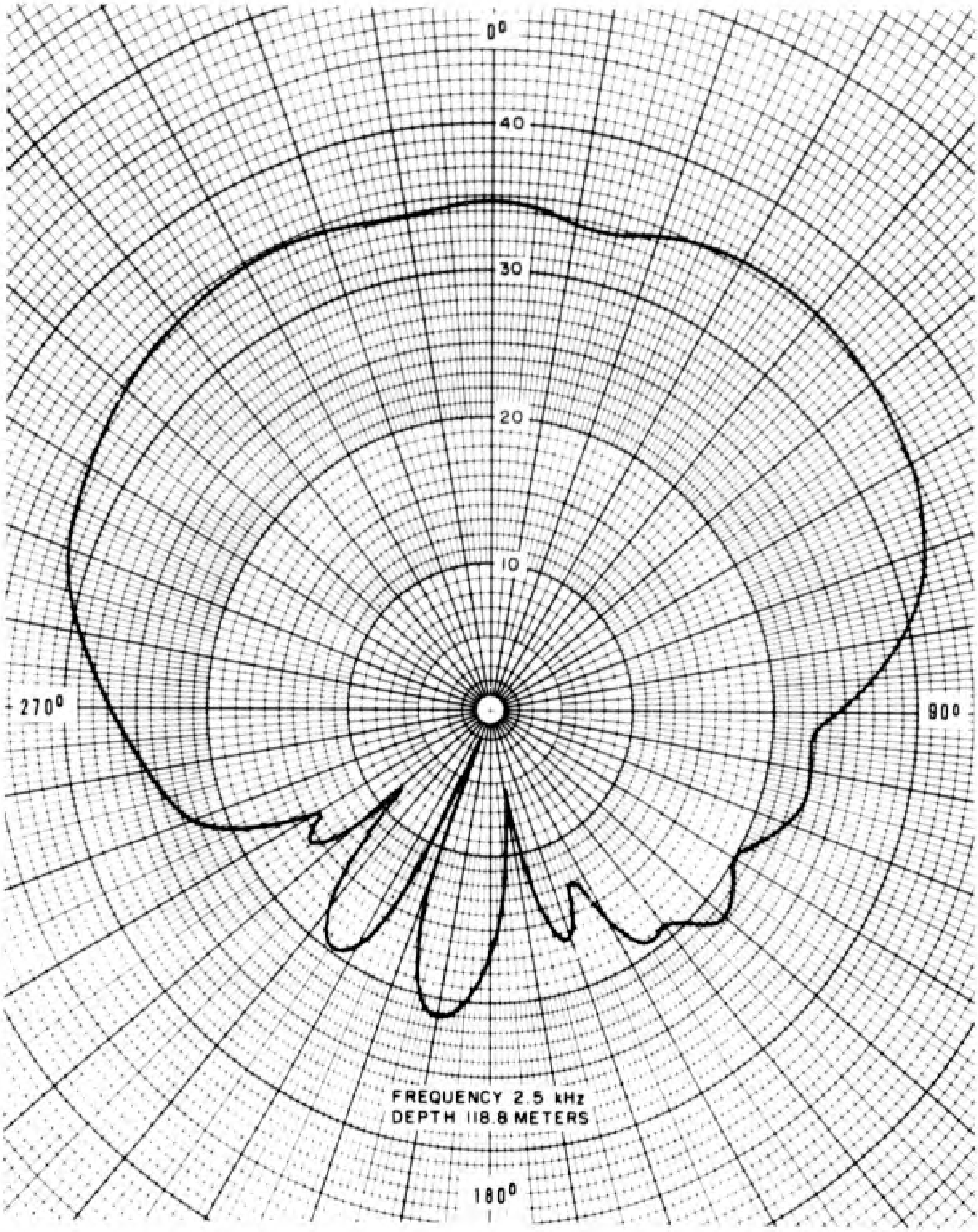

Figure 3-14. Directivity Pattern of Hydrophone 4 at 2.5 kHz

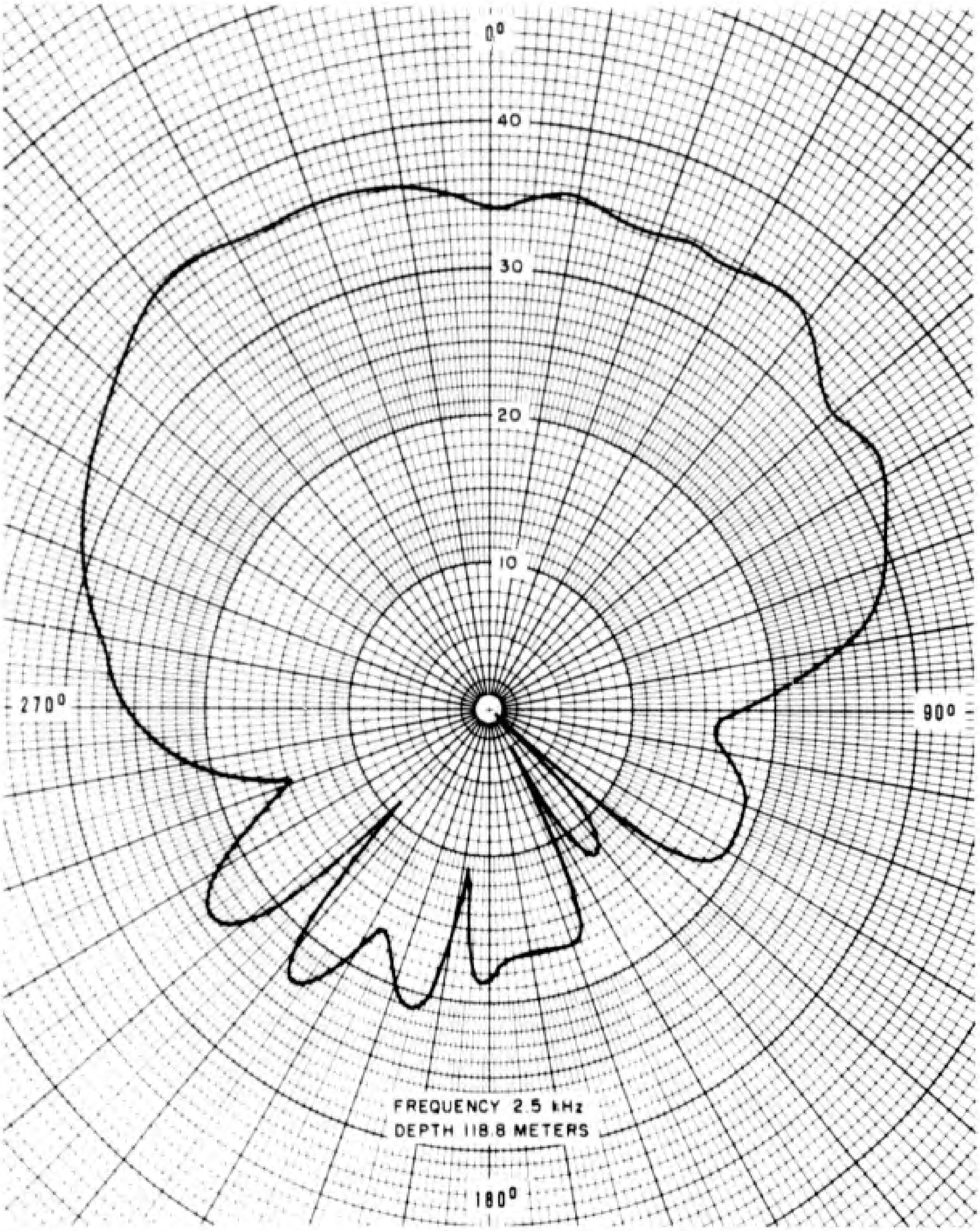

Figure 3-15. Directivity Pattern of Hydrophone 5 at 2.5 kHz

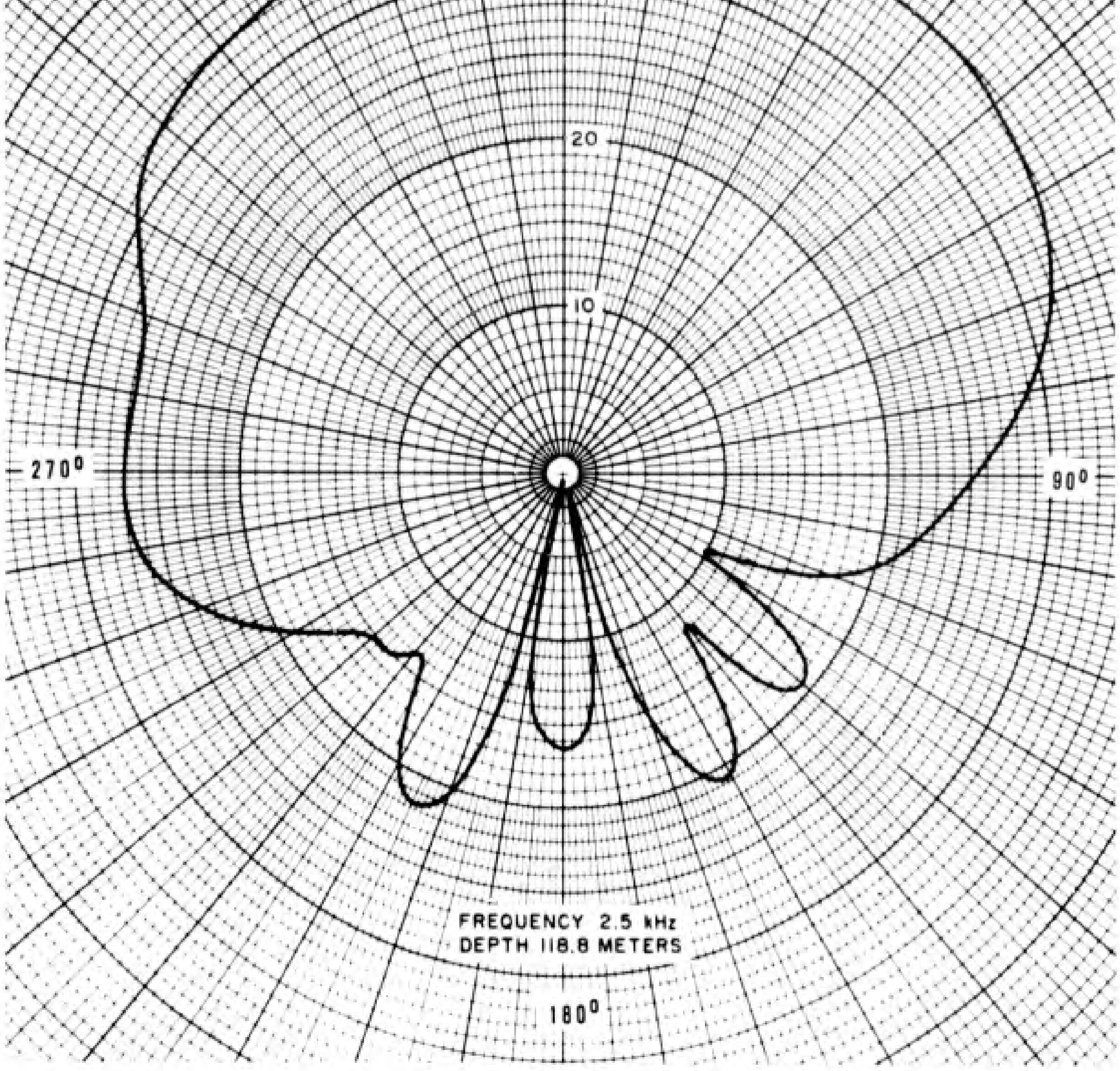

Figure 3-16. Directivity Pattern of Hydrophone 6 at 2.5 kHz

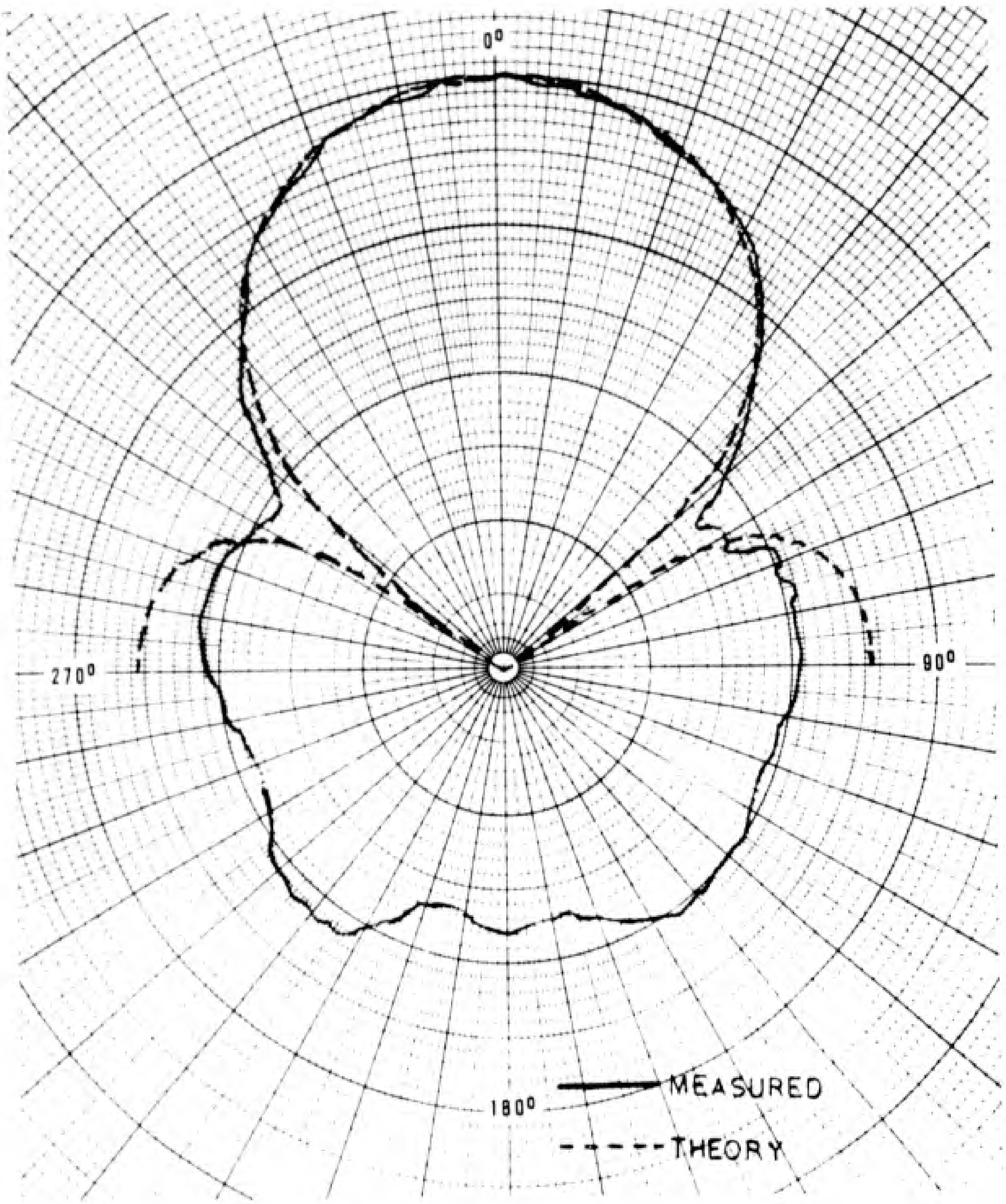

Figure 3-17. Zero-Degree Beam Pattern, Hydrophones 1 Through 6 at 1 kHz

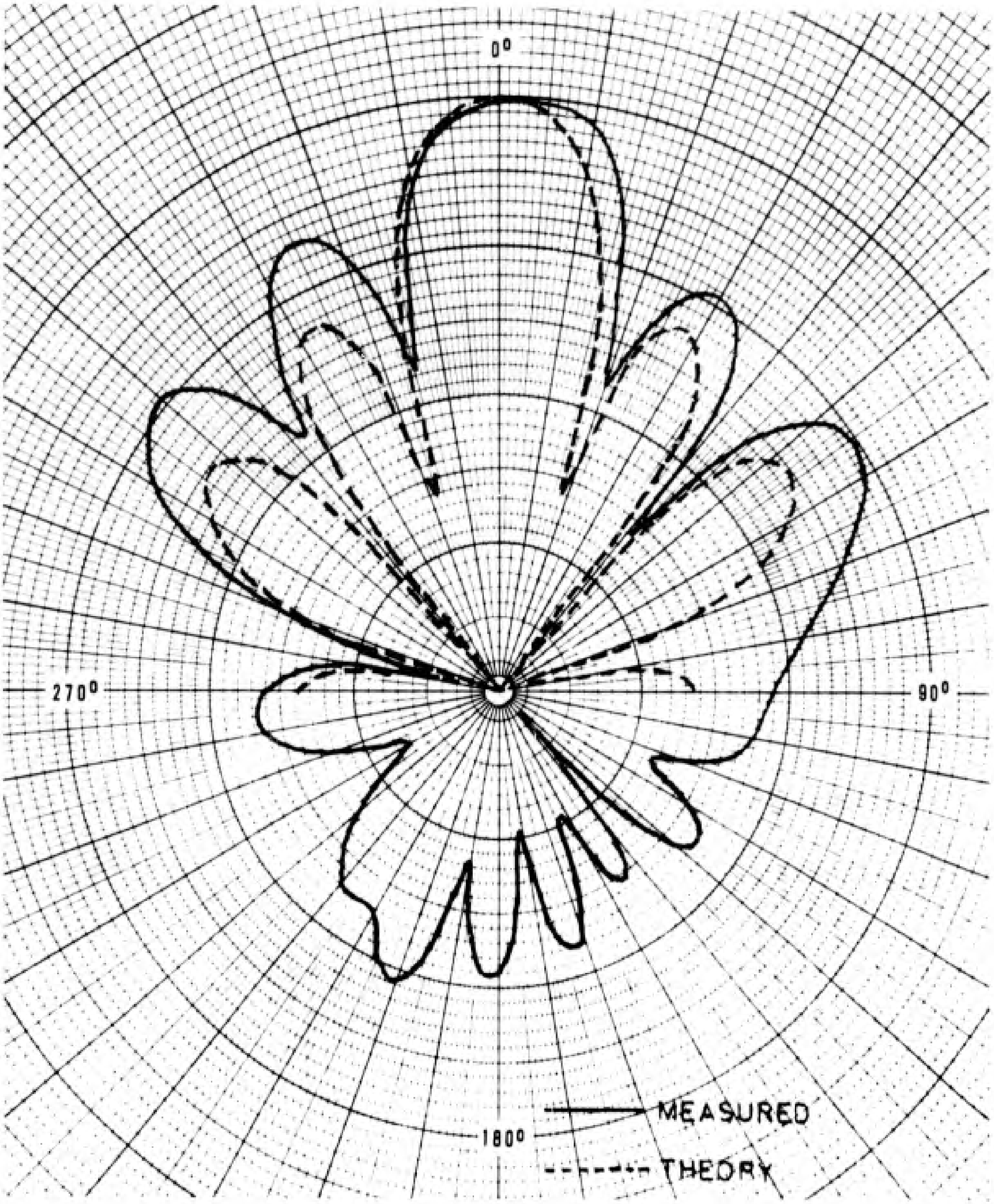

Figure 3-18. Zero-Degree Beam Pattern, Hydrophones 1 Through 6 at 2.5 kHz

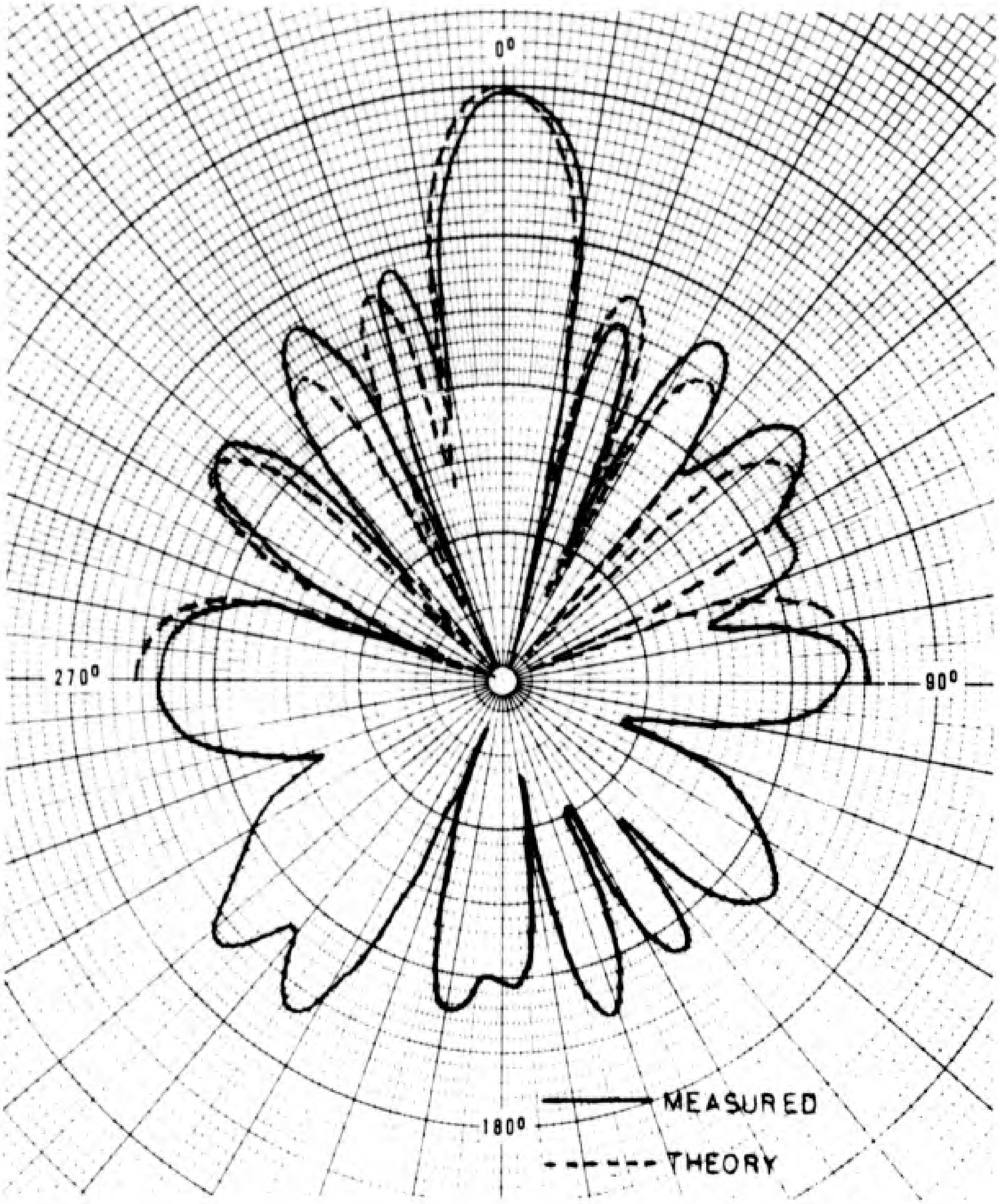

Figure 3-19. Zero-Degree Beam Pattern, Hydrophones 1 Through 6 at 3.5 kHz

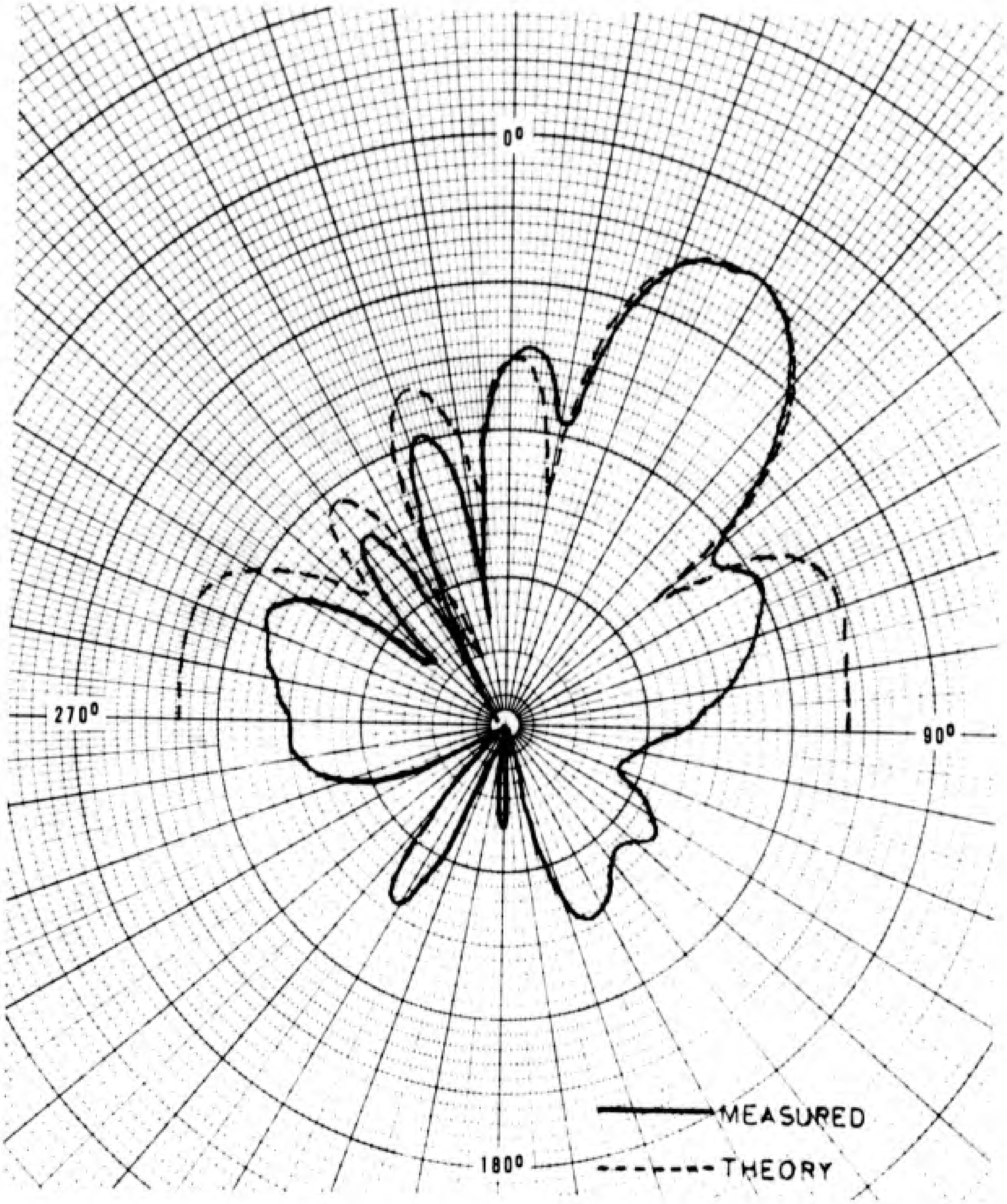

Figure 3-20. 30-Degree Beam Pattern, Hydrophones 1 Through 6 at 2.5 kHz With No Shading

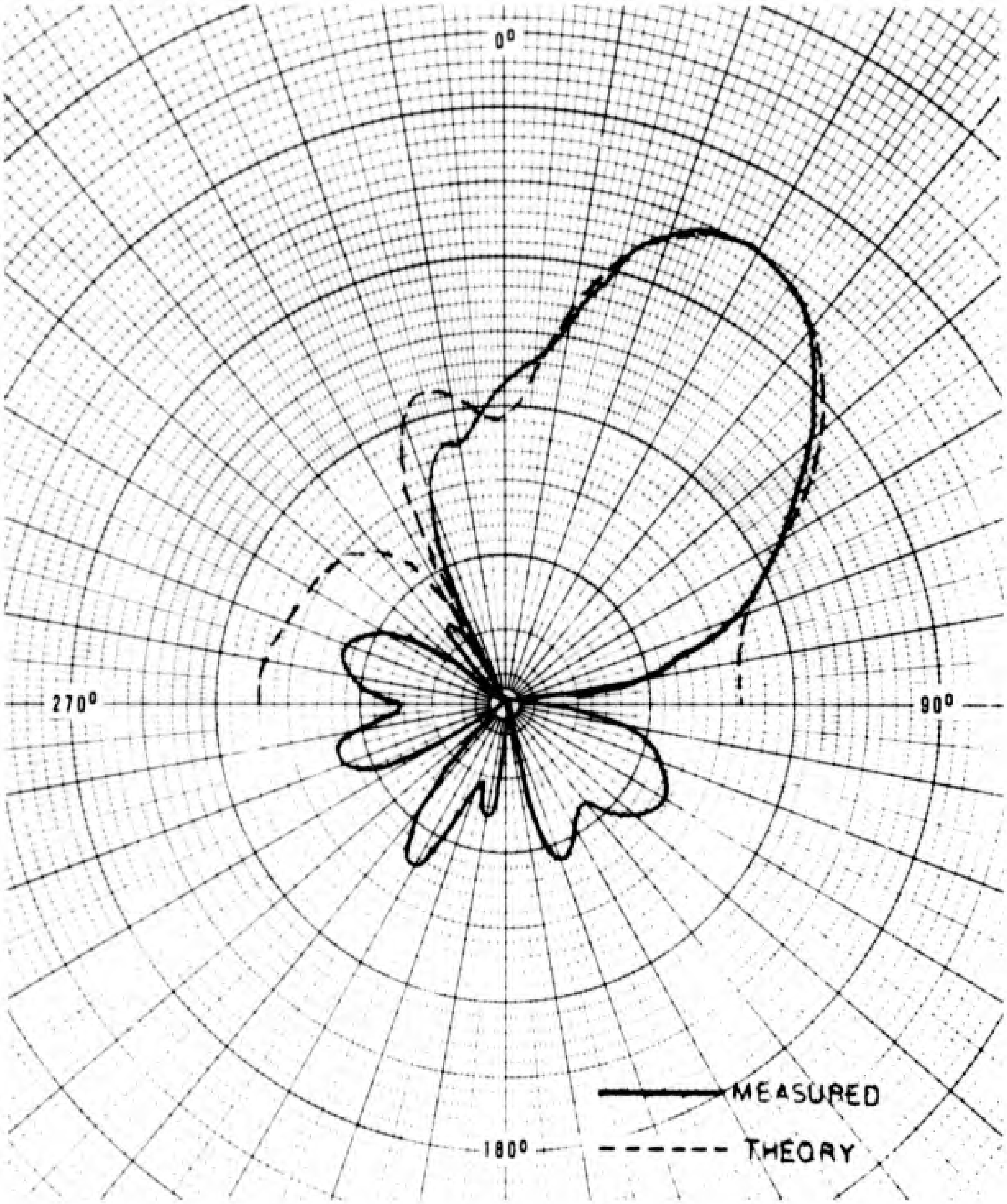

Figure 3-21. 30-Degree Beam Pattern, Hydrophones 1 Through 6 at 2.5 kHz with 20 dB Shading

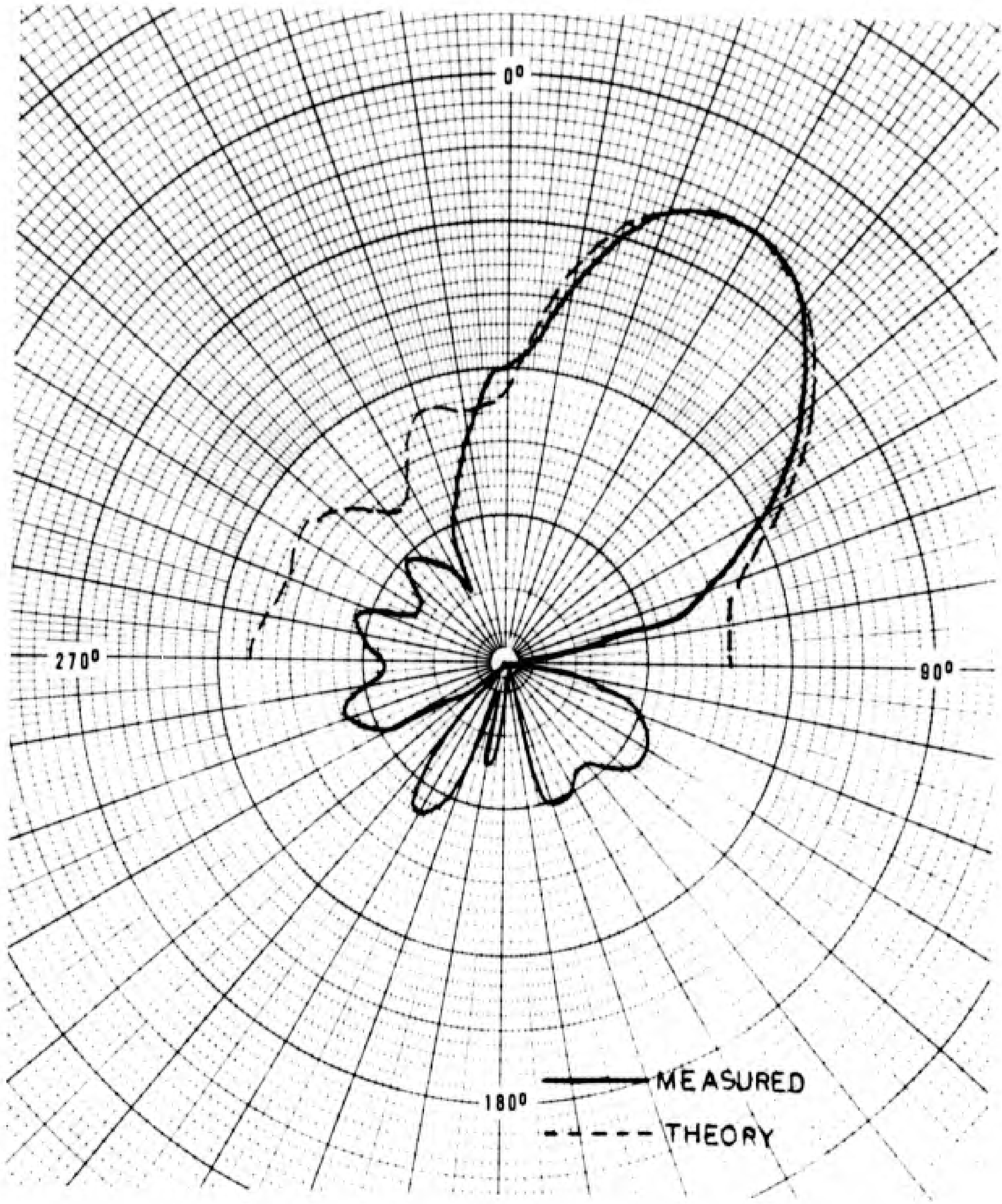

Figure 3-22. 30-Degree Beam Pattern, Hydrophones 1 Through 6 at 2.5 kHz with 30 dB Shading

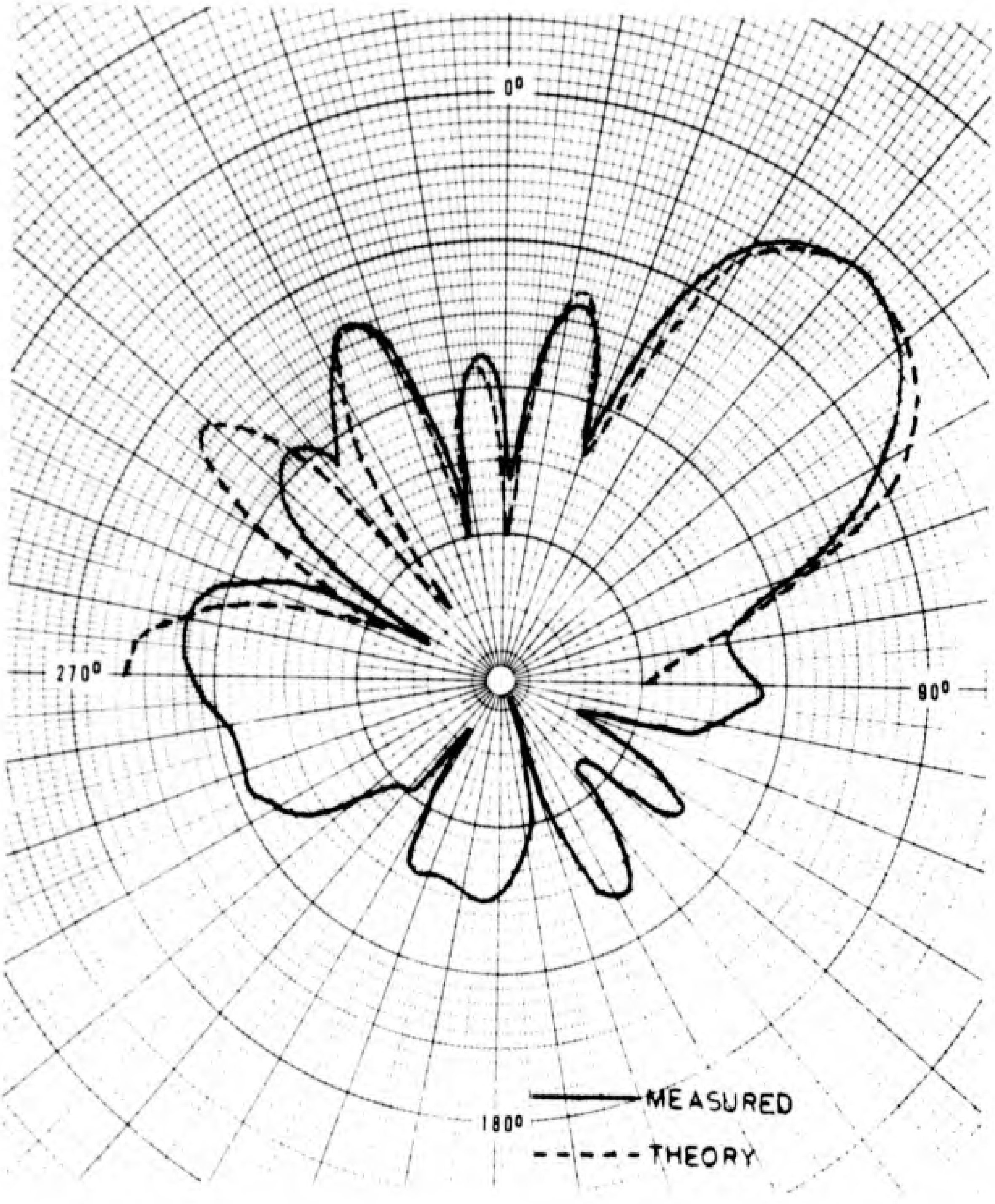

Figure 3-23. 45-Degree Beam Pattern, Hydrophones 1 Through 6 at 2.5 kHz With No Shading

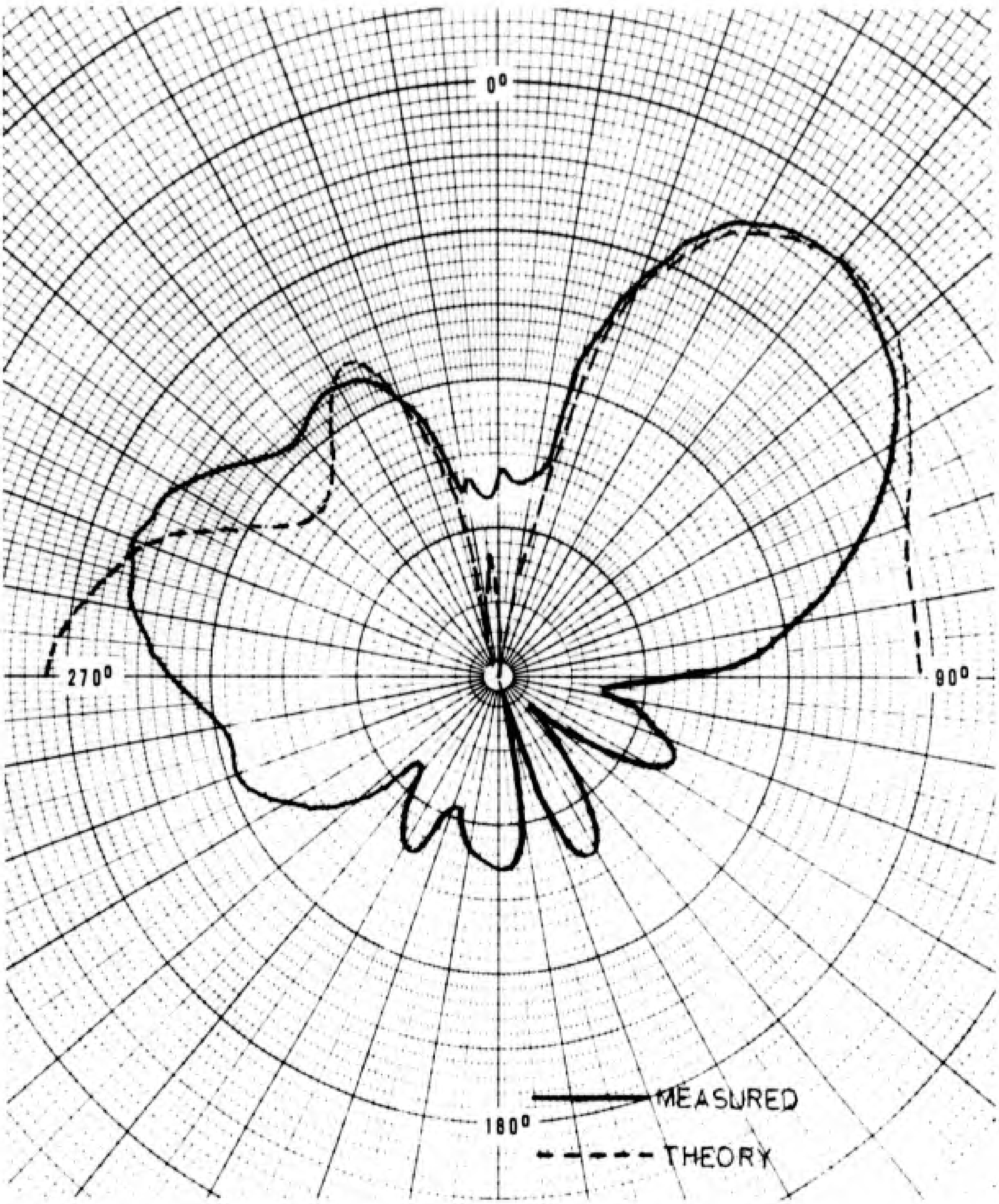

Figure 3-24. 45-Degree Beam Pattern, Hydrophones 1 Through 6 at 2.5 kHz with 20 dB Shading

SECTION 4

SONITE

4.1 INTRODUCTION

Sonite is a highly porous, fiber-reinforced, ceramic material manufactured by the Johns-Manville Corporation. It was originally designed as a thermal insulation under the trade name MIN-K. According to the manufacturer, Sonite has been specifically formulated as a low acoustic impedance material over a wide pressure range for use in deep submergence applications.

During the manufacturing process, Sonite is compressed to yield initial densities ranging from 20 to 35 pcf. Under static pressure, such as would be encountered in an ocean environment, both the density of and speed of sound in Sonite increase. In order to give repeatable performance under pressure changes, the material must be prestressed through several cycles to the highest pressure it is expected to encounter. After being prestressed, Sonite exhibits elastic mechanical and acoustical properties up to the prestress limit. Its acoustic impedance increases linearly with pressure but remains low compared to water. Tests by Johns-Manville (reference 4) have shown that Sonite's major properties are unaffected by temperatures from 4 to 30 degrees Centigrade.

4.2 THEORETICAL CONSIDERATIONS

The major component of Sonite is a microscopic particulate material. Small amounts of fiber and phenolic are added to stabilize its structure and increase handleability. Since the particulate material has an open cell structure, the cells tend to collapse under stress. However, if the Sonite is prestressed, the particles will not catastrophically collapse unless the prestress is exceeded. Up to this limit the individual particles undergo reversible deformation. As measured in reference 4, the properties of Sonite, under pressure cycling, become stable only after several cycles. This can be explained by realizing that during each stress cycle, the Sonite particles will rearrange themselves until an equilibrium position is reached. The reorientation process is believed to be exponential with a relaxation constant of two cycles.

Expressions for Sonite density and acoustic velocity as a function of prestress, initial density, and applied stress have been derived (reference 5) and are

$$\rho = \frac{\rho_o}{1 - \alpha \ln (P_m/P_{in}) - \dfrac{P}{B_{in} + \beta \left[\alpha \ln (P_m/P_{in})\right]^n}}$$

$$v = \left[\frac{C_{in} + \gamma \left[\alpha \ln (P_m/P_{in})\right]^m + \delta P}{\rho}\right]^{1/2}$$

where

ρ = density

v = acoustic propagation velocity

ρ_o = initial density

P_m = prestress

P_{in} = initial stress supported by the sample

P = applied stress

B_{in} = initial compressive stiffness

B = compressive stiffness

C_{in} = initial stiffness

m, n = experimental parameters within the system related to detailed coupling mechanism

$\alpha, \beta, \gamma, \delta$ = proportionality factors

It can be seen that the properties of Sonite can be changed to fit a particular requirement by applying the proper prestress, P_m.

The effects of the additional components used in the manufacture of Sonite are important. At low pressures, before Sonite has firmly compacted, the fiber and phenolic contribute to the material's mechanical behavior. At moderate pressures, because the load-bearing particles are much stronger, the effects become negligible. The phenolic also acts to increase the shear stiffness of Sonite by forming weak bonds between the microscopic particles locking them in place. Increasing shear stiffness, the dominant factor in Sonite, forces a corresponding increase in the sound velocity and thus raises the acoustic impedance. In general, anything that tends to bond the particles together will increase velocity; breaking the bonds will decrease velocity.

As a general guide to the use of Sonite, in order to avoid problems associated with its basic structure, it is recommended that the maximum applied stress be 20-percent less than the prestress and at least five cycles of prestress should be used to stabilize the material. To avoid contamination, which can form bonds between the particles and degrade Sonite's properties, the material must be carefully handled and encapsulated.

4.3 EXPERIMENTAL INVESTIGATION

Sonite is extremely porous and must be protected from direct contact with water. This fact complicates the problem of obtaining test data which reflects the acoustic properties of Sonite alone.

For the experiments conducted at the Sperry Sonar Test Facility, nine 12 x 12 x 1-inch panels were used. These panels were formed into one three-foot square structure by cementing thin (1/16 inch) aluminum panels to both sides and sealing the edges with cement. At the depths available for test purposes (12 feet) no problems with leaks were encountered.

The test configuration is shown in figure 4-1. Two series of runs were made, one with the reference hydrophone 1-5/8 inches from the baffle and the other at a distance of 3-1/4 inches. Frequency response data from 1 to 20 kHz were taken with the baffle and hydrophone located as shown in figure 4-1 and with the baffle and hydrophone rotated 180 degrees so that the baffle was between the hydrophone and projector. Horizontal patterns at various frequencies were also obtained with both hydrophone spacings.

Test results are shown in figures 4-2 through 4-4. Figures 4-2 and 4-3 are the frequency responses for hydrophone-to-baffle spacings of 1-5/8 inches and 3-1/4 inches, respectively. The responses at 180 degrees, compared to free field, are a measure of the baffle insertion loss. They indicate that 1 inch of Sonite can attenuate sound in the 1 to 20 kHz region by at least 10 dB. However, the relatively small size of the test baffle causes diffraction to limit the baffle performance. Figure 4-4 is a comparison between measured and predicted responses at a hydrophone spacing of 1-5/8 inches. Agreement is good over the 1 to 10 kHz frequency range. The predicted results, calculated by the Sperry multilayer baffled-hydrophone response computer program, include the effect of the two 1/16-inch aluminum panels cemented to the Sonite. However, another calculation, with a baffle composed of only Sonite, showed that this effect is negligible due to the small thickness of the aluminum. The acoustic impedance of Sonite (20 pcf) used in the calculations was 0.132 that of water. This is slightly lower than the more recent value of 0.145 (after 10 cycles of 0-1000 psi) reported by Johns-Manville in reference 4. However, the Sonite used in the tests had not been pressure cycled but had just been pressed to yield a density of 20 pcf.

Test results on Sonite to date are limited in scope but indicate its usefulness as a baffle material. Its light weight, coupled with an apparent ability to maintain a low acoustic impedance under high static pressures, makes it a good candidate for future investigation and experimentation.

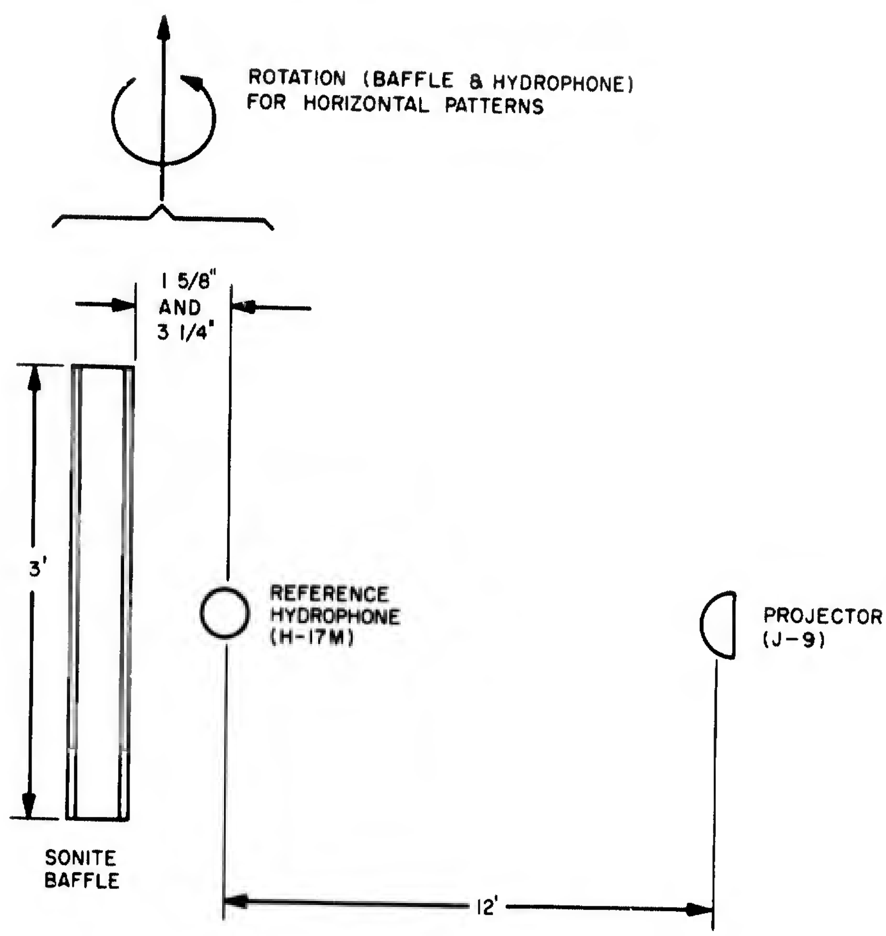

Figure 4-1. Sonite Test Configuration

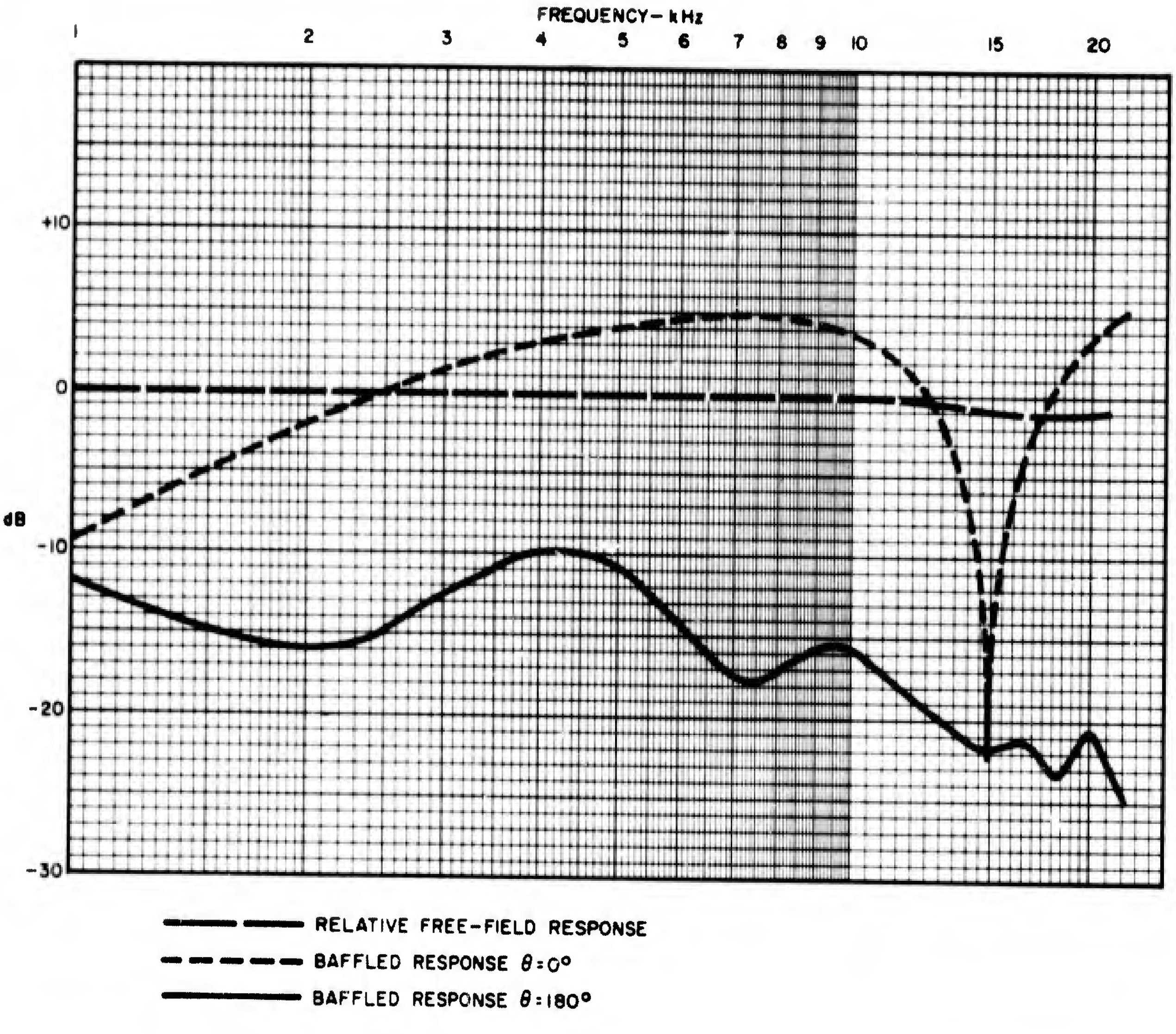

Figure 4-2. Relative Hydrophone Response In Presence of Sonite Baffle, Spacing 1-5/8 Inches

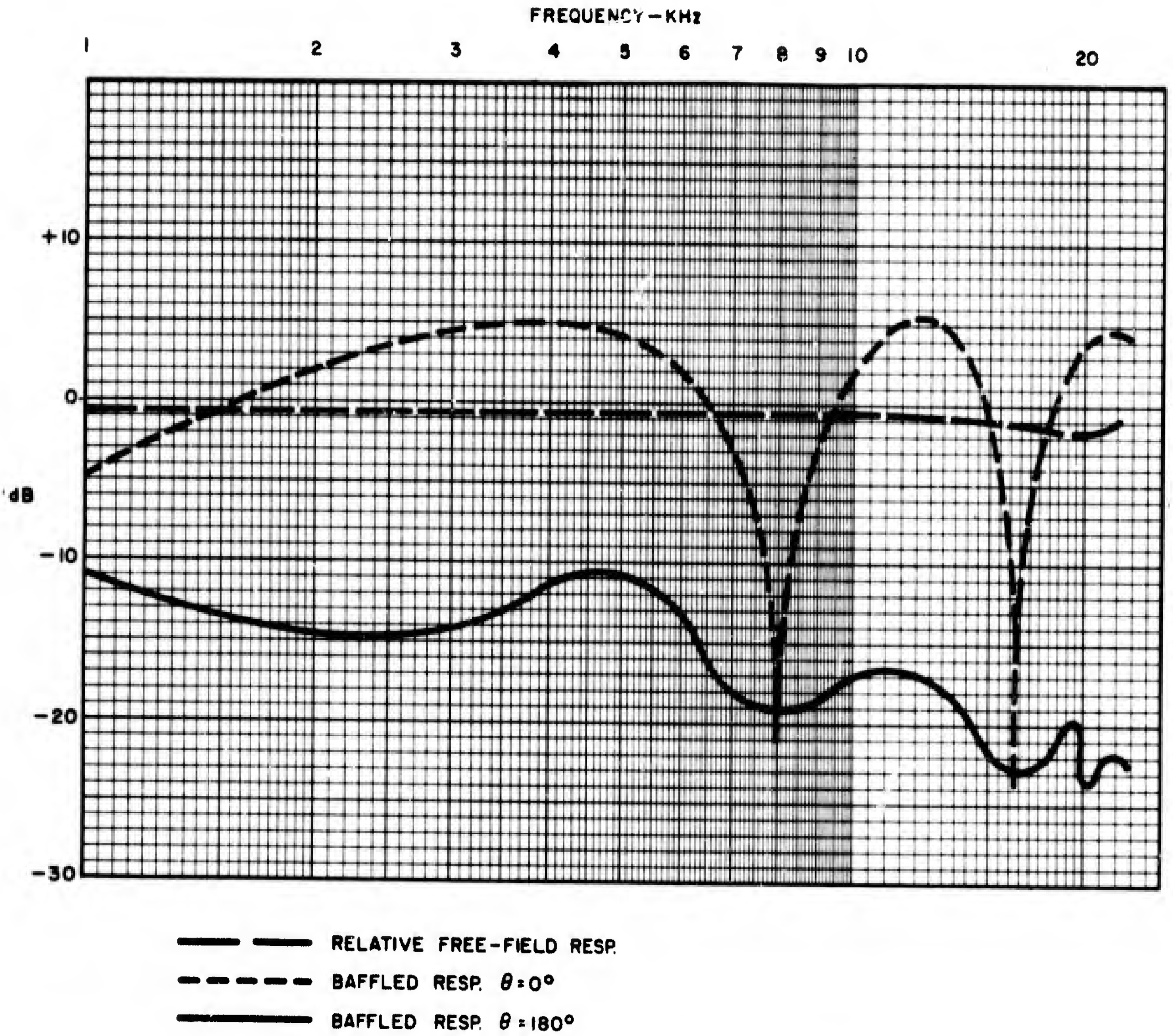

Figure 4-3. Relative Hydrophone Response In Presence of Sonite Baffle, Spacing 3-1/4 Inches

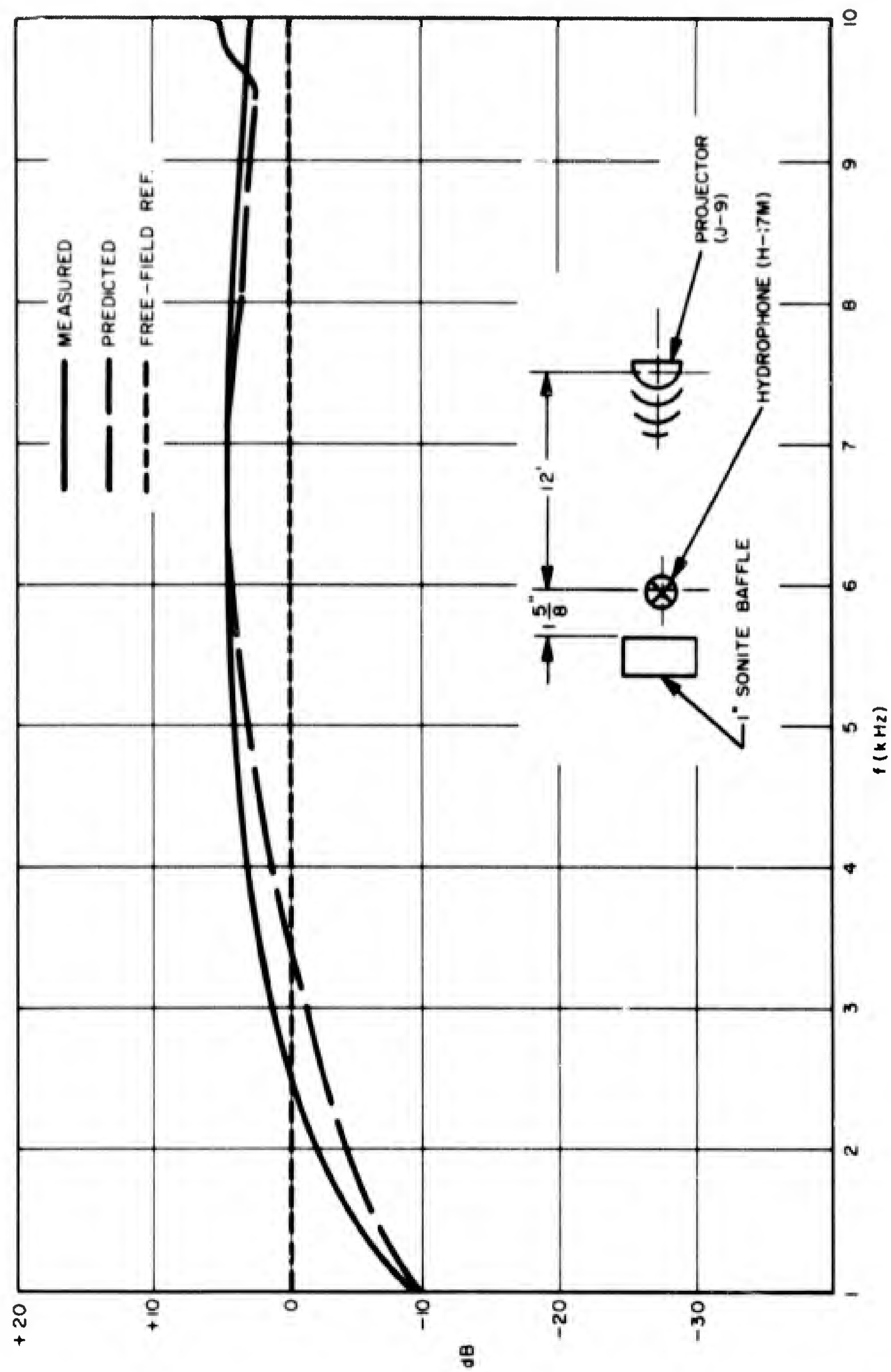

Figure 4-4. Comparative Response of Sonite Baffle

SECTION 5

SUMMARY

The following is a summary of the results of the investigations made during the period covered in this report.

- A baffle composed of an infinitely long cylinder, with walls made of layers of various materials, has been analyzed. Results of the analysis have been utilized in a computer program which calculates the response of a hydrophone placed anywhere outside the baffle. Limited comparisons between experimental and predicted data have shown extremely good agreement, although more work remains to be done.
- Studies were made to determine if a uncompensated spring-mass type of baffle could be designed to meet underwater noise reduction requirements. Lumped parameter models were used to calculate the performance of various configurations. Results of tests performed on a spring-mass baffle show that the lumped parameter models developed in this study are valid for predicting the performance when the effective thickness is small compared to one wavelength. Excellent agreement between predicted and measured data was obtained at the low frequencies. The tests further showed that good performance can be obtained with these spring-mass baffles over a wide range of frequencies and hydrostatic pressures.
- Sonite, a fiber-reinforced, ceramic material manufactured by the Johns-Manville Corporation, has been experimentally studied to learn about its performance as a low-impedance baffle element. Tests performed at the Sperry Sonar Test Facility on a Sonite panel, together with laboratory data concerning its behavior under pressure, indicate that this material shows promise for deep submergence noise reduction applications. Further experiments, especially at high hydrostatic pressures and using large baffle sizes, are need to fully characterize its performance.

SECTION 6

REFERENCES

1. Underwater Acoustic Noise Reduction Program-Interim Report, Sperry Gyroscope Division, SGD-4232-0014, April 1968.

2. Underwater Noise Reduction Study-Interim Report Phase II, Sperry Gyroscope Division, SGD-4232-0225, April 1969.

3. Philip M. Morse and Herman Feshbach, Methods of Theoretical Physics, McGraw-Hill

4. Physical Properties of Sonite-Final Report, Arnold E. Jabin, Report No. 3901-26, April 27, 1970, Johns-Manville Research and Engineering Center, Manville, New Jersey.

5. A Physical Model of Sonite Pressure-Release Material. Carl R. Johansen, NUC TN 387, Naval Undersea Research and Development Center, June 1970.